Dynamic Process Simulation of Limestone Calcination in Normal Shaft Kilns

Dissertation

zur Erlangung des Akademischen Grades

Doktoringenieurin

(Dr.-Ing.)

von: Dipl.-Ing. Agnieszka Bes

geb. am: 15.11.1974

in: Zabrze / Polen

genehmigt durch die Fakultät für Verfahrens- und Systemtechnik
der Otto-von-Guericke-Universität Magdeburg

Zusammenfassung

Die Kosten des Kalkbrennprozesses werden in hohem Maße durch die Brennstoffkosten bestimmt. Die gestiegenen Brennstoffkosten stellen in diesem Industriezweig ein großes Problem dar. Insbesondere durch den explosionsartigen Anstieg des Kokspreises müssen viele Mixed-Feed-Öfen in den nächsten Jahren auf andere Brennstoffe umgestellt werden. Auch Abfall wird als Brennstoff in zunehmendem Maße eingesetzt.

Es muss jedoch eine stets gleich bleibende Qualität des Kalks gesichert werden. Diese ist gekennzeichnet durch eine bestimmte Reaktivität (Hart-, Mittel-, Weichbrand) und einen sehr niedrigen Rest-CO_2-Gehalt. Messungen von Temperatur- und Konzentrationsprofilen sind auf Grund der Bewegung der Schüttung und der hohen Prozesstemperaturen in der Brennzone noch nicht möglich. Betriebsversuche sind schlecht möglich, da die Öfen eine Trägheit von mehreren Tagen besitzen. In Laboröfen kann der Prozess nicht nachgebildet werden. Daher bietet sich eine dynamische Prozesssimulation an.

Kernpunkt der Simulation ist die Berechnung der Kalksteinzersetzung im Normal Schachtofen. Die mathematische Schwierigkeit besteht darin, dass Kalkstein und Gas im Gegenstrom geführt werden und die Differentialgleichungen beider Ströme im gesamten Bereich über Reaktionsterme gekoppelt sind. An Hand der Simulation wird u. a. gezeigt, wie sich die Brennzone mit dem Durchsatz verlängert, bis keine vollständige Entsäuerung mehr möglich ist, wie mit erhöhtem Energieeinsatz die Entsäuerungszeit verkürzt und die Brenntemperaturen angehoben wird und wie mit dem Ausbrandverlauf des Brennstoffs der Verlauf der Gastemperatur beeinflusst werden kann. Die Berechnungen wurden für verschiedene Brennstoffe (Schwachgas, Erdgas, Braunkohle) durchgeführt. Es wurde angenommen, dass alle Partikeln sind Kugeln (d = 0.08m). Die radiale Temperatur- und Konzentrationsänderungen wurden vernachlässigt.

Contents

1. Introduction

Lime production is a global industry that contributes greatly to social and economic development throughout the world. Many beneficial industrial and consumer applications are made possible by the use of lime. A variety of business sectors including industrial manufacturing, utility suppliers, and environmental technologies, rely on the affordability, versatility and practicality of lime. The mining and distribution of lime stimulates commerce in other business sectors such as, transportation, shipping, storage, tooling suppliers, and heavy equipment suppliers.

The cost of the lime production is mostly influenced by the fuel cost. The increase of the fuel prices is one of the most important problems for the lime industry. The rapid coke price increase in last three years caused the tendency of substituting coke with other fuels. One of the alternatives is a gas with a low calorific value (weak gas). On the other hand, the quality of quicklime has to be unchanged. Quicklime's quality depends on its reactivity to water (soft-, medium-, and hard-burned) and the residual CO_2 content.

No measurements of temperature and concentration profiles are possible due to the solid flow and high process temperature in the burning zone. Response to the change of any of the operating parameters is noticeable only after a couple of days. Reproducing of the process in a laboratory scale furnace is very expensive. In this case the dynamic process simulation seems to be an interesting alternative.

Similar issue was researched by Verma [19], [20] for a mixed-feed kiln, fired with coke. Each zone was modelled separately and they were not coupled. There were differences between the temperature values at the boundaries of each zone. The other scientists, who dealt with similar subject, were Gordon, Blank, Madison and Abovian [21]. The process was modelled for natural gas that was burned in side burners outside the furnace. The fuel reaction was not included in a model.

1.1 Lime Production

World production of lime grew steadily from just under 60 million tonnes in 1960 to a peak of almost 140 million tonnes in 1989. The most recent world recession led to a drop in production to 116 million tonnes in 2002. Published estimates of the global production of quicklime (Table 1-1) suggest that the total is approximately 117 million tonnes in 2003.

| Country	1994	1995	1996	1997	1998	1999	2000	2001	2002	2003[e]
Austria	0.70	-	-	-	-	-	-	-	2.00	2.00
Belgium	1.75	1.80	1.80	1.80	1.75	1.75	1.75	1.75	1.70	-
Brazil	5.70	5.70	5.70	5.70	5.70	5.70	5.70	6.27	6.30	6.50
Canada		2.45	2.40	2.50	2.46	2.58	2.60	2.55	2.22	2.25
China	19.50	20.00	20.00	20.50	21.00	21.50	21.50	22.00	22.50	23.50
France	3.10	2.60	3.00	2.80	2.80	2.40	2.40	2.40	2.50	2.50
Germany	8.50	8.00	8.00	8.00	7.60	7.60	7.60	7.00	7.00	6.80
Iran	-	-	-	-	-	-	-	-	2.00	2.00
Italy[1]	3.50	3.50	3.50	3.50	3.50	3.50	3.50	3.50	3.00	3.00
Japan[2]	7.70	7.90	7.67	7.85	8.10	7.75	7.65	8.10	8.05	7.40
Mexico	6.50	6.60	6.60	6.60	6.60	6.60	6.50	6.50	6.50	6.50
Poland	2.50	2.50	2.50	2.50	2.50	2.50	2.50	2.20	2.00	2.00
Romania	1.60	1.70	1.70	1.75	1.70	1.70	1.70	1.70	1.70	-
Russia	-	-	-	-	-	7.00	8.00	8.00	8.00	8.00
South Africa (sales)	-	1.70	1.69	1.59	1.50	1.50	1.35	1.61	1.60	1.60
United Kingdom	2.50	2.50	2.50	2.50	2.50	2.50	2.50	2.50	2.00	2.00
United States	17.40	18.50	19.10	19.70	20.10	19.60	19.60	18.90	17.90	18.20
Other countries	37.00	34.00	35.00	32.80	28.10	21.70	21.20	23.00	22.40	23.00
Total (rounded)	118.00	120.00	121.00	120.00	116.00	116.00	116.00	118.00	116.00	117.00

[e] Estimated

[1] Includes hydraulic lime

[2] Quicklime only

Table 1-1: World production of quicklime and hydrated lime, including dead-burned dolomite sold and used, 1994-2003 according to [1],[2],[3], [4],[5] in million tonnes per annum.

The United States and China, each accounting for about 20 million tonnes, or ~18% of world output, were followed by Germany and Japan with about 7% of world output.

In most EU countries the lime industry is characterised by small and medium-sized companies. Recently a small number of large international companies have gained a considerable market share. Nevertheless, there are still more than 100 companies operating in the European Union. With an annual production of around 20 million tonnes of lime, the EU countries produce about 15% of sales-relevant world lime production. The largest producers are Germany, Italy and France, together accounting for about two third of the total volume. The total lime production in countries of EU in 1995 is shown in Figure 1-1.
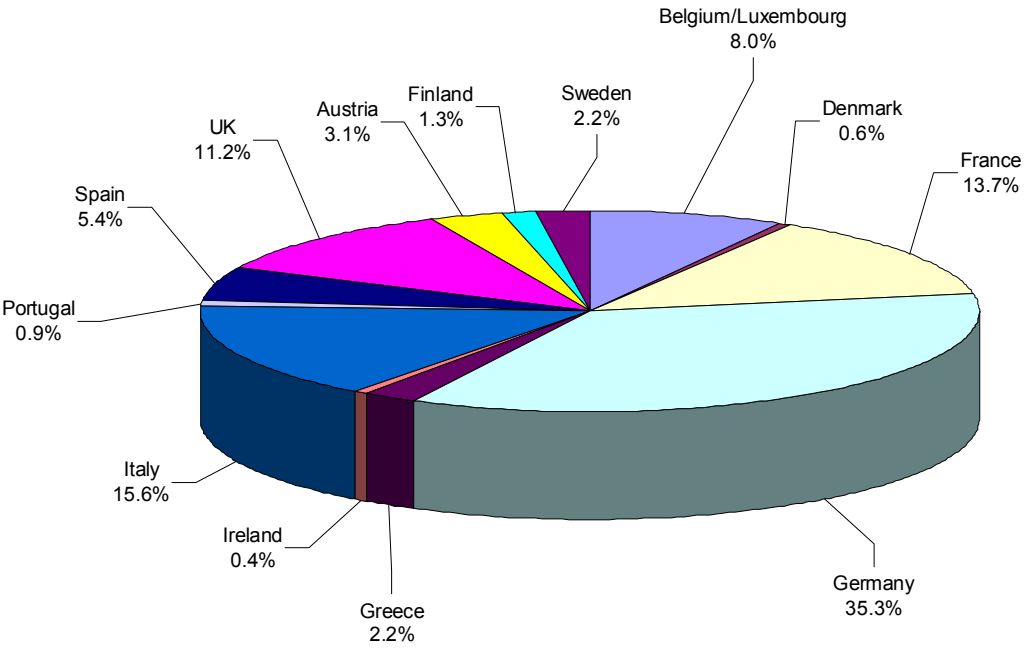
Figure 1-1: EU production of lime in 1995. [6]

The principal industries using lime in the EU are steel making, and the processing of non-ferrous metals to lower the slag melting temperature. The other application of lime is the desulphurisation of the flue gas (about 40% of total consumption in 1995), paper and cardboard making (2%) and chemistry-petrochemistry (10%). Lime is also employed in agriculture as soil conditioner on acid soils (12%) and in the agro-food business to refine sugar (5%).

The lime industry is a highly energy-intensive industry with energy cost accounting for up to 50% of total production cost. Kilns are fired with solid, liquid and gaseous fuels. The use of natural gas has grown substantially over last years. Table 1-2 shows the distribution of the fuel types used in EU in 1995.

5

Fuel	1995
Natural gas	48%
Coal (including hard coal, coke, lignite and pet coke)	36%
Oil	15%
Other	1%

**Table 1-2: Distribution of fuels used by the European lime industry in 1995 [7]**

The specific energy usage for different types of kilns is shown in Table 1-3

Kiln type	Energy usage [10^9 J / t CaO]
Rotary	5.8 – 5.9
Shaft	4.1 – 4.2
Annular	3.9 – 4.1
Parallel Flow Regenerative	3.6 – 3.7

Table 1-3: Specific energy usage for different types of kilns [7]

  The annual fuel cost, necessary for production of quicklime in 74 lime shaft kilns with the output of 90 000 t_{lime}/a each (Figure 1-2), would be 85 million € per year, assuming the flue gas temperature 150°C, lime output temperature 100°C and no carbon monoxide in the flue gas. If the furnace does not operate in an optimal way the flue gas temperature would be 250°C, lime output temperature - 100°C and there would be 6% of carbon monoxide in the flue gas. For this case the fuel cost for production of the same amount of quicklime is 160 million € per year. Reduction of the amount of carbon monoxide in the flue gas by 1% would reduce the fuel cost of ~ 20 million € (~12% of the initial cost) while decreasing the flue gas temperature from 200°C to 150°C would reduce the fuel cost by 5 million € (~5% of the initial cost). For the calculations it was assumed that one tonne of coke costs 150 €.
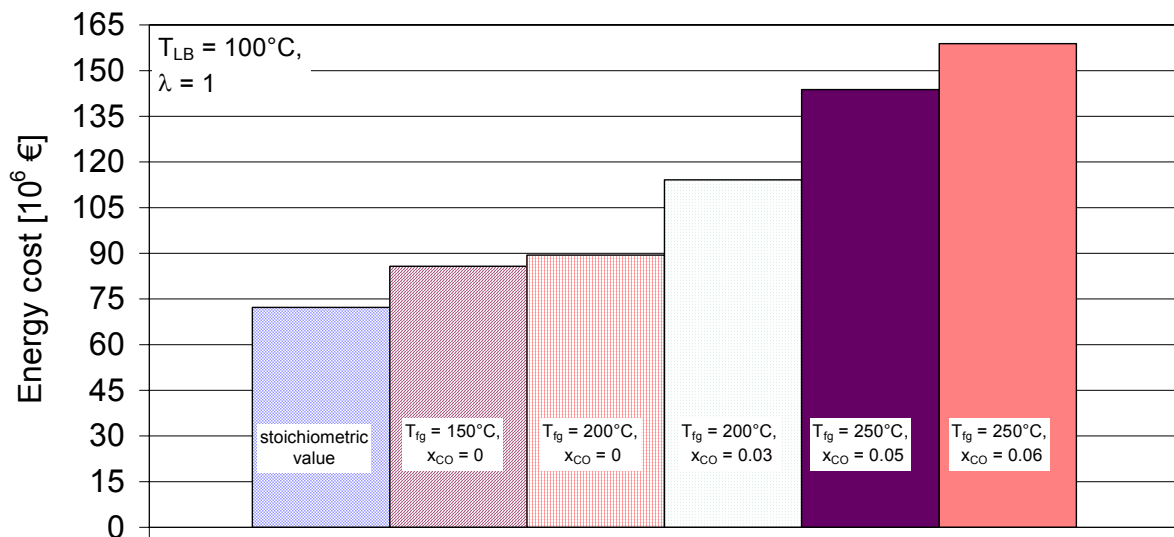
Figure 1-2: Energy cost for quicklime production in 74 lime shaft kilns with the output of 90 000 tpa each.

1.2 Limestone

Limestone is calcium carbonate (CaCO3), which is formed by the compaction of the remains of coral animals and plants on the bottoms of oceans around the world. It can be a soft white substance (chalk) through to a very hard substance (marble). Most commercial limestone deposits are a softish brown rock. Limestone is a sedimentary rock composed of the mineral calcite (calcium carbonate) and/or the mineral dolomite (magnesium carbonate) along with small amounts of other minerals.

Types of limestone are defined by their magnesium carbonate ($MgCO_3$) concentrations (ASTM C 51):

a. Dolomitic limestone consists of 35 to 46% magnesium carbonate.

b. Magnesian limestone consists of 5 to 35% magnesium carbonate.

c. High calcium limestone contains less than 5% magnesium carbonate.

Limestone is crushed and screened to serve a wide variety of applications including:

a. pH adjustment (water treatment)

b. Formulated product filler (masonry cements, ready mix concrete, asphalt, joint compounds, etc...)

c. Flue gas desulphurisation

d. Production of stone blocks

Limestone is a substitute for lime in many applications, such as agriculture, fluxing, and sulphur removal. Limestone, which contains less reactive material, is

7

slower to react and may have other disadvantages compared with lime depending on application; however, limestone is considerably less expensive than lime.

1.3 Quicklime

Calcium oxide, also called lime, quicklime, or caustic lime, is one of man's oldest and most vital chemicals. Lining fire pits with rocks, ancient man discovered that the heat turned limestone into a new and different material. The rocks, now soft and white, reacted with water to give off heat. The ancient Romans used lime in building and road construction uses which continue to the present day. Today, properly sized limestone is converted to quicklime through calcination in rotary or shaft kilns.

The term calcination refers to the process of limestone thermal decomposition into quicklime and carbon dioxide. The following chemical reaction takes place in the kiln with dolomitic limestone:

$$CaCO_3 + MgCO_3 + HEAT = CaO + MgO + 2CO_2$$

Heat is created in the kiln by burning pulverised coal, natural gas or oil. Kilns are normally operated at temperatures of 1100°C or higher to drive carbon dioxide from the limestone.

Quicklime is the least expensive and most widely-used alkali. It is used for a wide variety of industrial applications:

a. Agriculture: Lime increases fertilizer efficiency. Liming an acid soil raises the soil pH, the levels of calcium and magnesium, accelerates micro-biological activity and increases the rate of release from the soil of organic matter and nutrient elements.

b. Aluminium Industry: Lime helps remove silica from bauxite ore during the manufacture of alumina.

c. Building industry: Lime is used in the manufacture of lime silica bricks, insulation and building board materials. It is used in the mortar to lay bricks and the render of walls. Lime is also added to concrete and plaster to improve their performance.

d. Food industry: Lime is reacted with crude sugar juice for the production of both cane and beet sugars. Lime is an ingredient in baking soda and helps keep fruit and vegetables fresh.

e. Industrial Waste Water Treatment: Lime neutralizes acid wastes generated in industry thereby impeding corrosion and protecting the natural environment. Lime also removes silica, manganese, fluorides, iron and other impurities from water.

f. Metals Extraction Industries: Lime serves as a "flotation" vehicle in the recovery of copper, mercury, zinc, nickel, lead, gold and silver.

g. Paper manufacture: Pulp and paper manufacturers use lime to recover caustic soda during the conversion of wood chips to pulp. Lime bleaches the pulp and also dissolves non-cellulose components of straw and disintegrates it's fibres during the manufacture of strawboard and pasteboard.

h. Pollution control: Lime is used to absorb sulphur dioxide from exhaust gases in smelters and power generation plants.

i. Road construction: Lime converts unstable clay sub-grades by breaking down clod formations. It creates soil that will not swell or shrink. It can provide a cementing action that stabilizes soil into a steadfast layer impervious to water penetration.

j. Sewage treatment: Lime reduces pollution by removing organic matter, phosphates and nitrogen from waste water. It prevents over vegetation in streams and lakes, controls odours from waste ponds and precipitates heavy metals

k. Soil stabilisation: Lime can be used to stabilise soil in wet, boggy conditions to allow earthworks to continue.

l. Steel Industry: Lime is used as a flux for purifying steel and for removal of phosphorous, sulphur and silicon impurities. Lime lubricates steel rods as they are drawn through dies to form wire. As a whitewash coating, lime prevents ingots sticking to the moulds during pig iron casting. A bath of lime neutralizes traces of pickling acid adhering to steel products.

m. Tanneries: Lime removes hair and plump hides preparatory to leather tanning.

n. Water Treatment: Lime treats potable and industrial water supplies, including drinking water for cities and process water used in industry. It softens water by removing bicarbonate hardness and disinfects against bacteria.

1.4 Lime Shaft Kilns.

The choice of lime kiln is of a paramount importance to a lime producer. It must be suitable for burning the selected feed-stone and for producing the required quality of quicklime. It must have sufficiently low capital and operating costs to produce quicklime at a competitive price. Its capacity must also be appropriate for the market requirements. A large variety of techniques and kiln designs have been used over the centuries and around the world. The concept of the shaft kiln has been modernised in a number of designs, the characteristics of few of them are summarised in Table 1-4.

Some designs are more suitable for low outputs (below 100 tpd), while others can be used for much higher outputs (up to 800 tpd). Acceptable size for the feed-stone ranges from a minimum of 20 mm to a top size of up to 175 mm and even up to 350 mm. Some kilns are suitable for operation on gaseous, liquid and solid fuels, while the options for others are more restricted.

Kiln type	Fuels	Output range [tpd]	Range of stone size [mm]
Shaft			
Mixed-feed	S	60 - 200	20 - 200
Double-inclined	G, L, S	10 - 160	20 - 100
Multi-chamber	G, L, S	40 - 225	20 - 150
Annular	G, L, S	80 - 600	10 - 250
P.F.R - standard	G, L, S	100 - 600	25 - 200
P.F.R - fine lime	G, S	100 - 300	10 - 30
Other shaft - central burner	G, S	40 - 80	40 - 150
- external chambers	G, L	40 - 120	80 - 350
- beam burner	G, L, S	50 - 800	20 - 175
- internal arch	G, L, S	15 - 250	25 - 120
Rotary			
Long	G,L,S	160 - 1500	dust - 60
Preheater	G,L,S	150 - 1500	0 - 60
Other kilns			
Travelling grate	G,L,S	80 - 130	15 - 45
"Top shaped"	G,L,S	30 - 100	5 - 40
Fluidised bed	G, L	30 - 150	<2
Flash calciner	G, L	300 - 1500	0 - 2
Rotating hearth	G, L, S	100 - 300	10 - 40

Table 1-4: Summary of typical characteristics of the most common kilns [7].G – gaseous, L – liquid, S – solid

Different types of lime shaft kilns have been developed to reduce energy cost and to increase productivity. There are:

- Normal shaft kiln with different modifications
- Double-inclined shaft kiln
- Multi-chamber kiln
- Annular shaft kiln
- Parallel-flow regenerative kiln

In the European limestone industry among others normal shaft furnaces are being used for limestone calcination.

There are approximately 240 lime-producing installations in the European Union, which are distributed across the Member States as shown in Table 1-5 [7].

Country	Lime Plants
Austria	7
Belgium	6
Denmark	2
Finland	4
France	19
Germany	67
Greece	44
Ireland	4
Italy	32
Luxembourg	0
Netherlands	0
Portugal	12
Spain	26
Sweden	6
United Kingdom	9
Total	238

Table 1-5: Number of lime plants in EU Member States in 1995 [7]

There are about 850 kilns operating in Europe, most of which are shaft kilns - 35% of all furnaces (

Table 1-6).

	Rotary kiln	Shaft kiln	Annular shaft kiln	März kiln	Other	Total	Proportion [%] per country	total
Austria	0	7	1	3	1	12	58.3	0.9
Belgium	8	0	5	14	2	29	0.0	0.0
Czech Republic	4	13	0	7	0	24	54.2	1.6
Denmark	2	0	0	0	0	2	0.0	0.0
Finland	5	6	2	2	2	7	0.0	0.0
France	4	18	21	20	1	64	28.1	2.2
Germany	7	74	31	12	12	136	54.4	9.1
Greece	1	2	1	39	1	44	4.6	0.2
Ireland	1	3	0	1	0	5	60.0	0.4
Italy	0	30	5	25	0	60	50.0	3.7
Norway	0	3	0	0	0	3	100.0	0.4
Poland	2	57	0	2	0	61	93.4	7.0
Portugal	0	0	2	1	9	12	0.0	0.0
Slovakia	4	12	0	2	0	18	66.7	1.5
Spain	4	16	1	21	0	42	38.1	2.0
Sweden	6	5	0	0	0	11	45.5	0.6
Switzerland	0	1	0	1	1	3	33.3	0.1
Turkey	0	7	17	13	190	227	3.1	0.9
UK	8	37	0	11	1	57	64.9	4.5
Total	56	285	86	172	218	817	34.9	34.9

Table 1-6: Proportion of the shaft kilns in European countries (1995) according to [8]]

1.4.1 The Normal Shaft Kiln

Traditional shaft kilns operate continuously and are fired with fuel introduced into the calcining zone (Figure 1-3). Various fuels have been used, including bituminous coal, producer gas, fuel oil and natural gas.

In vertical lime kilns when fuel is injected at the wall of a kiln, it usually does not penetrate more than 1 m into the burden. This limits the effective kiln diameter to about 2 m, and thus restricts the productive capacity of such kiln to about 80 tpd.

Various techniques were used to enable the diameter of the kiln, and hence it's productive capacity, to be increased. On producer gas kilns, the large volume of the low calorific value gas favoured greater penetration, and was often assisted by the injection of additional or "primary" air into the calcining zone (e.g. the Priest design). Some oil-fired kilns used recycled kiln gases to increase the penetration of the vaporised oil. Others gassified the oil in refractory-lined combustion chamber, using 50% stoichiometric air, and injected it 1 m into the burden via water-cooled pipes thereby enabling a 4 m diameter shaft to be used.
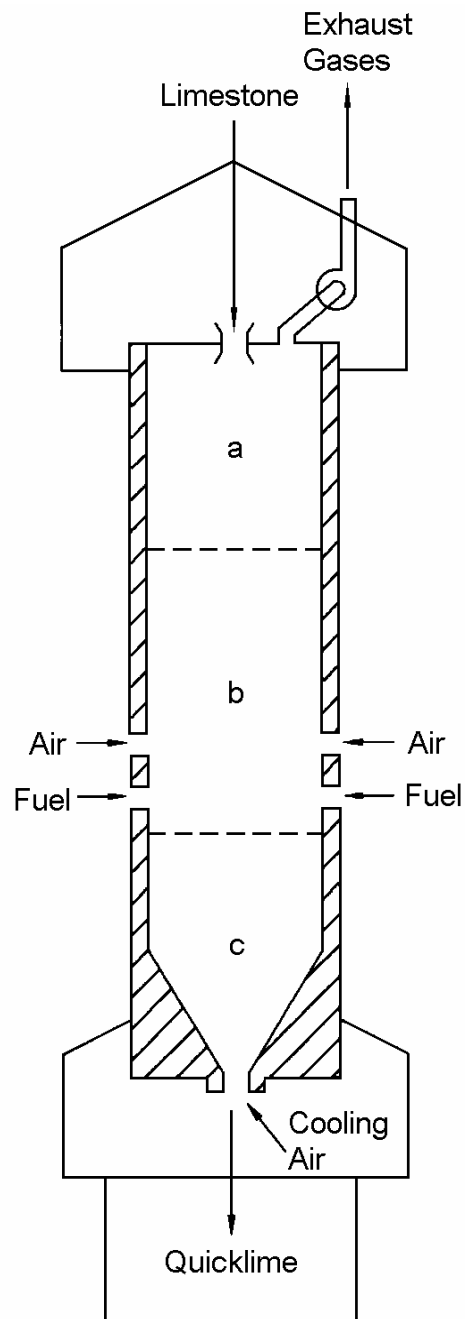
Figure 1-3: Cross-section of a normal shaft kiln. (a) the preheating zone; (b) the calcining zone; (c) the cooling zone [9]

1.4.2 The Double-inclined Kiln

The double inclined kiln is shown in Figure 1-4. It is essentially rectangular in cross-section, but incorporates two inclined sections in the calcining zone. Opposite each inclined section, off-set arches create spaces into which fuel and preheated combustion air are fired via three combustion chambers.

Cooling air is drawn into the base of the kiln. Part of it is withdrawn at 350-400°C and is re-injected via the combustion chambers. The tortuous path for the gases and the burden, coupled with firing from both sides, ensures an efficient distribution of heat and enables stone as small as 10mm to be calcined. The

14

maximum feed size is 100 mm. A range of solid, liquid and gaseous fuels can be used.

Limestone

Exhaust Gases

Fuel

a

Air

Fuel

b

Air

Combustion Air

Cooling Air

Quicklime
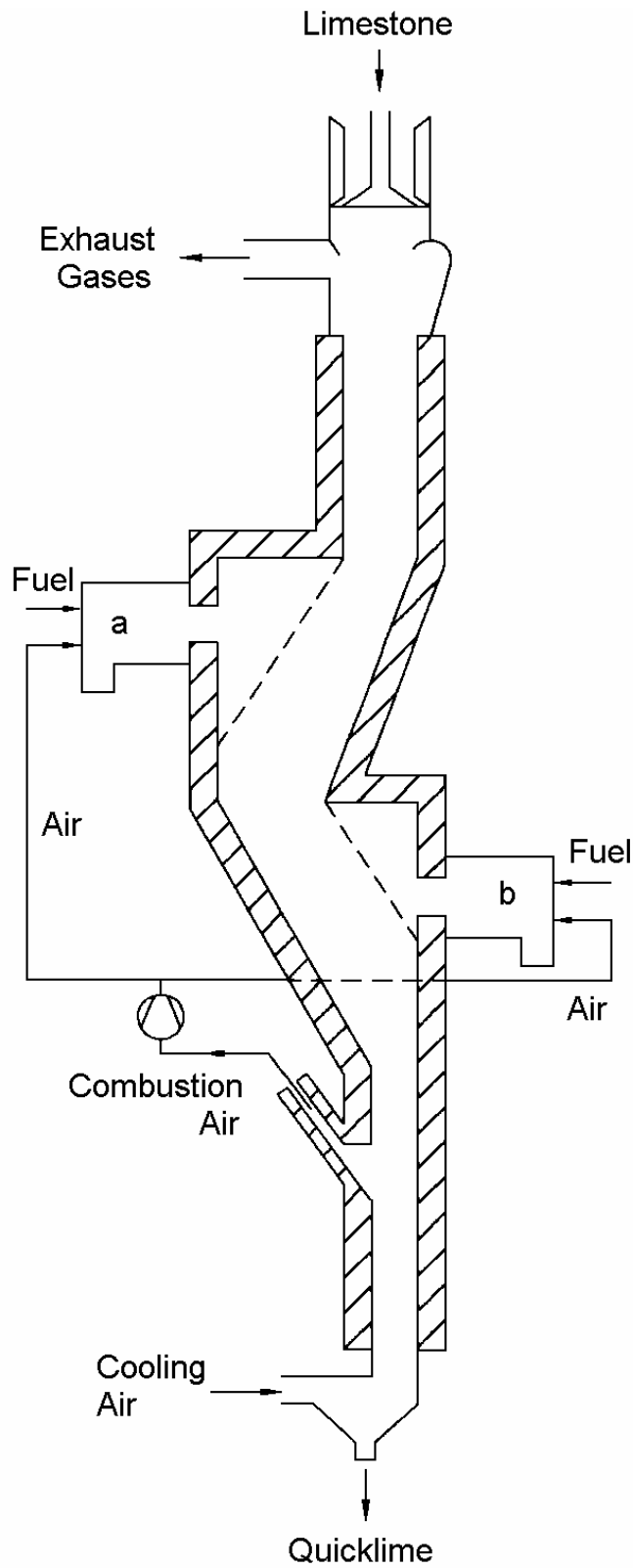
Figure 1-4: Cross-section of a double-inclined shaft kiln (a) upper combustion chamber; (b) lower combustion chamber. Based on a figure from [Ullmann's, 1990]

1.4.3 The Multi-chamber Kiln

This is a development of the double-inclined kiln. It consists of 4 or 6 alternately inclined sections in the calcining zone, opposite each of which is an offset arch. The arch serves the same purpose as in the double-inclined kiln. Cooling air is preheated by lime in the cooling zone and is withdrawn, de-dusted and re-injected via the combustion chamber. The main characteristic of this kiln is that the temperature of the lower combustion chamber can be varied to control the reactivity of the lime over a wide range. The kiln can be fired with solid, liquid and gaseous fuels (or a mixture). It can accept stone with a minimum size of 20 mm up to maximum size of 150 mm.

1.4.4 The Annular Shaft Kiln

The annular shaft kiln is shown in Figure 1-5. The characteristic feature of the kiln is a central cylinder, which:

- Restricts the effective thickness of the burden

- Ensures good heat distribution

- Enables part of the combustion gases from the lower burners to be drawn down the kiln (creating a relatively low temperature finishing zone in which both the gases and the burden move co-currently)

- Enables kiln gases to be withdrawn into a heat exchanger (where fitted) which preheats part of the combustion air.

The burden is drawn through the annulus between the central cylinder and the walls of the kiln, past the two layers of burners. Most of the fuel is fired through the upper burners, together with a sub-stoichiometric quantity of primary air. The remaining oxygen required to burn the fuel efficiently is provided by the kiln gases arising from the lower burners, which operate with the excess of oxygen. Part of the products of combustion from the lower burners rises up the kiln to the upper burners. The reminder is drawn down the kiln and into the central cylinder, together with the cooling air. The necessary suction for this flow is provided by an air-operated ejector. The resulting mixture of kiln gases and cooling air has a temperature of about 900°C and serves to moderate the flame temperature in the lower zone to about 1350°C. About 30% of the kiln gases passing through the preheating zone may be withdrawn at about 750°C to preheat the primary air in an external recuperator. The % CO_2 in the exhaust gases is about 34% by volume (dry) when fired with heavy fuel oil.

The kiln accepts a feed-stone with a top size in the range 30 to 250 mm and a bottom size as low as 10 mm. It can burn gas, oil or solid fuels.
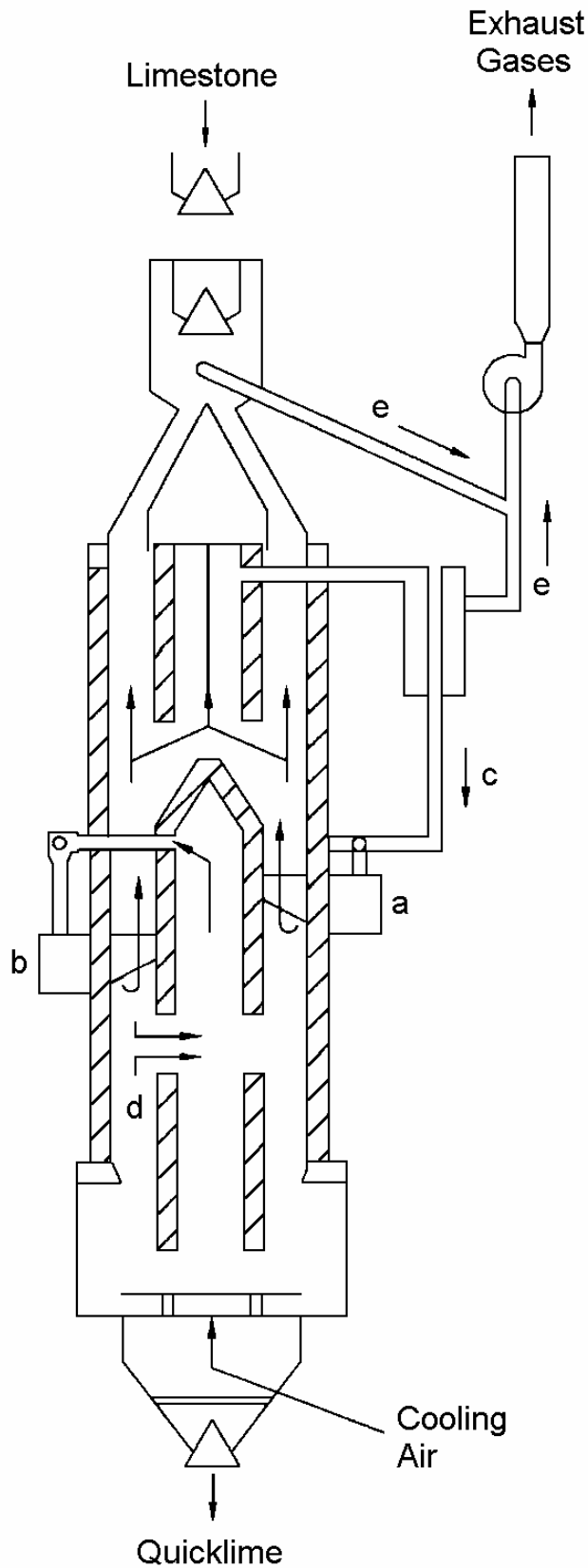
Figure 1-5: Cross-section of an annular shaft kiln; (a) upper burners; (b) lower burners; (c) combustion air to upper burners; (d) combustion air to lower burners; (e) exhaust gases Based on a figure from [Ullmann's, 1990]

1.4.5 The Parallel-flow Regenerative Kiln

The parallel-flow regenerative kiln is shown in Figure 1-6. Its characteristic feature is that it consists of two interconnected vertical cylindrical shafts (some early designs had three shafts, while others had rectangular shafts, but the operating principles were the same).

Batches of limestone are charged alternately to each shaft. The burden is drawn downwards through a preheating/regenerative heat exchange zone, past the fuel lances and into the calcining zone. From there the quicklime passes into the cooling zone.

The operation of the kiln consists of two equal stages, of 8 to 15 min. duration at full output. In the first stage, fuel is injected through the lances in shaft 1 and burns in the combustion air blown down that shaft. The heat released is partly absorbed by the calcinations of limestone in shaft 1. Air is blown into the base of each shaft to cool the lime. The cooling air in shaft 1, together with the combustion gases and the carbon dioxide from calcinations, passes through the interconnecting cross-duct into the shaft 2 at about 1050°C. In shaft 2, the gases from shaft 1 mix with the cooling air blown into the base of shaft 2 and pass upwards. In so doing, they heat the stone in the preheating zone of that shaft. If this mode of operation were to continue, the exhaust gas temperature would rise to well over 500°C.

However, after 8 to 15 min., the second stage commences. The fuel and air flows to shaft 1 are stopped, and "reversal" occurs. After charging limestone to shaft 1, fuel and air are injected to shaft 2 and the exhaust gases are vented from the top of shaft1.

The above method of operation incorporates two key principles.

The stone-packed preheating zone in each shaft acts as a regenerative heat exchanger, in addition to preheating the stone to calcining temperature. The surplus heat in the gases (low grade heat) is transferred to the stone in shaft 2 during the first stage of the process. It is then transferred from the stone to the combustion air in the second stage (and, in so doing, becomes high-grade heat). As a result, the combustion air is preheated to about 800°C.

The calcination of the quicklime is completed at the level of the cross-duct at a moderate temperature of about 1100°C. This favours the production of highly reactive quicklime, which may, if required, be produced with a low $CaCO_3$ content.
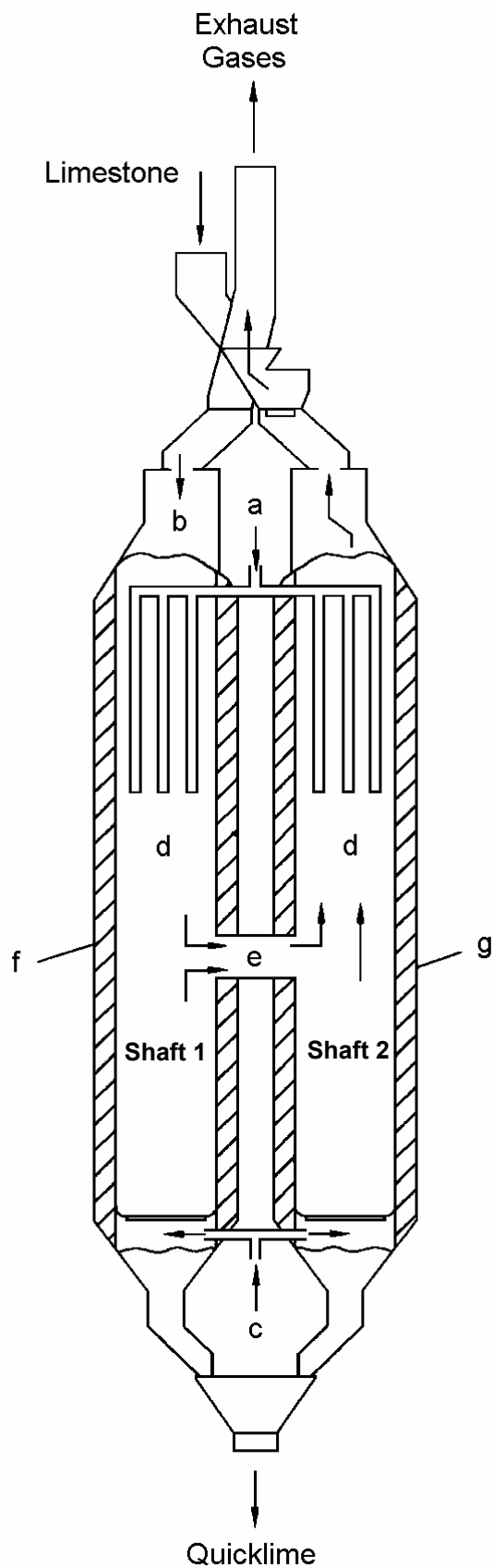
Figure 1-6: Cross-section of a parallel-flow regenerative kiln; (a) fuel; (b) combustion air; (c) cooling air; (d) kiln gases; (e) cross-duct; (f) shaft 1; (g) shaft 2. Based on a figure from [Ullmann's, 1990]

The standard kiln can be designed to accept feed-stones in the range of 25 to 200 mm. It can be fired with gas, oil or solid fuel (in the case of solid fuel, its characteristics must be carefully selected). A modified design is able to accept a feed-stone in the range 10 to 30 mm. Because the kiln is designed to operate with a high level of excess air (none of the cooling air is required for combustion), the level of CO_2 in the exhaust gases is low at 20% by volume (dry).

1.4.6 The Rotary Kiln

The traditional rotary kiln consists of a rotating cylinder (110 to 140 m long) inclined at an angle of 3 to 4° to the horizontal. Limestone is fed into the upper end and fuel and combustion air are fired into the lower end. Quicklime is discharged from the kiln into a lime cooler, where it is used to preheat the combustion air. Many kilns have internal features to recover heat from the kiln gases and to preheat the limestone, while permitting the passage of air. The design of burner is important for the efficient and reliable operation of the kiln. The flame should be of the correct length –when it is too short, it causes excessive temperatures and refractory failure, too long and it does not transfer sufficient radiant heat in the calcining zone with the result that the back-end temperature raises and thermal efficiency decreases. The flame should not impinge on the refractory. Oxygen enrichment of the combustion air, and particularly of that under the flame, is used to raise flame temperature and increase radiant heat transfer. It can increase output by 20% and reduce heat usage per tonne lime by 10%.
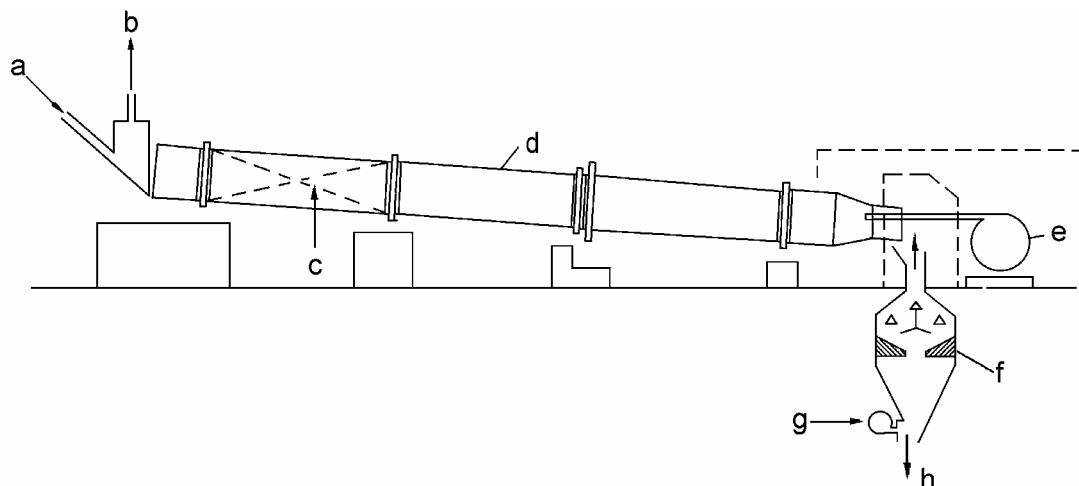
Figure 1-7: Cross section of a rotary kiln; (a) limestone; (b) exhaust gases; (c) refractory trefoils; (d) kiln shell; (e) fuel plus secondary air; (f) lime cooler; (g) cooling air; (h) quicklime. Based on a figure from [Ullmann's, 1990]

Rotary kiln can accept a wide range of sizes from 60mm down to dust. An interesting feature of the tumbling bed in the kiln is that larger stones migrate towards

the outside of the bed, while smaller ones concentrate at the centre of the bed. This results in the larger stones being exposed to higher temperatures and avoids over-calcination of the finer fractions.

Because of the ease with which they can be controlled, rotary kilns can produce a wider range of reactivities and lower $CaCO_3$ levels than shaft kilns. The variability, however, tends to be greater than that of shaft kilns.

Relatively weak feed-stones, such as shell deposits, and limestone that decrepitates, are unsuitable as feed to shaft kiln but may prove to be acceptable for rotary kilns.

Rotary kilns can be fired with a wide range of fuels. As heat transfer in the calcining zone is largely by radiation, and as the infra-red emissivities increase in the sequence gas, oil and solid fuel, the choice of fuel can have a marked effect on heat usage. Radiation and convection losses from the kiln are high relative to other designs of lime kiln.

A feature of rotary kiln is that sulphur from the fuel, and, to a lesser extent from the limestone, can be expelled from the kiln in the kiln gases, without over-burning the lime, by a combination of controlling the temperature and the % CO in the calcining zone. Thus high reactivity, low sulphur limes can be produced using relatively inexpensive high sulphur fuels – subject to any emission limits for SO_2 in the exhaust gases.

1.4.7 The Mixed-feed Shaft Kilns

Mixed-feed kiln is that kind of furnace in which the limestone and fuel are both charged into the top of a shaft kiln. Coke-fired mixed-feed kilns can have the lowest heat usage of all kilns. Another feature of mixed-feed kilns is that they can be operated to produce the consistently low reactivity lime favoured by some producers. They can also produce higher reactivity lime, but the $CaCO_3$ contents are higher than can be obtained from more modern designs.

Mixed-feed kilns currently in operation generally use coke or anthracite as the fuel for lime burning. Where coke is used, it needs to be sufficiently large to be trapped between the lumps of limestone and also needs to be strong enough to resist being crushed or abraded by the burden. It should have low reactivity with respect to the reduction of carbon dioxide ($C + CO_2 \rightarrow 2CO$), which would result in a loss of effective calorific value.

The kiln accepts feed-stone with a size in the range 30 to 150 mm.

A feature of the mixed-feed kiln is the ease of lighting it off and putting it out. The main problems of such kilns are:

- high CO content in the exhaust gases
- influence of the coke type and size on a temperature profiles
- coke and limestone distribution in bed
- the limestone decomposition is not complete

2. Energy balance

2.1 Process description

A lime shaft kiln is basically a moving bed reactor with the upward-flow of hot gases passing counter-current to the downward-flow of a feed consisting of limestone particles undergoing calcination. A kiln basically has three operating sections: the preheating, the burning and the cooling zone. The preheating zone is that part of the kiln where the limestone is heated to its dissociation temperature. The burning zone is that part of the kiln in which reaction of the burden takes place. The cooling zone is that part of the kiln in which the lime emerging from the burning zone is cooled before discharge. It begins when the gas temperature is lower than solid temperature. The feed consisting of limestone particles is loaded into the kiln at the top, and the calcined product is withdrawn from the bottom. Air under ambient conditions enters at the bottom and the hot kiln gases leave from the top of the kiln. Fuel is injected into the furnace between burning and cooling zone.
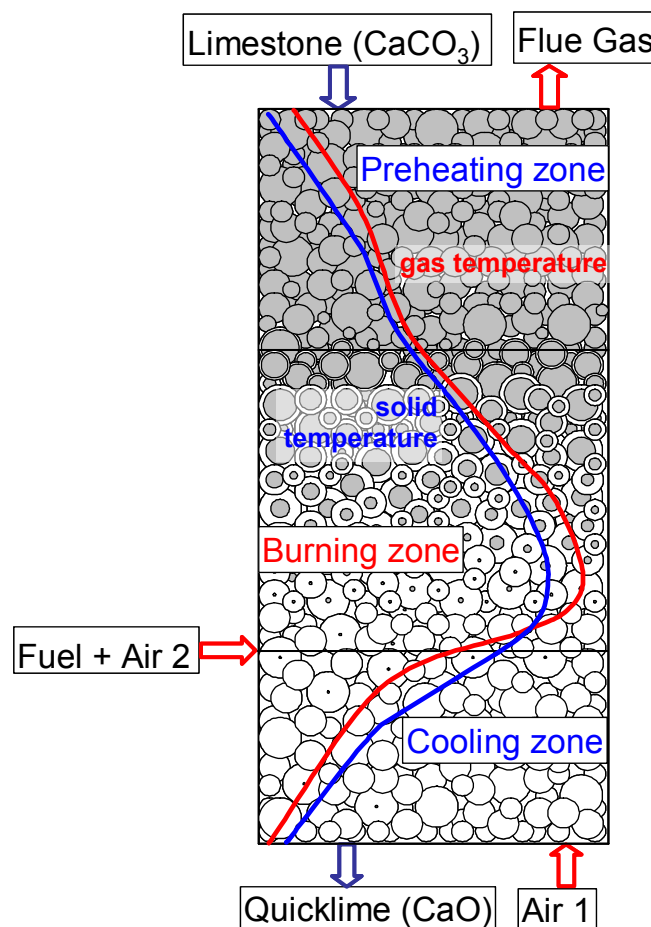
Figure 2-1: Temperature and concentration profiles in lime shaft kiln.

The preheating zone utilises the hot gases from the calcination zone whilst the cooling zone preheats the combustion air thus maximising heat recovery and increasing fuel efficiency. Figure 2-1 shows the temperature profiles of limestone surface and gas. The carbon dioxide in the gas phase is produced by fuel combustion and the decomposition of limestone.

2.2 Fuels

The most common fuels used in shaft kilns are coke, natural gas, weak gas and pulverized lignite. As recently the price of coke increased rapidly there is a tendency to substitute it with cheaper fuels [10]. Table 2-1 and Table 2-2 show the composition of these fuels, the air demand and net calorific values.

	CH_4	C_2H_6	H_2	CO_2	CO	N_2	$\tilde{L}$ $\left[m^3_{air}/m^3_{fuel}\right]$	L $\left[kg_{air}/kg_{fuel}\right]$	h_u [MJ/kg]
Weak gas	-	-	0.02	0.16	0.66	0.16	1.64	2.44	6.6
Natural gas L	0.82	0.03	-	0.01	-	0.14	9.1	15.1	38.3
Natural gas H	0.93	0.05	-	0.01	-	0.01	9.69	15.64	47.3

Table 2-1: Composition, air demand and net calorific value of the gaseous fuels used.

	C	H	O	S	N	$L\left[kg_{air}/kg_{fuel}\right]$	h_u [MJ/kg]
Anthracite (d.a.f.)	0.92	0.04	0.02	0.01	0.01	12.0	32.8
Lignite (d.a.f.)	0.7	0.05	0.25	-	-	7.3	20
Coke (d.a.f.)	0.98	-	-	0.01	0.01	12	28.7

Table 2-2: Composition (dry and ash free), air demand and net calorific value of solid fuels.

The fuel combustion rate is not known as the kinetic of radial mixing in a normal shaft kiln is unknown. There are different ways of introducing fuel into the furnace e.g. lances, beam-burners.

Therefore the function describing the fuel burnout was taken to approximate the fuel combustion. Günther [22] described the burnout of the free diffusion flame with the function $U_{fuel} = exp(-az^2)$, where a is constant and z stands for the co-ordinate. Constant a depends on the kind of fuel and therefore in the model described in this work it was taken as a parameter.

2.3 Energy balance

In order to describe the operation and the design of a shaft kiln, it has to be divided into three operating sections: the preheating, the reaction and the cooling zone as it is shown in Figure 2-2. The preheating zone is this part of the kiln, where the stones are preheated from ambient temperature to their dissociation temperature; the reaction zone is this part of the kiln where both reactions (limestone decomposition and fuel combustion) take place, and the cooling zone is this part, where lime is cooled down before discharge. To calculate the energy consumption the reaction and the cooling zone have to be treated together and the preheating zone has to be separated. This division is necessary because the gas temperature T_g between the preheating and the reaction zone has to be higher than the solid equilibrium temperature at that position T_{eq}, so that the 2nd law of the thermodynamics is fulfilled.
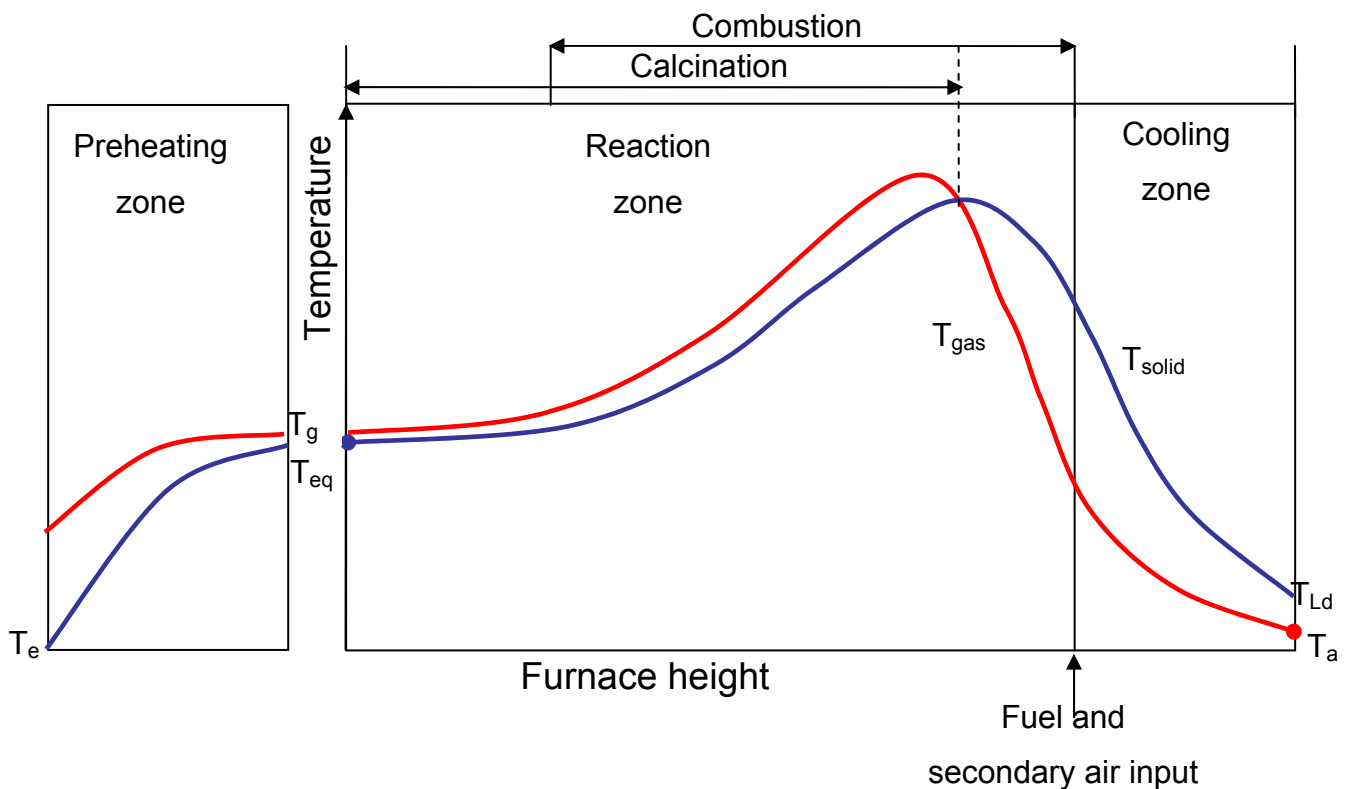
Figure 2-2: Demonstrative temperature profiles in the lime shaft kiln

The energy input and output flows in the reaction and the cooling zone are schematically depicted in Figure 2-3.
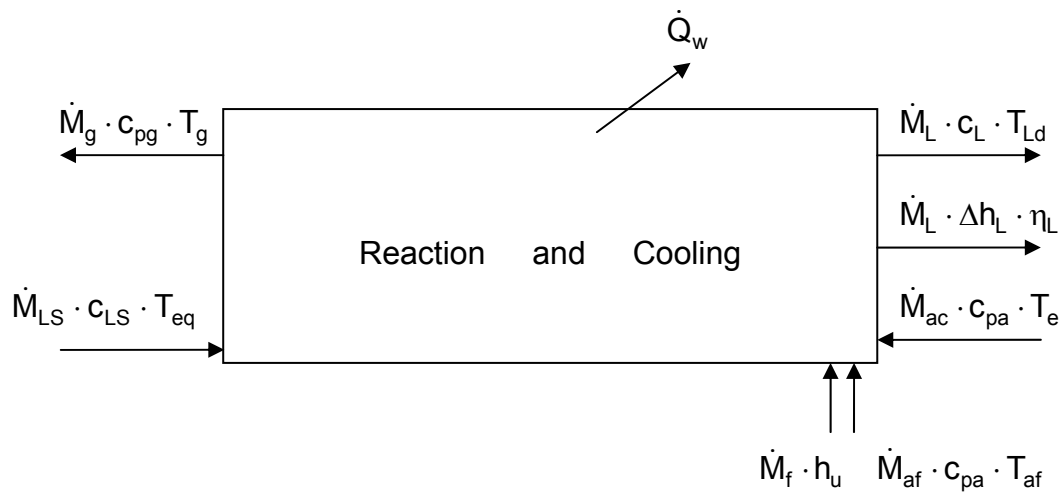
Figure 2-3: Heat inputs and outputs in the reaction and the cooling zone.

The main heat input is the mass of fuel $\dot{M}_f$ multiplied by its heating value h_u. The limestone input temperature is the equilibrium temperature T_{eq}. The air flow is divided into the air flow through the cooling zone $\dot{M}_{ac}$ and the air flow blown into the kiln with the fuel $\dot{M}_{af}$. The air blown in with the fuel can be preheated. Therefore, its temperature was denoted as T_{af}. The heat input of the two air flows $\dot{M}_a \cdot c_{pa} \cdot T_e$ is calculated relative to the ambient temperature T_e. The amount of the air necessary for the lime cooling $\dot{M}_{ac}$ will be discussed in detail in chapter 4.1.

The main energy output is the energy consumed by the limestone decomposition $\dot{M}_L \cdot \Delta h_L \cdot \eta_L$. Here, η_L is the conversion degree ($1 - \eta_L$ gives the residual CO_2 content), $\dot{M}_L$ is the mass flow of lime and Δh_L = 3.18 MJ/kg_{lime} is the reaction enthalpy related to the ambient temperature. The experimental research results in the value $\Delta \tilde{h}$ =178 ± 1 MJ/kmol. The other heat outputs are the heat output with the lime $\dot{M}_L \cdot c_L \cdot T_{LB}$, with the gas $\dot{M}_g \cdot c_{pg} \cdot T_g$ ($\dot{M}_g$ is the amount of the flue gas) and the heat loss through the wall $\dot{Q}_w$. The decomposition of the magnesite fraction and the evaporation enthalpy of the moisture in the limestone are neglected. The calorific value of the combustibles in the flue gas, if any, should not be overlooked. This results in the energy balance:

$$\dot{M}_f \cdot h_u + \dot{M}_{ac} \cdot c_{pa} \cdot T_e + \dot{M}_{af} \cdot c_{pa} \cdot T_{af} + \dot{M}_{LS} \cdot c_{LS} \cdot T_{eq}$$
$$= \dot{M}_L \cdot c_L \cdot T_{Ld} + \dot{M}_L \cdot \Delta h_L \cdot \eta_L + \dot{M}_g \cdot c_{pg} \cdot T_g + \dot{Q}_w \tag{2-1}$$

The air mass flow depends with the air demand L on the kind of fuel and with the air excess number λ on the operating conditions:

$$\dot{M}_a = \dot{M}_{ac} + \dot{M}_{af} = \lambda \cdot L \cdot \dot{M}_f. \tag{2-2}$$

The flue gas mass flow $\dot{M}_g$ consists of the air flow $\dot{M}_a$, the fuel flow $\dot{M}_f$ and the CO_2 flow produced by the calcination $\dot{M}_{LS} \cdot y_{CO_2}$:

$$\dot{M}_g = \dot{M}_a + \dot{M}_f + \dot{M}_{LS} \cdot y_{CO_2}. \tag{2-3}$$

Here, $\dot{M}_{LS}$ is the mass flow of limestone and y_{CO2} is the mass fraction of CO_2 in the limestone

$$\dot{M}_{LS} = \dot{M}_L \cdot \frac{1}{1 - y_{CO_2}}. \tag{2-4}$$

The CO_2 mass fraction varies for different limestones. It is typically in the range of $y_{CO_2} = 0.40 - 0.44$ kg CO_2 per kg limestone.

From Eq. (2-1) to (2-4) the energy consumption per kg of lime is obtained ($T_{af} = T_e$):

$$\frac{\dot{M}_f \cdot h_u}{\dot{M}_L} = \frac{c_L \cdot T_{Ld} + \Delta h_L \cdot \eta_L + \dfrac{y_{CO_2}}{1 - y_{CO_2}} \cdot c_{pg} \cdot T_g - \dfrac{1}{1 - y_{CO_2}} \cdot c_{LS} \cdot T_{eq} + \dfrac{\dot{Q}_w}{\dot{M}_L}}{1 + [\lambda \cdot L \cdot c_{pa} \cdot T_e - (1 + \lambda \cdot L) \cdot c_{pg} \cdot T_g]/h_u} \tag{2-5}$$

The energy balance requires the mean values of the specific heat capacities, which can be obtained from the real values. The specific heat capacity depends on the temperature. This relationship is given in chapter 3.3.1.

To solve the Eq. (2-5) it is necessary to know the value of the equilibrium temperature T_{eq}, which has to be lower than the gas temperature. Both temperatures are unknown. The equilibrium temperature depends on the carbon dioxide concentration and thus on the kind of fuel and the operating conditions. This dependence will be described in the following chapter.

2.4 Equilibrium temperature

The temperature, at which the decomposition begins, is a function of the carbon dioxide partial pressure in the gas phase. This partial pressure varies for different fuels. The carbon dioxide concentration in the flue gas leaving the reaction zone x_{CO_2fg} can be calculated from the mass balance:

$$\dot{M}_{gf} \cdot x_{CO_2f} + \dot{M}_{CO_2L} = (\dot{M}_{gf} + \dot{M}_{CO_2L}) \cdot x_{CO_2fg}. \tag{2-6}$$

The mass flow of CO_2 produced by the fuel combustion $\dot{M}_{gf} \cdot x_{CO_2f}$ and the mass flow of CO_2 produced by the limestone decomposition $\dot{M}_{CO_2L}$ leave the reaction zone with the total gas flow:

$$\dot{M}_g = \dot{M}_{gf} + \dot{M}_{CO_2L}. \tag{2-7}$$

The mass flow of the combustion gas $\dot{M}_{gf}$ depends on the mass flow of the fuel $\dot{M}_f$:

$$\dot{M}_{gf} = (1 + \lambda \cdot L) \cdot \dot{M}_f. \tag{2-8}$$

The mass flow of CO_2 produced by the limestone decomposition can be replaced by the lime mass flow

$$\dot{M}_{CO_2L} = \dot{M}_{LS} \cdot y_{CO_2} = \dot{M}_L \cdot \frac{y_{CO_2}}{1 - y_{CO_2}} \tag{2-9}$$

and the lime mass flow can be replaces by the energy consumption E:

$$E = \frac{\dot{M}_f \cdot h_u}{\dot{M}_L}. \tag{2-10}$$

This results in:

$$x_{CO_2fg} = \frac{E \cdot (1 + \lambda \cdot L) \cdot x_{CO_2f}(\lambda) + \frac{y_{CO_2}}{1 - y_{CO_2}} \cdot h_u}{E \cdot (1 + \lambda \cdot L) + \frac{y_{CO_2}}{1 - y_{CO_2}}}. \tag{2-11}$$

From the equation above it can be seen that the CO_2 fraction in the flue gas depends on the energy usage E, the air excess number λ and with h_u and x_{CO_2f} on the kind of fuel.

The concentration of the carbon dioxide in a combustion gas has to be calculated with the molar balances of the four species C, H_2, O_2 and N_2. For the input ensues:

$$\tilde{\upsilon}_C = \tilde{x}_{CH_4} + \tilde{x}_{CO_2} + n \cdot \tilde{x}_{C_nH_m} + \tilde{x}_{CO} \tag{2-12}$$

$$\tilde{\upsilon}_{H_2} = 2 \cdot \tilde{x}_{CH_4} + \tilde{x}_{H_2O} + m/2 \cdot \tilde{x}_{C_nH_m} + \tilde{x}_{H_2} \tag{2-13}$$

$$\tilde{\upsilon}_{O_2} = 0.5 \cdot \tilde{x}_{H_2O} + \tilde{x}_{CO_2} + 0.5 \cdot \tilde{x}_{CO} + \tilde{x}_{O_2a} \cdot \lambda \cdot \tilde{L} \tag{2-14}$$

$$\tilde{\upsilon}_{N_2} = \tilde{x}_{N_2} + \tilde{x}_{N_2a} \cdot \lambda \cdot \tilde{L} \tag{2-15}$$

Here $\tilde{x}_i$ is the volume concentration of the components in the fuel and in the air (a).

The moles are removed with the components in the combustion gas. For the specific amount of the combustion gas m^3_{gas}/m^3_{fuel} follows:

$$\tilde{\upsilon} = \tilde{\upsilon}_C + \tilde{\upsilon}_{H_2} + \tilde{\upsilon}^*_{O_2} + \tilde{\upsilon}_{N_2} \tag{2-16}$$

where

$$\tilde{\upsilon}^*_{O_2} = \tilde{x}_{O_2a} \cdot (\lambda - 1) \cdot \tilde{L} \tag{2-17}$$

is the non-reacted oxygen. For the CO_2 volume concentration $\tilde{x}_{CO_2f}$ ensues:

$$\tilde{x}_{CO_2f} = \frac{\tilde{\upsilon}_C}{\tilde{\upsilon}} \tag{2-18}$$

From this the mass concentration is obtained:

$$x_{CO_2f} = \tilde{x}_{CO_2f} \frac{\rho_{CO_2}}{\rho_g} . \tag{2-19}$$

The carbon dioxide volumetric concentration for different fuels and air excess numbers are shown in Figure 2-4 . The lower the energy consumption and the air excess number are, the higher is the carbon dioxide concentration. Weak gas gives the highest and the natural gas H the lowest concentration.
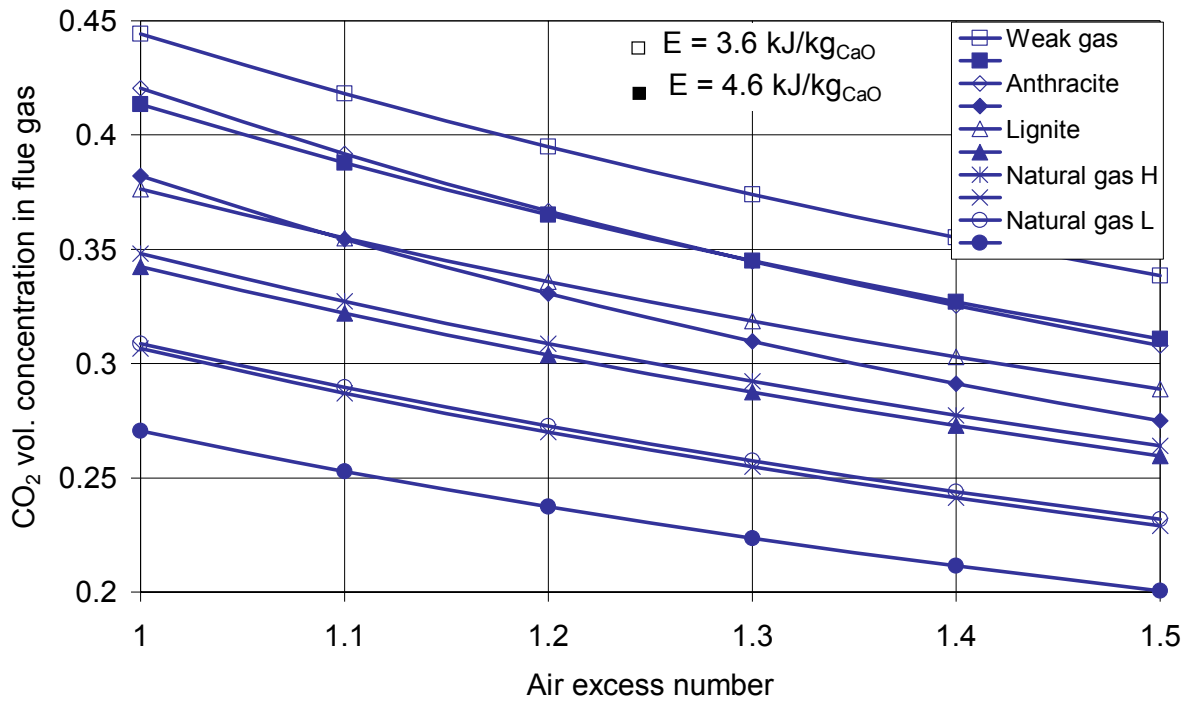
Figure 2-4: Carbon dioxide volumetric concentration in a flue gas.

The equilibrium correlation between the CO_2 concentration and the temperature varies from paper to paper. The literature sources suggest that the equilibrium temperature at CO_2 pressure 1 bar is in the range from 880°C to 920°C. Therefore, own measurements have been conducted with DTG. The experiments gave the decomposition temperatures of 915-917°C at CO_2 pressure 1 bar for limestones of different origin. These results are approximated by the following correlation:

$$p_{eq} = 2.15 \cdot 10^7 \exp\left(-\frac{167}{R \cdot T_{eq}} \frac{kJ}{mol}\right) bar \qquad (2\text{-}20)$$

where 167 kJ/mol is the decomposition enthalpy at ~900°C.

The decomposition temperatures for different fuels and air excess numbers are shown in Figure 2-5. This dependence is the same as of the carbon dioxide vol. concentration.
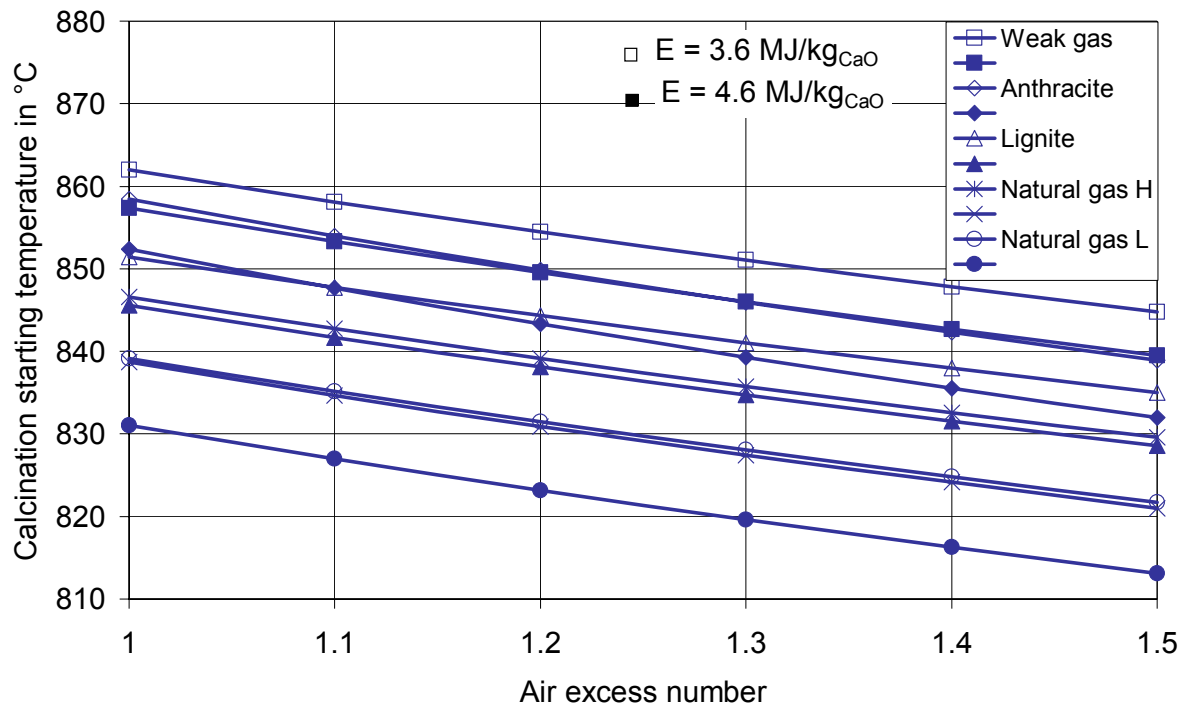
Figure 2-5: Calcination starting temperature.

2.5 Energy consumption

With the set of equations given before the energy consumption can be calculated iteratively. In Eq. (2-5) all values are now known except from the gas temperature T_g between the preheating and the reaction zone. This temperature depends on the heat exchange, the zone length and the lime throughput and thus on the kinetic of the process. The larger the heat transfer and the higher the kiln are, the smaller is the difference between gas and solid temperature. The process kinetic will be described in detail in a following paper. Because the gas temperature is unknown its value was taken as a parameter for the following calculations.

Figure 2-6 shows the energy consumption as a function of the gas and solid temperature difference at the transition to the reaction zone (T_g - T_{eq}) for typical fuels. For the calculations a heat loss through the wall of 170 kJ/kg$_{lime}$, a CO_2 concentration in the limestone y_{CO2} =0.42, the residual CO_2 concentration of 0%, a lime discharge temperature of T_{Ld} = 80°C and an air excess number of λ = 1.2 were assumed. These assumptions are discussed later. The energy consumption for the temperature difference (T_g - T_{eq}) equal 0 is the minimum value possible. The energy consumption increases linearly with the temperature difference. As it will be shown in a following paper this temperature difference is lower than 5 K for most of the kilns. Therefore, the influence of this difference is relatively low and was set to 1 K in the following. In

31

Figure 2-6 it can be seen that for the same conditions the energy consumption for the weak gas is the highest and for natural gas H is the lowest. The energy consumptions for lignite, anthracite and natural gas L are similar. For comparison the value of the decomposition enthalpy is drawn in. This value is theoretically the minimum value.
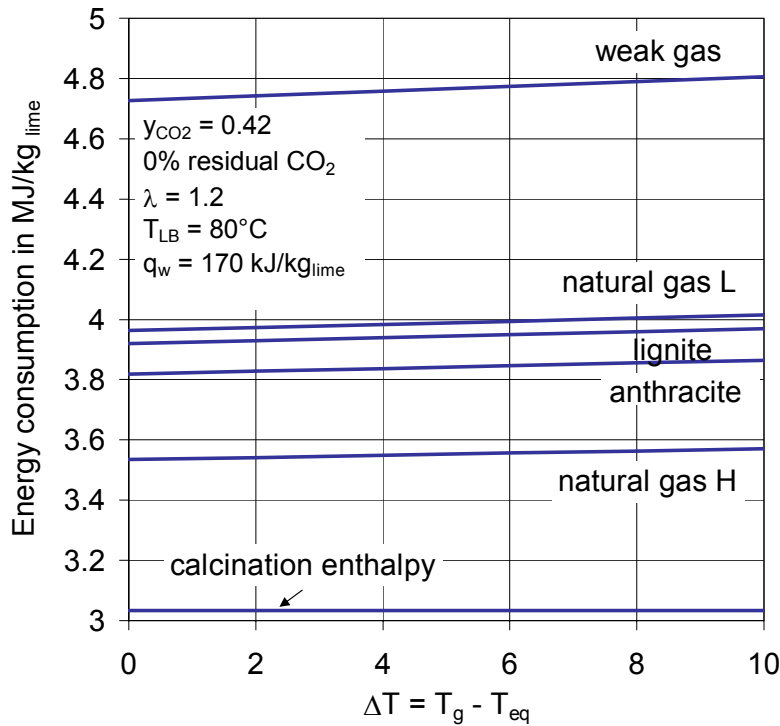
Figure 2-6: Energy consumption for different fuels in dependence on the gas and solid temperature difference at the zone transition.

The calculations were done for the air excess number 1.2 in order to compare different fuels, though the fuels require different λ during the combustion. Figure 2-7 shows the energy consumption for different fuels in dependence on the air excess number for $\Delta T = 1K$. The air excess number has stronger influence on the energy consumption for the weak gas than on other fuels.
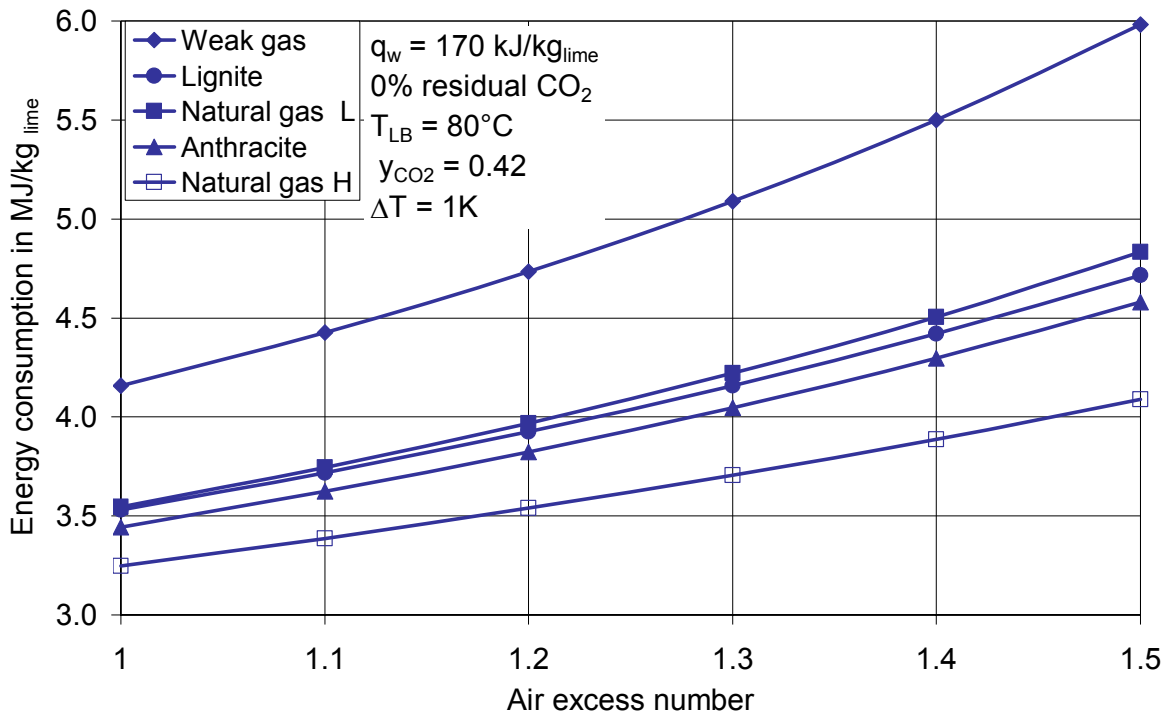
Figure 2-7: Energy consumption for different fuels in dependence on the air access number.

Figure 2-8 shows the energy consumption in dependence on the CO_2 concentration in the limestone and the residual CO_2 content in the lime for lignite as an example. The energy consumption increases nearly linearly with the CO_2 mass fraction. The energy consumption decreases by approximately 0.08 MJ/kg_{lime} with every percent of the residual CO_2.
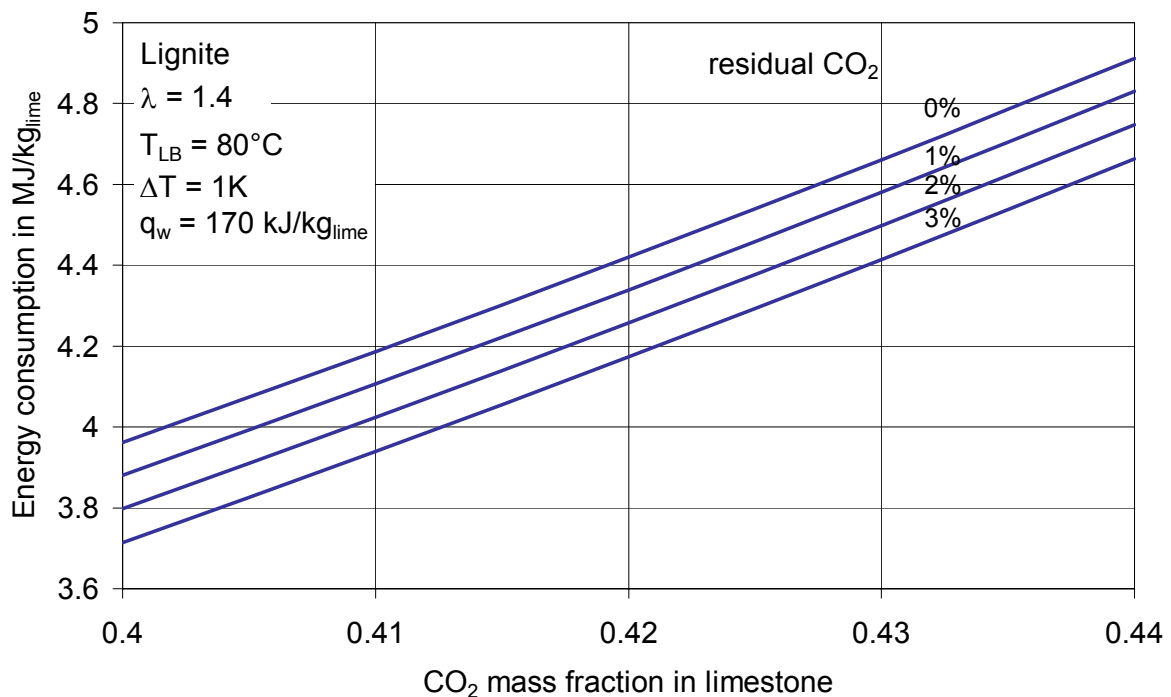
Figure 2-8: Energy consumption for different CO_2 mass fraction in limestone and in lime.

At last, with Figure 2-9 the influence of the heat loss will be discussed. The energy consumption is shown again in dependence on the air excess number for the two fuel natural gas H and lignite with the same conditions as before, however additionally for an adiabatic wall, this means no heat loss. It can be seen that the difference is 0.25 - 0.30 MJ/kg$_{lime}$, which is about 50 to 75% more than the heat loss of 0.17 MJ/kg$_{lime}$. The reason is that the energy to cover the heat loss has to be generated with a low pyrotechnical efficiency because the temperature of the gas leaving the reaction zone is so high. Therefore, the real (total) heat loss is much higher than the portion transferred through the wall.
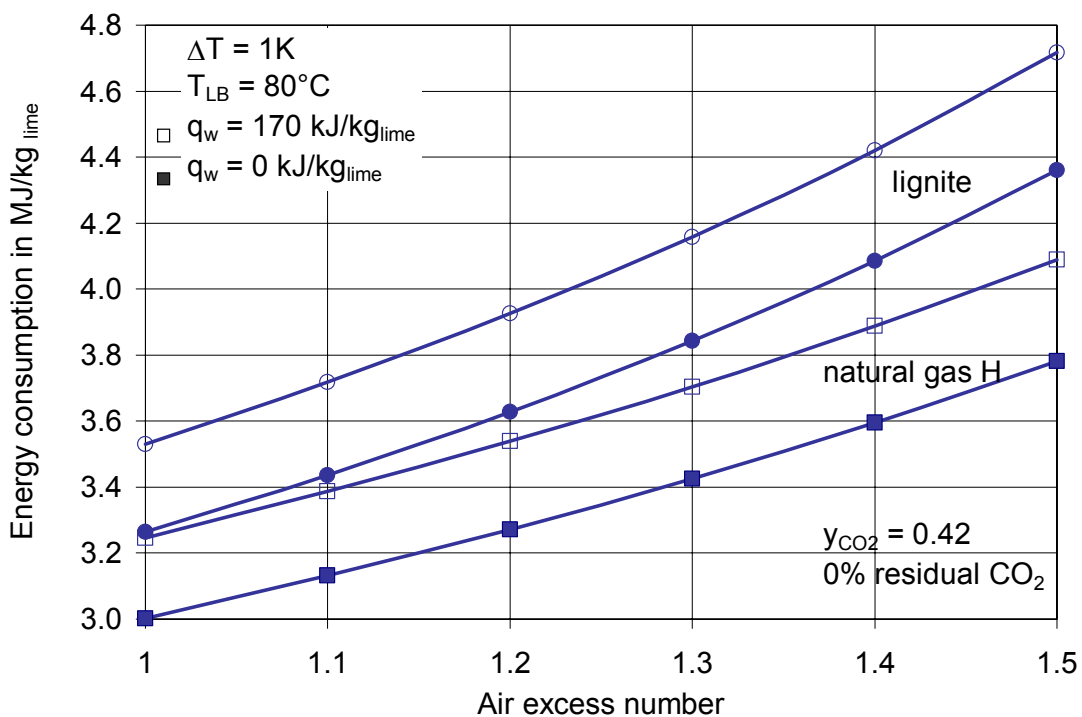
Figure 2-9: Energy usage with and without heat loss through the wall.

Figure 2-10 shows the energy usage in dependence on the flue gas temperature and the carbon monoxide content in the flue gas. The calculations were carried out for the assumed lime output temperature of 50°C, the limestone, coke and air input temperature of 10°C, air excess number equal 1 and the coke calorific value h_u = 28000 kJ/kg. The CO emission of 1-2% is usually typical for a kiln with a good performance. For a kiln with a very bad performance the CO emission is higher and it can reach ~6%.

The quality of quicklime depends on the process temperature. The energy demand to produce medium burned quicklime is 4.2 – 4.3 [GJ / t$_{CaO}$] while to produce hard burned quicklime 4.5 – 4.6 [GJ / t$_{CaO}$] is required. In mixed-feed kilns the mixture

of coke and anthracite is usually used as a fuel in order to obtain the hard burned lime. If the furnace would be fired with pure anthracite only the medium burned lime could be produced. Increase of coke to lime ratio would result in higher CO concentration in a flue gas.
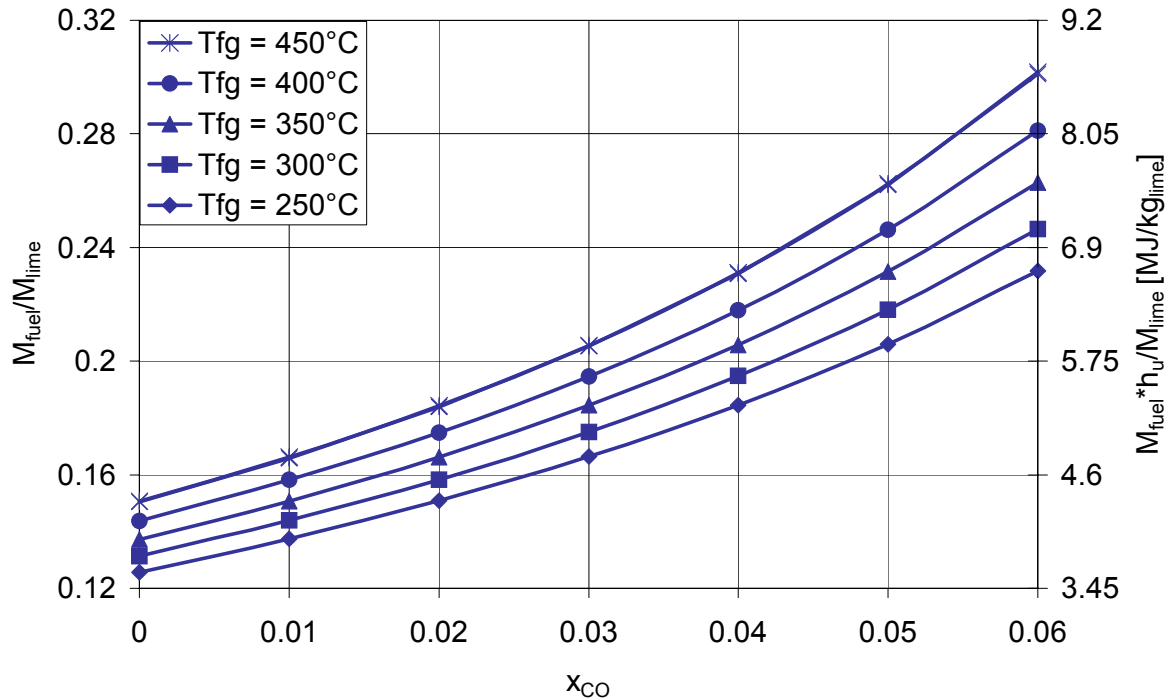
Figure 2-10: Energy usage as a function of the flue gas temperature and CO content in the flue gas. Plots involve coke as a fuel.

2.6 Flue gas temperature

The theoretically minimum energy consumption is the calcination enthalpy, which is 3.18 MJ/kg$_{lime}$ for the pure limestone and 3.03 MJ/kg$_{lime}$ for the limestone consisting of 42% of CO_2 as it was depicted in Figure 2-6. The difference to this minimum value is mainly the enthalpy of the flue gas. The enthalpy flow of the lime discharge is lower than 10% of that of the flue gas. The high value of the flue gas enthalpy is caused by the condition that its temperature at the transition from the reaction to the preheating zone must be higher than the decomposition temperature, as it was already mentioned.

In order to discuss the energy recovery from the flue gas, its temperature and amount will be considered at first. The flue gas temperature T_{fg} can be calculated from the energy balance of the preheating zone:

$$\dot{M}_{LS} \cdot c_{ps} \cdot \left(T_{eq} - T_e\right) = \dot{M}_g \cdot c_{pg} \cdot \left(T_g - T_{fg}\right) \qquad (2\text{-}21)$$

Figure 2-11 shows the flue gas temperature for the fuels used. It increases strongly with the air excess number. For weak gas the highest temperatures are obtained as it was expected, because of the highest energy consumption. The values are in the range of 350 - 550°C. Natural gas H has the lowest temperatures, which are in a range of 50 – 300°C. The flue gas temperature of the other fuels is in a range of 150 – 400°C. Therefore, only the values for lignite are depicted in the figure. It should be emphasised that these values are the temperatures directly above the bed. The values of the temperature measured in the flue gas channel are lower because of the mixing with the false air from the charge.
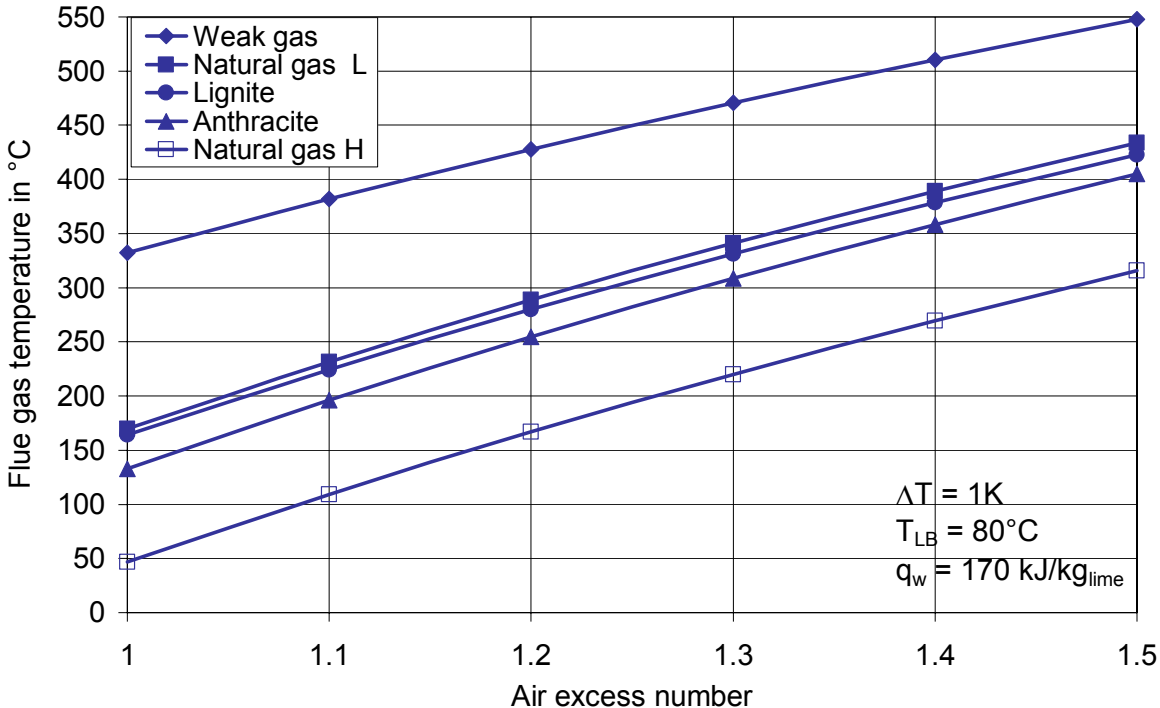
Figure 2-11: Flue gas temperature for different fuels in dependence on the air access number.

Figure 2-12 shows gas to solid mass flow ratios in the preheating zone. This ratio strongly depends on the kind of fuel and the air excess number. It has the highest values for the weak gas and the lowest for the natural gas H. These fuels have the highest and the lowest energy consumption respectively.
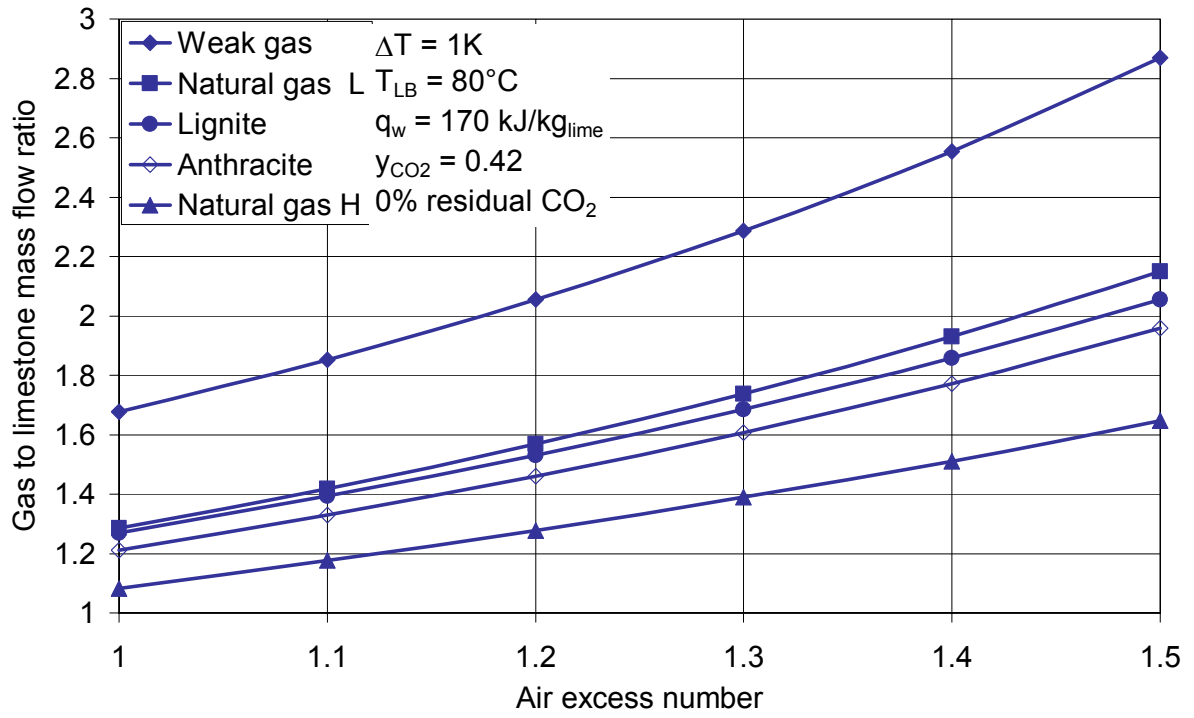
Figure 2-12: Gas to limestone mass flow ratio in the preheating zone.

3. Kinetics

3.1 Packed bed

Shaft kilns are basically packed bed reactors with the upward-flow of hot gases passing counter-current to the downward-flow of feed consisting of solid particles. The void fraction Ψ of a packed bed is defined as:

$$\Psi = \frac{\text{Bed volume} - \text{Packing volume}}{\text{Bed volume}}$$

(3-1)

Values of Ψ between 0.3 and 0.5 are typical.

Void fraction of a packed bed can be influenced by

- method of packing (random or regular, loose or dense)
- particle shape (sphere, cylinder …)
- particle size
- particle size distribution

For infinitely extended, regular packing of equally sized, large spheres the void fraction is:

0.476 for simple cubic packing

0.395 for cubic space centred packing

0.259 for cubic face centred packing

For random packing of equally sized, large spheres the void fraction is:

0.4 - 0.42   for loose packing

0.36 - 0.38   for dense packing

Figure 3-1 shows the influence of particle size distribution for bidispersed, random packing of spheres.
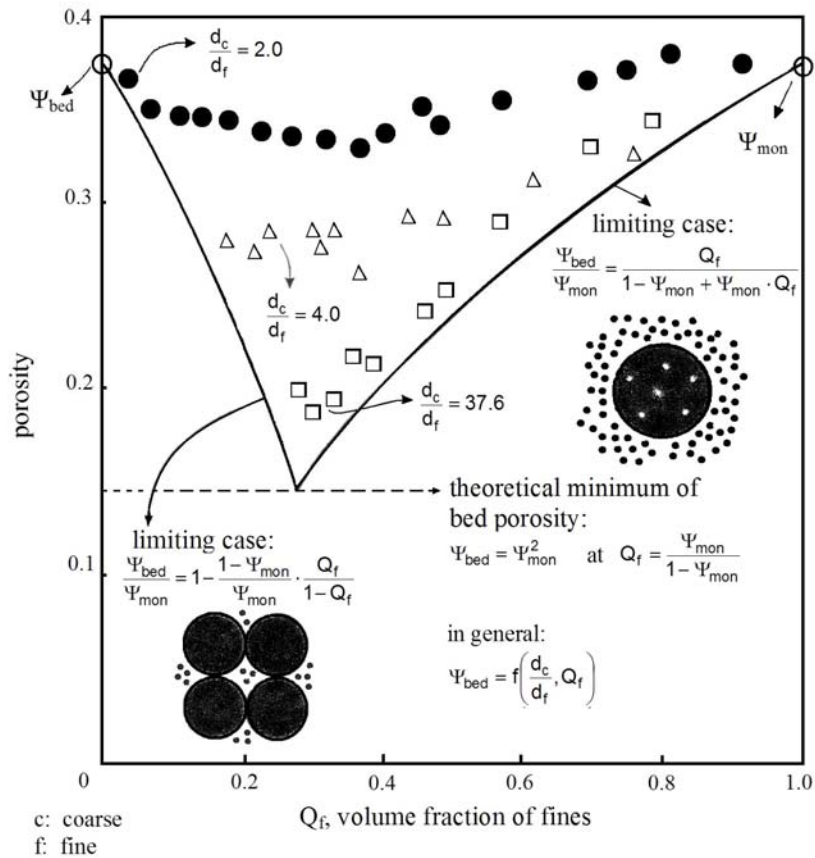
Figure 3-1: Bed porosity of bi-dispersed packing of spheres [12].

Radial porosity profiles in packed tube for imperfect spheres are shown in Figure 3-2.
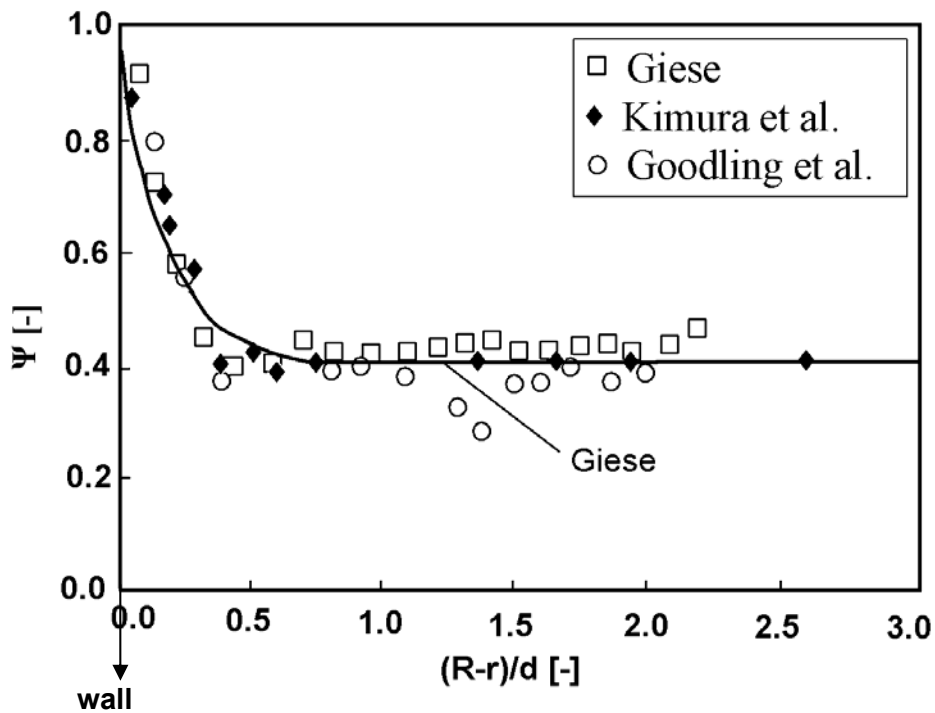
Figure 3-2: Radial porosity profiles in packed tube [12]. R – tube radius; r – radial coordinate; d – particle diameter.

The surface area for the heat transfer depends on the particle size, shape and the void fraction. The specific surface area O [m^2/m^3] of a packed bed is the wetted or transfer area per unit volume of bed:

$$O = \frac{\text{Total surface area of particles}}{\text{Bed volume}}$$

(3-2)

If a bed consists of particles of volume V_p and surface area A_p, then

$$O = \frac{A_p}{V_p} \cdot (1 - \Psi)$$

(3-3)

In general, the specific surface area can be calculated if the geometry of the particles and the void fraction in the bed are known.

3.2 Pressure drop in a packed bed

Flow through a packed bed can be regarded as fluid flow past some number of submerged objects.

The hydraulic diameter is defined [13]:

$$D_h = \frac{\text{Volume of bed available for flow}}{\text{Wetted surface in bed}} = \frac{\text{Void volume / unit volume}}{\text{Wetted surface / unit volume}} = \frac{\Psi}{O}$$

(3-4)

Using the above mentioned equations,

$$D_h = \left(\frac{\Psi}{1 - \Psi} \right) \cdot \frac{V_p}{A_p}$$

(3-5)

Pressure drop can be described with two different models:

- Model based on hydraulic diameter
- Model based on one particle cross-flow

3.2.1 Pressure drop equations based on a hydraulic diameter model

The Ergun equation [23] is based on the model conception that the real packed bed can be replaced by a parallel connection of flow channels, and the pressure drop calculation is similar to the one phase pipe flow, however with the hydraulic diameter of the packed bed as characteristic dimension.

The pressure drop across the packed bed can be obtained from Ergun equation [13], [23]:

$$\frac{\Delta p}{\Delta L} = 150 \cdot \frac{(1-\Psi)^2}{\Psi^3} \cdot \frac{\eta \cdot w}{\overline{d}_p^2} + 1.75 \cdot \frac{1-\Psi}{\Psi^3} \cdot \frac{\rho_f \cdot w^2}{\overline{d}_p} \tag{3-6}$$

where w stands for the velocity in the bed if no packing were present. This equation tells us the pressure drop along the length of the packed bed for a given fluid velocity. It also tells us that the pressure drop depends on the packing size, length of bed, fluid viscosity and fluid density. The first term of this equation describes the change in pressure under viscous flow while the second one accounts for change in pressure at turbulent flow (kinematic energy loss). The constants are based on experimental data for many shapes of particles, but the equation is most accurate for spherical particles. The Ergun equation was designed for fluid flow up to the fluidization point.

Bulk material is described by the characteristic diameter, Sauter-diameter $\overline{d}_p$:

$$\overline{d}_p = \left[\sum_{i=1}^{n} \left(\frac{V_i}{V} \cdot \frac{1}{d_{pi}} \right) \right]^{-1} \tag{3-7}$$

For the pressure drop in packed bed, consisting of spherical particles, exists the equation obtained by Brauer [24], which is similar to Ergun equation:

$$\frac{\Delta p}{\Delta L} = 160 \cdot \frac{(1-\Psi)^2}{\Psi^3} \cdot \frac{\eta \cdot w}{\overline{d}_p^2} + 3.1 \cdot \frac{1-\Psi}{\Psi^3} \cdot \frac{\rho_f \cdot w^2}{\overline{d}_p} \cdot \left[\frac{\eta \cdot (1-\Psi)}{\rho_f \cdot w \cdot \overline{d}_p} \right]^{0.1} \tag{3-8}$$

Brauer's correlation is based on experimental data and applies to a packed bed, consisting of spherical particles of the same diameter. Therefore in this case the Sauter-diameter is equal to the sphere diameter. For the calculation of a pressure drop for a bed consisting of spherical particles of different size, appropriate correction functions have to be considered [24].

3.2.2 Single particle cross-flow model

This model, created by Molerus [13], [25], is based on a flow over a single particle. When the particles are overflowed by a fluid a resistance force W is exerted on each particle. Depending on a number of particles n in a packed bed a resistance z·W is exerted on a bed, which is balanced by the pressure:

$$n \cdot W = \Delta p \cdot A \qquad (3\text{-}9)$$

The number of particles in a bed can be obtained from the mass balance. It is equal to the ratio of the volume of solid to the volume of a single particle with Sauter-diameter $\overline{d}_p$:

$$n = \frac{(1 - \Psi) \cdot A \cdot \Delta L}{\overline{d}_p^3 \cdot \frac{\pi}{6}} \qquad (3\text{-}10)$$

From the above mentioned equations results the pressure drop:

$$\frac{\Delta p}{\Delta L} \cdot \frac{\overline{d}_p^3}{6} \cdot \frac{1}{1 - \Psi} = W \qquad (3\text{-}11)$$

The dimensionless form is:

$$Eu = \frac{4}{3} \cdot \frac{\Delta p}{\rho_f \cdot w^2} \cdot \frac{\overline{d}_p}{\Delta L} \cdot \frac{\Psi^2}{1 - \Psi} \qquad (3\text{-}12)$$

The analysis of a cross-flow of single particle in the packed bed with the help of Navier-Stokes equation and the experimental data results in the equation for the Euler number. For the spherical particles [26], [27]:

$$Eu = \frac{24}{Re} \left\{ 1 + 0.692 \cdot \left[\frac{r_0}{\delta} + 0.5 \left(\frac{r_0}{\delta} \right)^2 \right] \right\} + \frac{4}{\sqrt{Re}} \left[1 + 0.12 \cdot \left(\frac{r_0}{\delta} \right)^{1.5} \right] + \left[0.4 + 0.891 \cdot \frac{r_0}{\delta} Re^{-0.1} \right] \qquad (3\text{-}13)$$

with

$$\frac{r_0}{\delta} = \left[\frac{0.95}{\sqrt[3]{1 - \Psi}} - 1 \right] \qquad (3\text{-}14)$$

and

$$Re = \frac{w\overline{d}_p}{\Psi\nu} \qquad\qquad\qquad (3\text{-}15)$$

Figure 3-3 shows the comparison of the pressure drop calculated with two methods described above. The calculations were done for the void fraction 0.4 and air as a gas. Air material properties were taken for the temperature of 600°C. The pressure drop in a packed bed increases for the higher superficial velocities. It is inversely proportional to the particle diameter. For the typical superficial velocity in a shaft kiln ~1m/s the pressure drop is twice as big for particles of 0.04m diameter as for the particles of 0.08m.
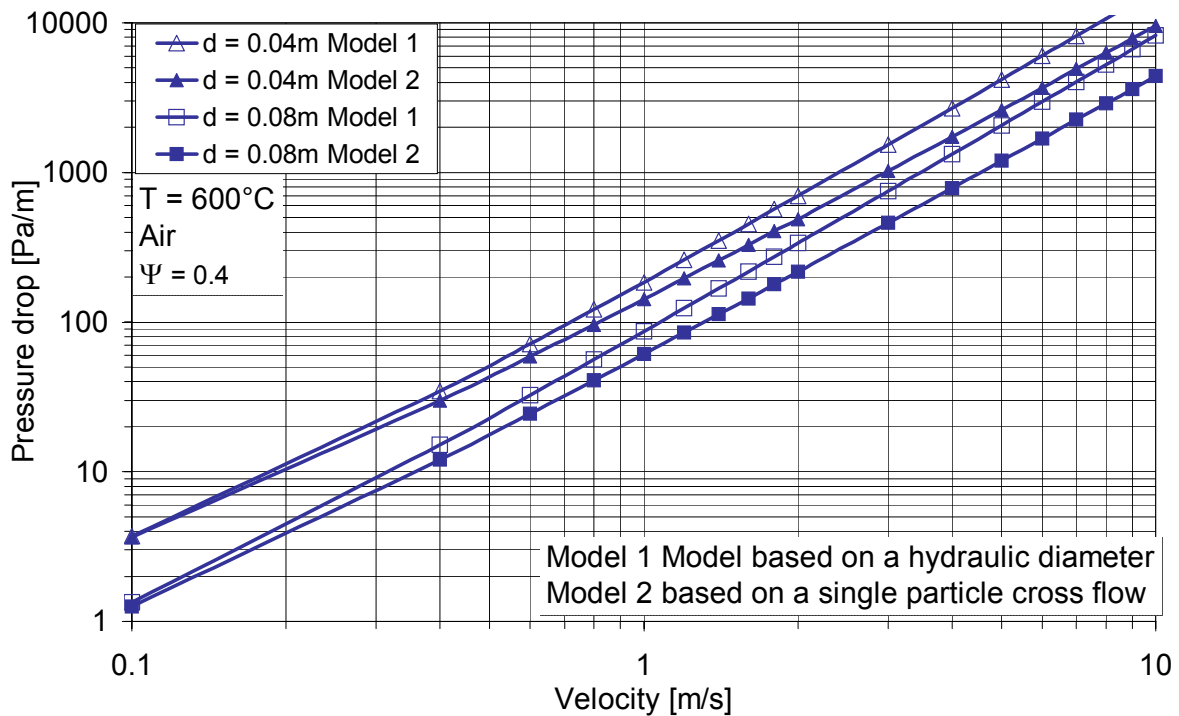
Figure 3-3: Pressure drop versus gas velocity. Comparison of Ergun equation and model based on a single particle cross flow. Plots involve void fraction 0.4

3.3 Convective heat transfer in a packed bed

3.3.1 Gas properties

If the temperature dependence of the material properties cannot be neglected they can be calculated with the following equations [14]:

$$\frac{\lambda}{\lambda_0} = \left(\frac{T}{T_0}\right)^{n_\lambda} ; \qquad \frac{\mu}{\mu_0} = \left(\frac{T}{T_0}\right)^{n_\mu} ; \qquad \frac{a}{a_0} = \left(\frac{T}{T_0}\right)^{n_\mu + 1 - n_c}$$

$$\frac{\rho}{\rho_0} = \left(\frac{T}{T_0}\right)^{-1} ; \qquad \frac{c_p}{c_{p0}} = \left(\frac{T}{T_0}\right)^{n_c} ; \qquad \frac{\nu}{\nu_0} = \left(\frac{T}{T_0}\right)^{n_\mu + 1}$$

where $T_0 = 273$ K.

The Prandtl number is temperature independent. Material properties of gases in temperature $T_0 = 273$ K are gathered in Table 3-1.

Gas	$\tilde{M}$ $\dfrac{kg}{kmol}$	ρ_0 $\dfrac{kg}{m^3}$	c_{p0} $\dfrac{kJ}{kg \cdot K}$	n_c $-$	λ_0 $\dfrac{W}{m \cdot K}$	n_λ $-$	μ_0 $\dfrac{mg}{m \cdot s}$	n_μ $-$	Pr $-$
N_2	28	1.26	1.00	0.11	0.024	0.76	16.8	0.67	0.70
CO	28	1.26	1.00	0.12	0.024	0.78	16.8	0.67	0.70
Air	29	1.29	1.00	0.10	0.025	0.76	17.4	0.67	0.70
O_2	32	1.44	0.90	0.15	0.025	0.80	19.7	0.67	0.70
CO_2	44	1.98	0.84	0.30	0.017	1.04	14.4	0.77	0.73
H_2O	18	0.81	1.75	0.20	0.016	1.42	8.7	1.13	0.95

Table 3-1: Material properties of gases in $T_0 = 273$ K according to[14].

The properties of gas mixtures can be calculated with the following formulas:

$$\rho_M = \sum \rho_i \cdot \tilde{x}_i \qquad (3\text{-}16)$$

$$\lambda_M \approx \sum \lambda_i \cdot \tilde{x}_i \qquad (3\text{-}17)$$

$$c_{pM} = \sum c_{pi} \cdot x_i = \frac{1}{\rho_G} \sum c_{pi} \cdot \tilde{x}_i \cdot \rho_i \qquad (3\text{-}18)$$

3.3.2 Model of heat transfer based on a flow over single particle

The values of the heat transfer coefficient between fluid and particles in a packed bed are significantly higher than the values of the heat transfer coefficient between fluid and a single sphere. The heat transfer coefficient for a packed bed can be obtained with help of a correlation for the Nusselt number ($Nu_{single\ sphere}$) for a flow around a single sphere and a form factor f_a [13], [28], [29].

$$Nu = f_a \cdot Nu_{single\ sphere} \tag{3-19}$$

$$Nu_{single\ sphere} = 2 + \sqrt{Nu_{lam}^2 + Nu_{turb}^2} \tag{3-20}$$

where

$$Nu_{lam} = 0.664 \cdot \sqrt{Re_\Psi} \cdot \sqrt[3]{Pr} \tag{3-21}$$

and

$$Nu_{turb} = \frac{0.037 \cdot Re_\Psi^{0.8} \cdot Pr}{1 + 2.443 \cdot Re_\Psi^{-0.1} \cdot \left(Pr^{2/3} - 1\right)} \tag{3-22}$$

$$Nu = \frac{\alpha \cdot d_s}{\lambda} \tag{3-23}$$

$$Re_\Psi = \frac{w_{free} \cdot d_s}{\nu \cdot \Psi} \tag{3-24}$$

$$Pr = \frac{\nu}{a} \tag{3-25}$$

$$d_s = \sqrt{\frac{A_p}{\pi}} \tag{3-26}$$

The diameter d_s of a sphere, which has the same geometrical surface as a given particle, is calculated with the formula above using the geometrical surface A_p of single particle. A_p can be determined from the volume-specific surface of the bed and the volume-specific number of particles. For a bed consisting of spheres of an equal size, d_s equals the diameter d of the sphere.

The velocity w_{free} is the velocity in the bed if no packing were present.

The form factor f_a, of a bed consisting of spheres of equal size, can be calculated with sufficient accuracy for the range $0.26 < \Psi < 1$, from the formula:

$$f_a = 1 + 1.5 \cdot (1 - \Psi)$$ (3-27)

for cylinders with a length l to diameter d ratio within the range $0.24 < l/d < 1.2$

$f_a = 1.6$; for cube $f_a = 1.6$; for Raschig rings $f_a = 2.1$

From the calculations based on before mentioned equations convective heat transfer coefficient (Figure 3-4) is found to be greatly influenced by the size of the particles in the range of gas velocity higher than 1 m/s. Increasing the void fraction from 0.4 to 0.6 significantly decreases the convective heat transfer coefficient in the range of gas velocity higher than 1 m/s. For superficial gas velocity < 1 m/s influence of the void fraction and the particles diameter is also important but not as critical. Calculations were done for the air at the temperature of 600°C.
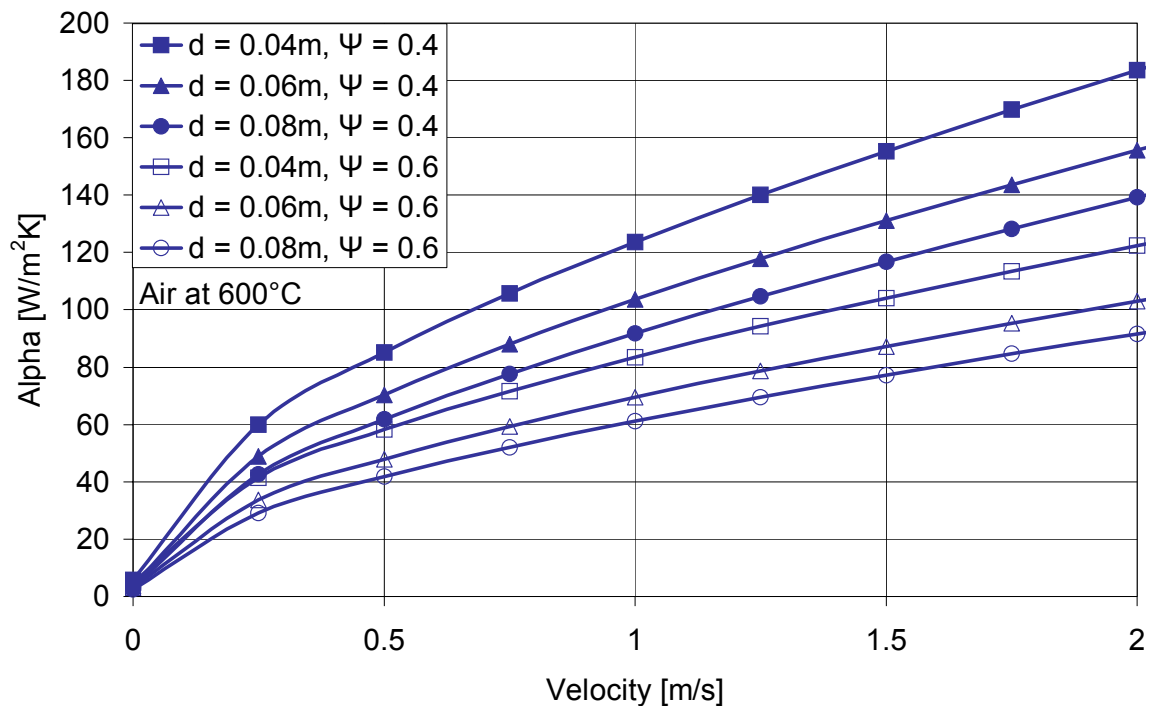
Figure 3-4: Heat transfer coefficient as a function of particle diameter d, void fraction Ψ, and superficial gas velocity at STP.

In the lime shaft kiln heat is mostly transferred by convection. This heat transport is influenced by the particle diameter, which does not change during the process and the gas temperature, which changes along the furnace. Figure 3-5 shows the dependence of the convective heat transfer coefficient on the temperature for the smallest (d = 0.04m) and the biggest particles (d = 0.08m). Calculations were done for spheres, void fraction 0.4 and air. The lower temperatures apply to the

46

cooling and the preheating zone while in the reaction zone the temperature varies between 1000°C and 1500°C. The parameter that mostly depends on the temperature is the superficial gas velocity, which is directly proportional to the temperature.
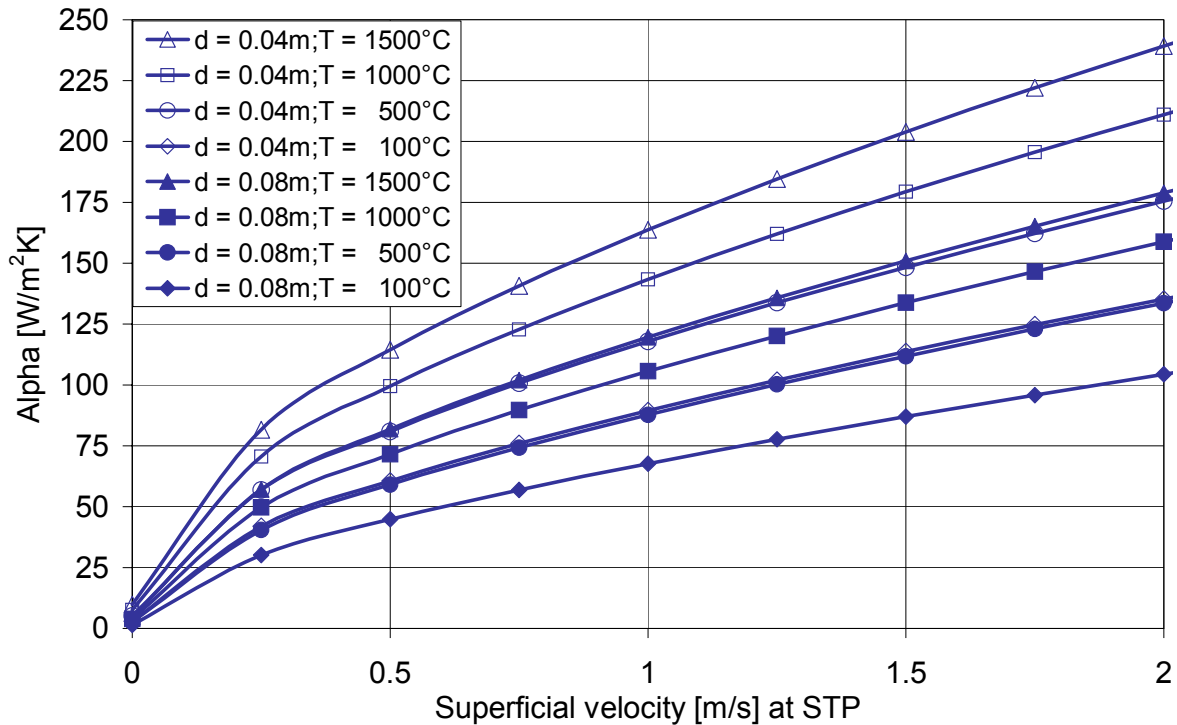
Figure 3-5: Heat transfer coefficient as a function of temperature and superficial gas velocity at STP.

3.3.3 Model of convective heat transfer based on a hydraulic diameter

If the filling in a packed bed could be described as a bundle of parallel pipes the hydraulic diameter d_h of the bed could be described with the following equation [15]:

$$d_h = \frac{2}{3} \cdot \frac{\Psi}{1-\Psi} \cdot d \qquad (3\text{-}28)$$

Expressing the Reynolds number with the hydraulic diameter gives the equation [15]:

$$Re = \frac{w \cdot d}{\nu} \cdot \frac{1}{1-\Psi} \qquad (3\text{-}29)$$

The Nusselt number is calculated similarly [15]:

$$Nu = \frac{\alpha \cdot d}{\lambda} \cdot \frac{\Psi}{1-\Psi} \qquad (3\text{-}30)$$

47

$$\mathrm{Nu} = 2 \cdot \frac{\Psi}{1-\Psi} + 1.12 \cdot \sqrt{\mathrm{Re}} \cdot \mathrm{Pr}^{0.33} + 0.0056 \cdot \mathrm{Re} \cdot \mathrm{Pr}^{0.33} \qquad (3\text{-}31)$$

and valid in a range 100 < Re < 40000 and 0.6 < Pr < 1000

Figure 3-6 shows the convective heat transfer coefficient calculated with both above mentioned models. For the model based on the cross-flow over single particle calculations were done for laminar flow and laminar and turbulent flow. In the shaft kiln there is a laminar flow or there is a transition between laminar and turbulent flow, therefore both cases were considered. For the typical superficial velocity of ~1m/s at STP the difference between the values of convective heat transfer coefficient calculated with the model based on a hydraulic diameter and the model based on the cross-flow over single particle is ~20%.
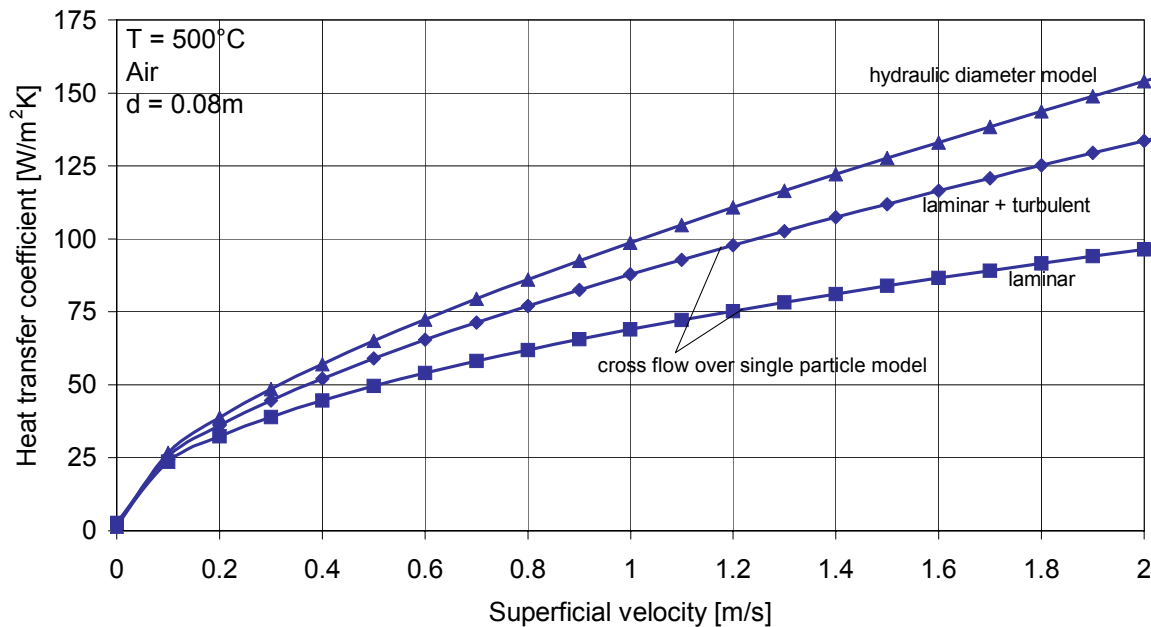
Figure 3-6: Heat transfer coefficient as a function of superficial velocity at STP - Comparison of cross-flow over single particle and hydraulic diameter model.

3.3.4 Transient heat transfer coefficient

In technical processes the solid particles are usually warmed up or cooled down through the heat exchange with gas passing counter-current. Often only the mean temperature of the particle can be considered and not the temperature field within the particle because additionally to the calculation of the axial temperature profile, the Fourier differential equation should be solved and this requires a lot of effort. For those purposes the modified heat transfer coefficient α_k is introduced [16]:

$$dQ = \alpha_k \cdot \left(T_{gas} - \overline{T}\right) \cdot A \cdot dt \qquad (3\text{-}32)$$

where

$$\alpha_k = \frac{1}{\dfrac{1}{\alpha} + \dfrac{s/2}{\kappa \cdot \lambda}} \qquad (3\text{-}33)$$

If the ambient temperature changes in a linear way [16]:

$$T_{gas} = T_{gas\,t=0} + B \cdot Fo \qquad (3\text{-}34)$$

the transient factor is described by the following formula:

$$\kappa = b + 2 \qquad (3\text{-}35)$$

which gives:

$$\kappa = \begin{cases} 3 & \text{plate} \\ 4 & \text{cylinder} \\ 5 & \text{sphere} \end{cases}$$

At constant ambient temperature the transient factor is calculated with the following equation:

$$\kappa = \left(\kappa_{Bi=0} - \kappa_{Bi=\infty}\right) \cdot \left[\frac{1}{2} - \frac{1}{\pi} \cdot \arctan\left(\ln\frac{2 \cdot Bi}{b + 4}\right)\right] \qquad (3\text{-}36)$$

where Bi is the Biot number and b the form factor.

$$Bi = \frac{\alpha \cdot s/2}{\lambda} \qquad (3\text{-}37)$$

$\kappa_{Bi=\infty}$		$\kappa_{Bi=0}$	
$\dfrac{\pi^2}{4} \approx 2.476 \quad \le \quad \kappa = \overline{\kappa} \quad \le \quad 3$			Plate
$2.892 \quad \le \quad \kappa = \overline{\kappa} \quad \le \quad 4$			Cylinder
$\dfrac{\pi^2}{3} \approx 3.290 \quad \le \quad \kappa = \overline{\kappa} \quad \le \quad 5$			Sphere

The influence of the transient heat conduction within the particle will be illustrated in the two following graphs. Figure 3-7 shows the values of the transient heat transfer coefficient into the particle. The mean conductivity of lime is assumed to be 0.6 W/m/K. For small particle diameters, the heat conduction within the particle is much higher than the convective heat transfer coefficient. It decreases dramatically with the increasing particle diameter. For big particles the values are similar to the convective heat transfer coefficient and they decrease slightly with the increasing particle diameter.

In principle, the preheating zone can be described with the same set of equations. Therefore, Figure 3-7 includes the values of the transient heat transfer coefficient for limestone which mean conductivity is assumed to be 1.5 W/m/K. The trend is the same as for the values calculated for the cooling zone, however the values are much higher.
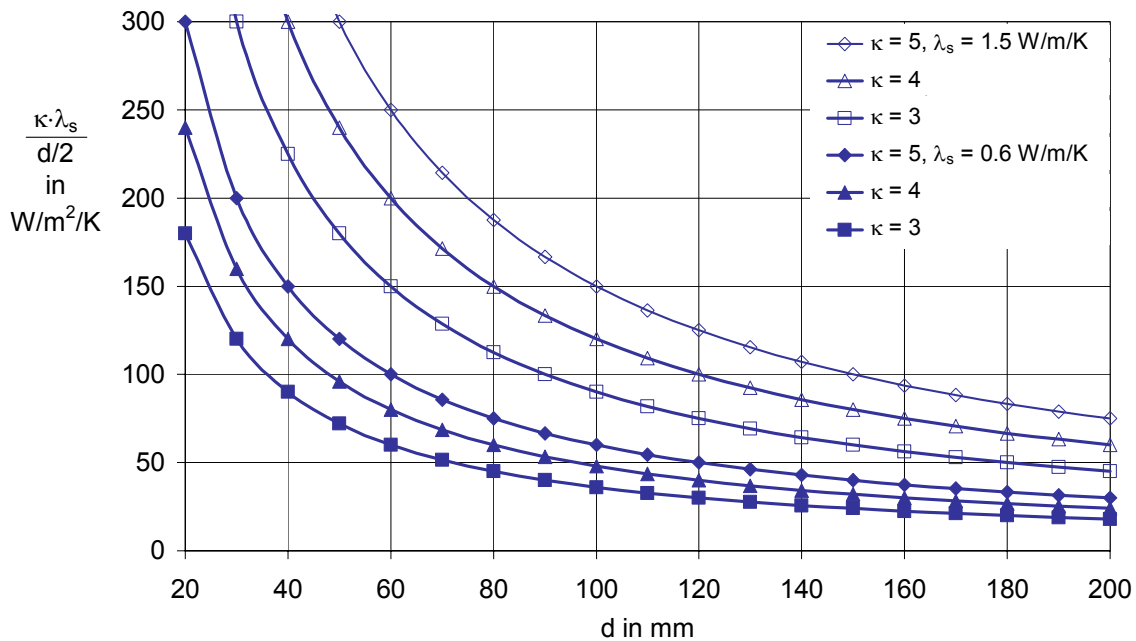
Figure 3-7: Values of heat transfer coefficient term of heat conduction into the particle.

As it is not possible to describe real lime particles as spheres, plates or cylinders a mean value of $\kappa = 4$ was taken for the following calculations of the cooling zone length. The influence of the heat conduction within particle is explained in Figure 3-8, where the ratio of the overall heat transfer coefficient u to the convective heat transfer coefficient is shown. The mean gas temperature in the cooling zone was taken as parameter. For fine particles the overall heat transfer coefficient is only 10 – 20 % smaller than the convective heat transfer coefficient, while for the big particles the overall heat transfer coefficient is reduced by 30 – 40 %.
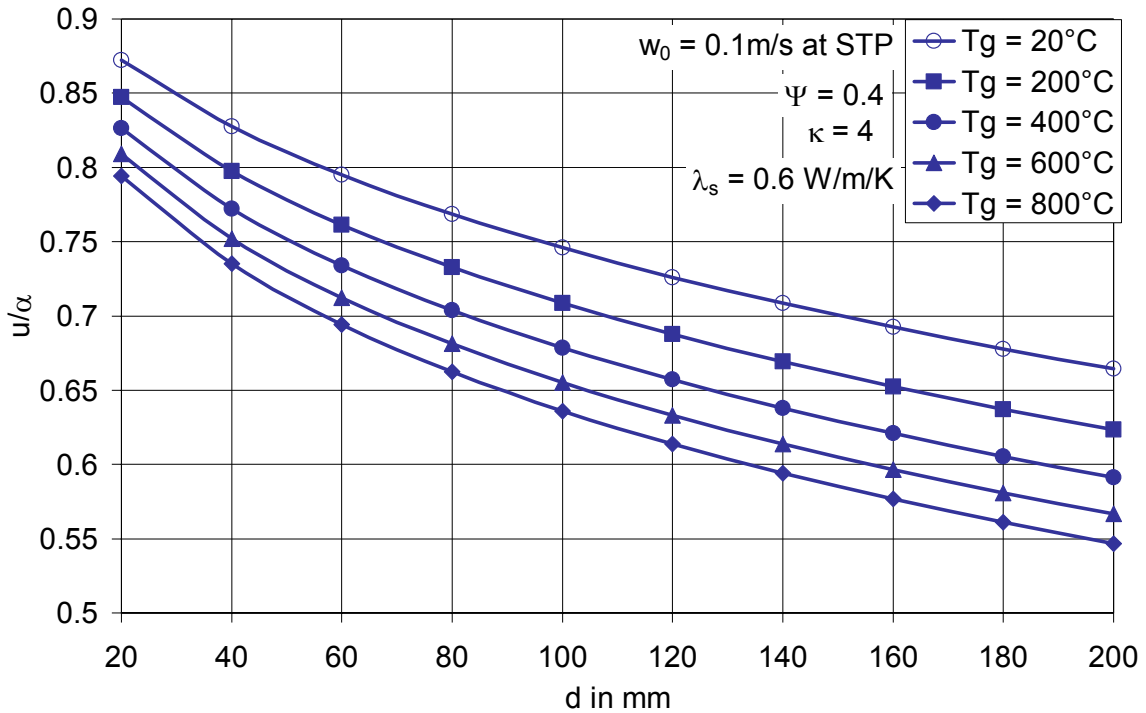
Figure 3-8: Influence of the heat conduction within particle on the overall heat transfer.

3.4 Dust radiation

Limestone dust in relatively significant concentrations is present in the lime shaft kiln. In mixed-feed kiln there is a mixture of limestone and coal dust. Dust is able to increase the radiation from hot gases significantly. The dust concentration is a substantial parameter for the total emitted radiation. In the following two computation models are described for the determination of the emissivity of dust.

3.4.1 Simplified model for small dust concentrations

For applications, in which the amount of the exponent in the following equations does not exceed a value of 0.5, the emissivity ε_{st} of the dust according to Biermann and Vortmeyer [13], [30] at negligible backscattering can be calculated with the equations:

$$\varepsilon_{st} = 1 - \exp\left(-\overline{Q}_{abs} \cdot A \cdot B_{st} \cdot s_{gl}\right)$$

(3-38)

or

$$\varepsilon_{st} = 1 - \exp\left(-k \cdot \frac{3}{2 \cdot \rho_{st}} \cdot d_p^{-2/3} \cdot B_{st} \cdot s_{gl}\right)$$

(3-39)

where

$$d_p = \frac{3}{2 \cdot \rho_{st} \cdot A}$$

(3-40)

and

$$k = \overline{Q}_{abs} \cdot d_p^{-1/3}$$

(3-41)

The meaning of the symbols is as follows:

$\overline{Q}_{abs}$ -   relative active cross-section for absorption of the dust

B_{st} kg/m^3 dust concentration

A m^2/kg specific surface of the dust

s_{gl} m   equivalent layer thickness

d_p m   mean particle diameter

k m$^{-1/3}$ material constant dependent on $\overline{Q}_{abs}$

ρ_{st} kg/m^3 dust density

These values, for limestone and coal dust, were experimentally determined by Biermann [13]:

	Coal	Limestone
ρ_{st} [kg/m^3]	2200	2700
A [m^2/kg]	56.0	38.7
d_p [10^{-6} m]	12.2	14.4·
$\overline{Q}_{abs} \cdot A$ [m^2/kg]	14.4	5.84
$\overline{Q}_{abs}$	0.257	0.150
k [m$^{-1/3}$]	11.2	6.17

Table 3-2: Data for limestone and coal dust.

Figure 3-9 and Figure 3-10 show the emissivities of coal and limestone dust respectively. Calculated values are very small and therefore the heat transfer by dust radiation in lime shaft kiln can be neglected.
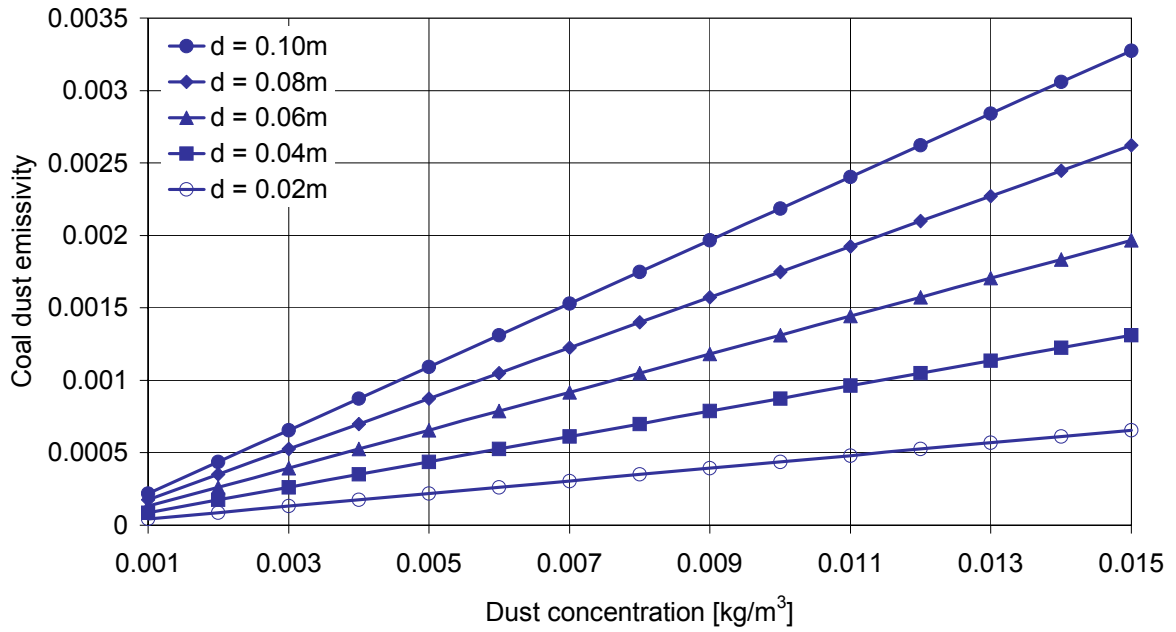
Figure 3-9: Coal dust emissivity as a function of its concentration and limestone particle diameter d.
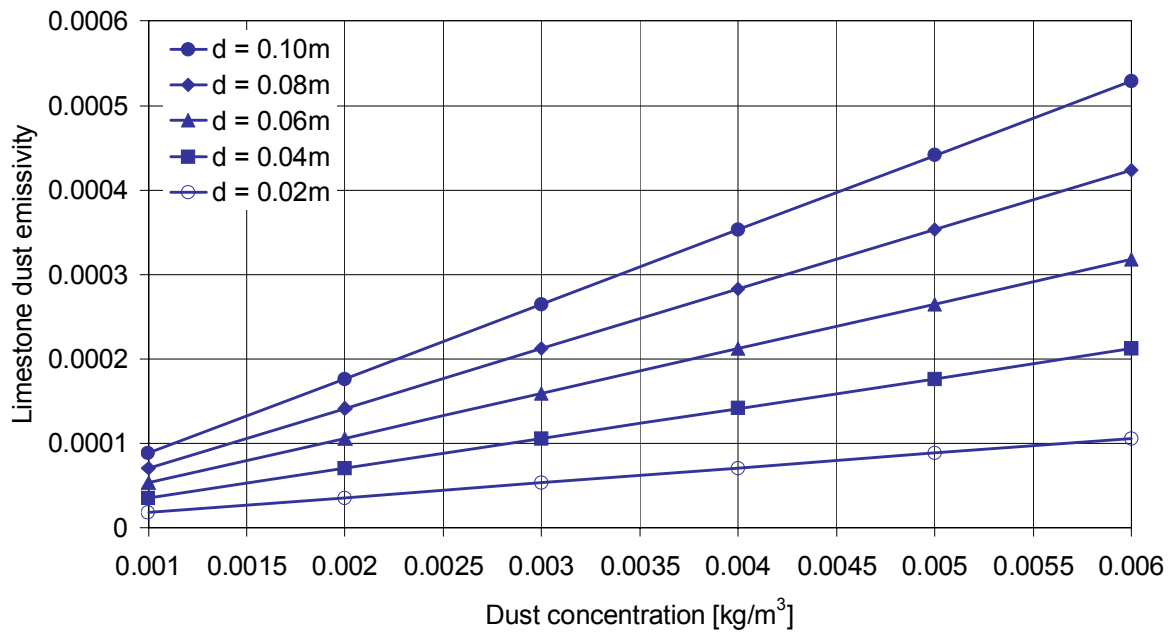
Figure 3-10: Limestone dust emissivity as a function of its concentration and limestone particle diameter d.

3.4.2 Dust radiation model for higher dust concentrations

This model includes the backscattering. The following equation allows the calculation of dust emissivity [13], [30]:

$$\varepsilon_{st} = (1-\beta)\frac{1-\exp(-\Phi)}{1+\beta\exp(-\Phi)} \qquad (3\text{-}42)$$

where:

$$\beta = \frac{\alpha-1}{\alpha+1} \qquad (3\text{-}43)$$

and

$$\alpha = \left(1+\frac{2\overline{Q}_{rstr}}{\overline{Q}_{abs}}\right)^{1/2} \qquad (3\text{-}44)$$

$$\Phi = \overline{Q}_{abs}AB_{st}s_{gl}\alpha \qquad (3\text{-}45)$$

$$A = \frac{3}{2\rho_{st}d_p} \qquad (3\text{-}46)$$

3.5 Model of gas radiation

In technical applications, the gas radiation in the infrared is of interest. In this region, the main emitters are CO_2 and H_2O, although other gases like CO, SO_2, NH_3, CH_4 and further hydrocarbons also emit here. In contrast, N_2 and O_2, the main constituents of air allow radiation in the infrared region to pass through with virtually no attenuation; they do not absorb, and therefore according to Kirchhoff's law do not emit either. Methods for calculation of gas radiation were worked out by Nusselt [32], Schack [33], Hottel [31],[34], Elsasser [35], Mayer [36], Goody [37] and Plass [38]. The emission of gas radiation depends on the size and shape of the gas space.
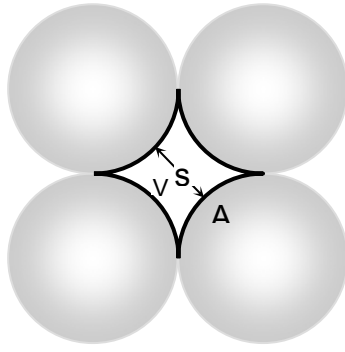
For the simple cubic packing the mean beam length of the gas space s can be determined with sufficient accuracy from the formula:

$$s = 0.9 \cdot \frac{4 \cdot V_{gas}}{A_{particle}} = \frac{(1 - \pi/6) \cdot d_p}{\pi} \approx 0.152 \cdot d_p \qquad (3\text{-}47)$$

where V stands for the volume of the gas space, A for the surface of the gas volume. Emissivity of CO_2 can be obtained with the following equation:

$$\varepsilon = A \cdot e^{-B \cdot T} \qquad\qquad T > 1300K \qquad (3\text{-}48)$$

$$A = 2.0 \cdot \left(\frac{p \cdot s}{10^5 Pa \cdot m}\right)^{0.54} \qquad 0.001 \leq \frac{p \cdot s}{10^5 Pa \cdot m} < 0.01 \qquad (3\text{-}49)$$

$$A = 0.51 \cdot \left(\frac{p \cdot s}{10^5 Pa \cdot m}\right)^{0.26} \qquad 0.01 \leq \frac{p \cdot s}{10^5 Pa \cdot m} \leq 1.5 \qquad (3\text{-}50)$$

$$B = 6.7 \cdot 10^{-4} \cdot \left(\frac{p \cdot s}{10^5 Pa \cdot m}\right)^{-0.085} \qquad 0.001 \leq \frac{p \cdot s}{10^5 Pa \cdot m} \leq 1.5 \qquad (3\text{-}51)$$

where p is CO_2 partial pressure.
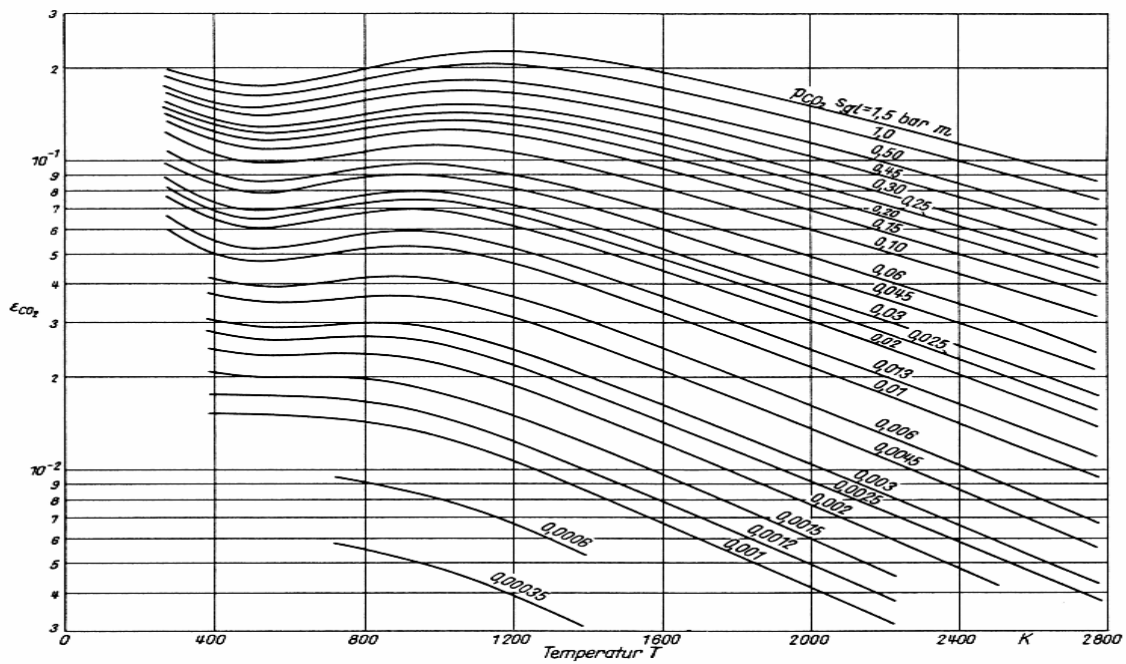
Figure 3-11: Emissivity ε_{CO2} of carbon dioxide at p = 1 bar as a function of the temperature T and the product of the partial pressure p_{CO2} and the mean beam length s_{gl} as a parameter [16]
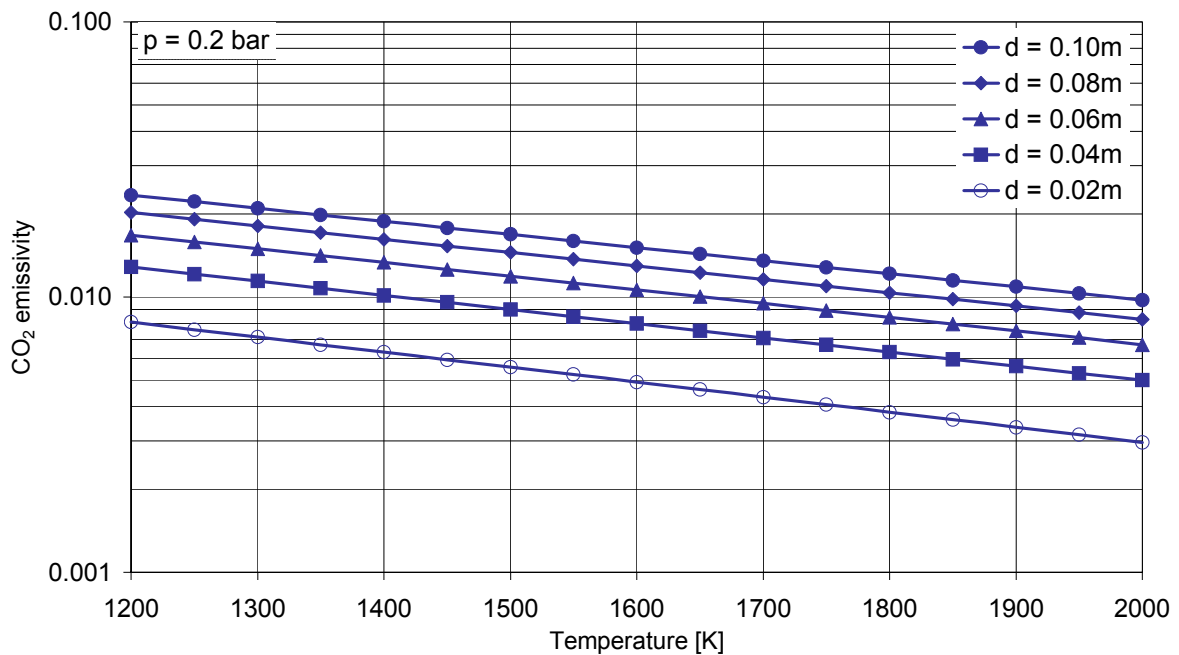
Figure 3-12: Emissivity ε_{CO2} of carbon dioxide at p = 1 bar as a function of the temperature T and the particle diameter. Plots involve CO_2 partial pressure p_{CO2} =0.2 bar.

The heat transfer coefficient for gas radiation can be obtained with the formula:

$$\alpha = 4 \cdot \frac{1}{\dfrac{1}{\varepsilon_{gas}} + \dfrac{1}{\varepsilon_{lime}} - 1} \cdot \sigma \cdot T_g^3 \qquad (3\text{-}52)$$

56

From the calculations based on before mentioned equations (Figure 3-13 and Figure 3-14) gas radiation coefficient is found to be greatly influenced by the size of the particles in the range of temperatures higher than 1000°C. Increasing the particle size from 20 mm to 60 mm significantly increases the gas radiation coefficient in this range of temperatures. The gas transfer coefficient is ~20 W/m^{2}K for the particle diameter 80 mm, gas temperature 1000°C and carbon dioxide partial pressure 0.4 bar, ~15 W/m^{2}K if CO_2 partial pressure equals 0.2 bar while the convective heat transfer coefficient under the same conditions is found to be ~100 W/m^{2}K. The gas radiation coefficient in the chosen small range of temperatures is linear, while for the broader temperature range it doesn't show the linear temperature dependence.
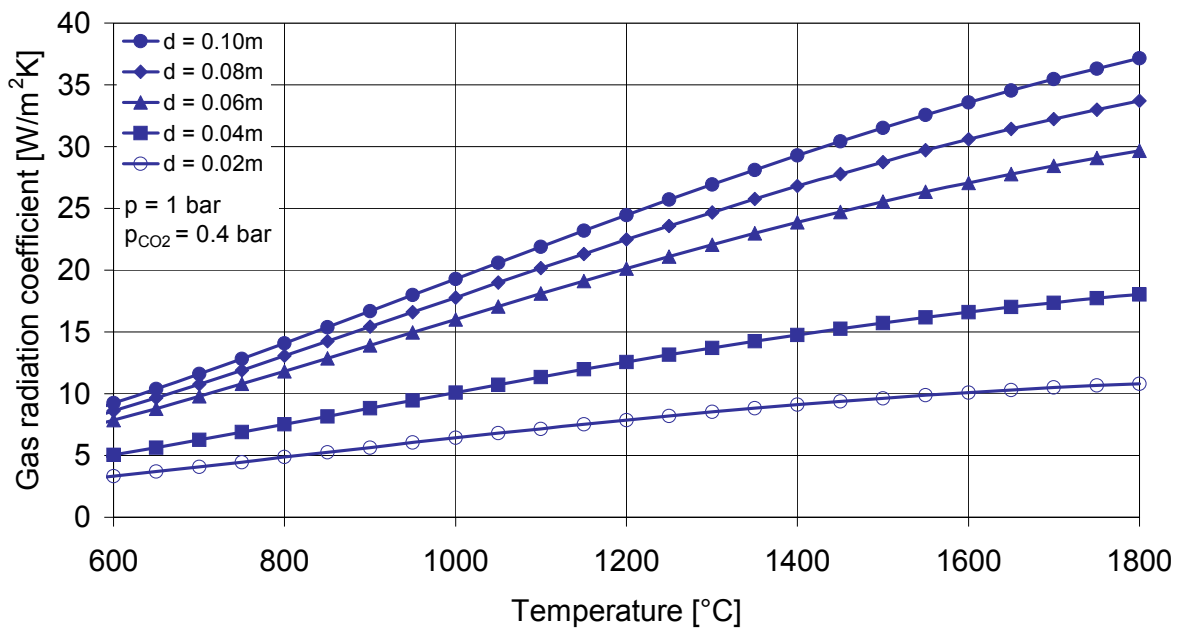
Figure 3-13: Gas radiation coefficient as a function of gas temperature and particle diameter.
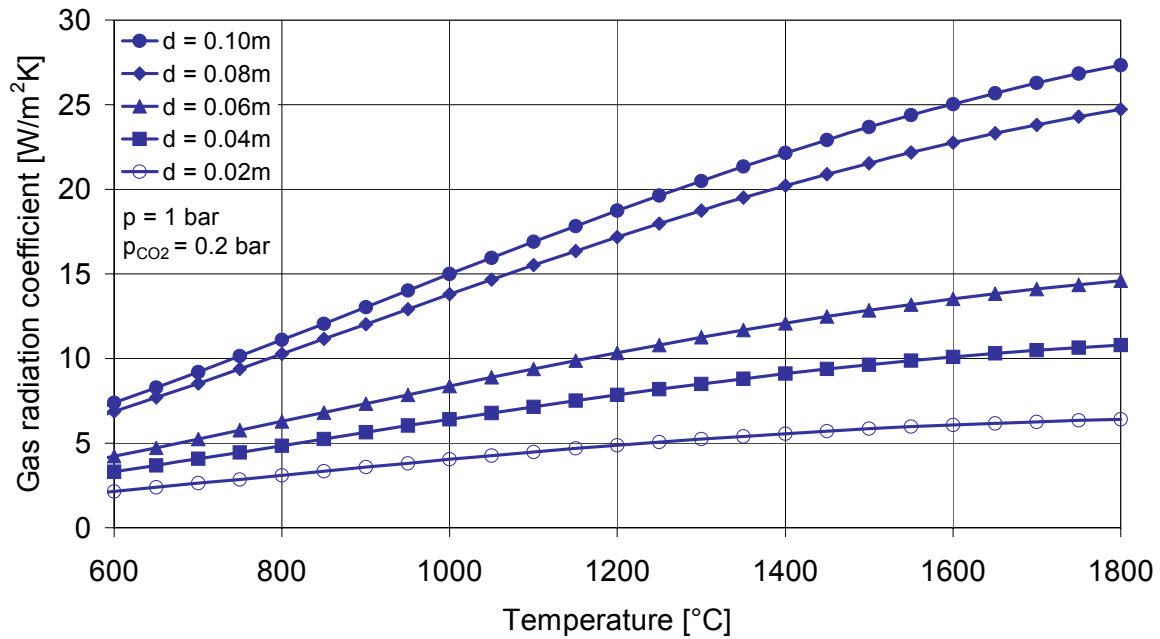
Figure 3-14: Gas radiation coefficient as a function of gas temperature and particle diameter.

Figure 3-15 shows the heat transfer coefficient for radiative and convective heat transfer in a shaft kiln. The calculations show that gas radiation is not that critical component in determining the total heat transfer coefficient for small particles and therefore in most of the cases can be neglected. For particles of diameter > 0.08m the radiative heat transfer coefficient increases to the value of ~20% of the value of convective heat transfer coefficient and has to be taken into account.
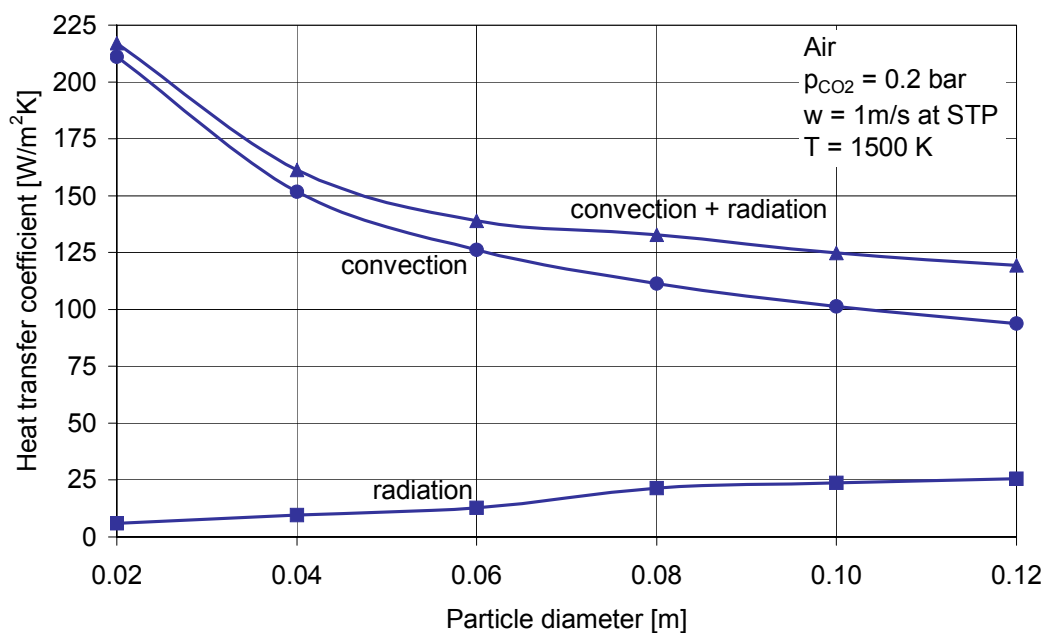
Figure 3-15: Heat transfer coefficients as a function of temperature and particle diameter.

3.6 Model of limestone decomposition

The passage of a limestone particle through a lime shaft kiln can be divided into five stages.

1. In the pre-heating zone the limestone is pre-heated from ambient temperature to about 800°C by the kiln gases (i.e. products of combustion plus CO_2 from calcination and excess air)

2. At about 800°C, the pressure of carbon dioxide produced by the dissociation of the limestone equals the partial pressure of the CO_2 in the kiln gases. As the temperature of the limestone rises, the surface layer begins to decompose, so that when the temperature of the stone reaches 900°C, the layer of lime may be 0.5mm thick (corresponding to about 5% by weight of quicklime for a 25mm particle)

3. Once the temperature of limestone exceeds the „decomposition temperature" of 900°C, the partial pressure exceeds 1 atmosphere and the process of dissociation can proceed beyond the surface of the particles.

4. If all of calcium carbonate dissociates before a given particle leaves the calcining zone, the lime begins to sinter.

5. The particles of lime, which may contain residual limestone, leave the calcining zone at 900°C and are cooled by air used for combustion

The reaction for the thermal decomposition of calcium carbonate may be written as :

$$CaCO_3 + heat \rightleftarrows CaO + CO_2 \uparrow$$
$$100g \qquad\qquad 56g \quad 44g$$
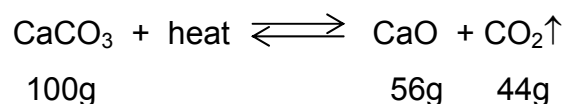
The shrinking core model (Figure 3-16) has been assumed for the decomposition of a limestone sphere undergoing calcination. At any given instant, there is a central core of undecomposed carbonate surrounded by a shell of calcium oxide with the reaction occurring at the interface between the core and the shell.
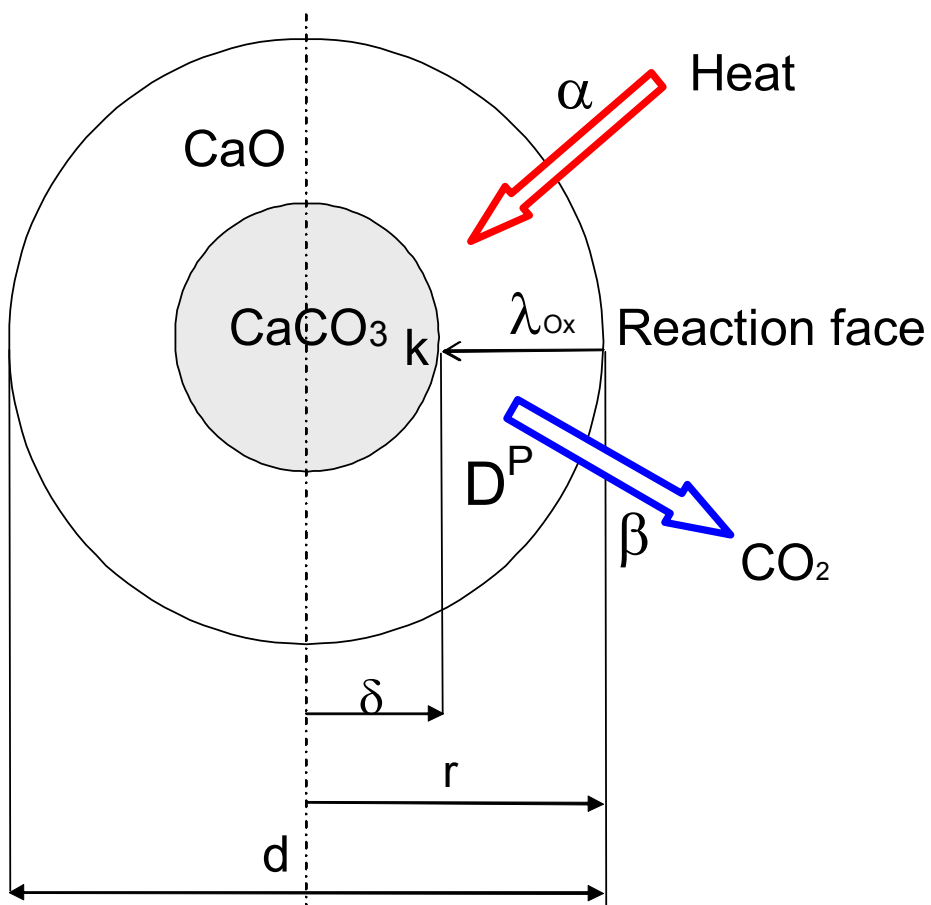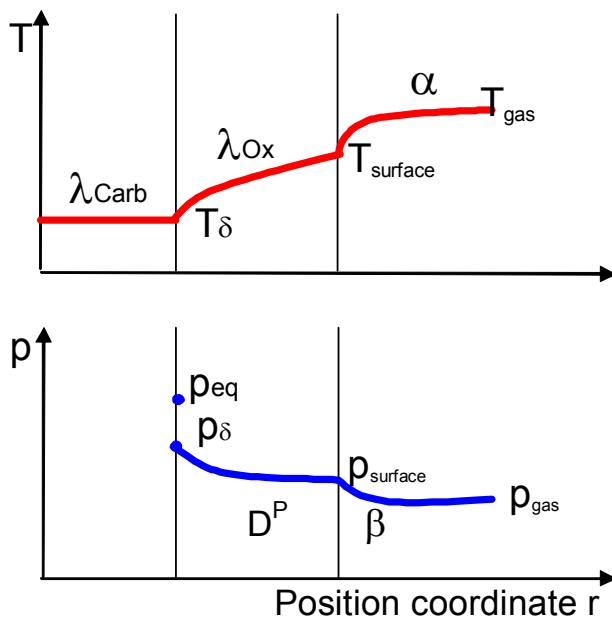
Figure 3-16: Model of the decomposition of limestone

In the calcination reactor with the temperature T_{gas} the heat is transferred by radiation and convection (symbolised by α) to the oxide layer with the surface temperature $T_{surface}$. By conduction (λ_{Ox}) the heat passes through the micro-porous oxide layer to the reaction face where the decomposition temperature T_δ is established. During the decomposition process the reaction enthalpy predominates the internal energy. Therefore, the further heat flow into the undecomposed core is very small, so that the temperature in the core is slightly lower than the temperature at the reaction layer. Sustained by the appropriate supply of heat, the chemical reaction (k) then takes place, for the driving force of which a deviation ($p_{eq} - p_\delta$) from equilibrium of the CO_2 partial pressure is necessary. The released CO_2 diffuses (D^P) through the porous layer to the surface and reaches by convection (β) the ambient atmosphere with the CO_2 partial pressure p_{gas}.

The decomposition behaviour of limestone may be mathematically described if the following assumptions are made:

- The pieces of calcium carbonate are regarded as spheres or cylinders.
- The heat supply is symmetrical, so that all processes can be treated as one-dimensional.
- The chemical and the structural composition of the raw material are homogenous.
- The reaction starts uniformly on the surface, always forming a geometrically smooth decomposition front, which advances continuously into the interior of the body.

The gradient of conversion can be obtained from two equivalent equations[14],[17],

$$\frac{dU}{dt} \cdot \left(R_\beta + R_D \cdot f_1'(U) + R_k \cdot f_2'(U)\right) = \frac{\left|\left(p_{1eq} - p_{1u}\right)\right| \cdot \tilde{M}}{\rho_{1s} \cdot RT} \qquad (3\text{-}53)$$

$$\frac{dU}{dt} \cdot \left(R_\alpha + R_\lambda \cdot f_1'(U)\right) = \frac{1}{\rho_{1s}} \cdot \left(T_u - T_\delta\right) \qquad (3\text{-}54)$$

where T_u is the ambient temperature

R_β is the mass transfer resistance:
$$R_\beta = \frac{s/2}{\beta \cdot b} \qquad (3\text{-}55)$$

R_D is the diffusion resistance:

$$R_D = \frac{(s/2)^2}{D^P \cdot 2 \cdot b}$$

(3-56)

R_k is the reaction resistance:

$$R_k = \frac{s/2}{k}$$

(3-57)

where k is the reaction coefficient.

R_α is the convective heat transfer resistance:

$$R_\alpha = \frac{\Delta \tilde{h}}{\tilde{M}_1} \cdot \frac{s/2}{\alpha \cdot b}$$

(3-58)

R_λ is the heat conduction resistance:

$$R_\lambda = \frac{\Delta \tilde{h}}{\tilde{M}_1} \cdot \frac{(s/2)^2}{\lambda \cdot 2 \cdot b}$$

(3-59)

The following equations are used for the function of the decomposition degree:

$$f_1' = 2 \cdot \ln(1-U)^{-1/3} \qquad \text{for cylinder} \qquad (3\text{-}60)$$

$$f_1' = 2 \cdot \left[(1-U)^{-1/2} - 1\right] \qquad \text{for sphere} \qquad (3\text{-}61)$$

$$f_2' = \frac{1}{b} \cdot (1-U)^{(1/b)-1} \qquad (3\text{-}62)$$

The decomposition process can be conceived either as a heat transport problem or a mass transport problem.

3.7 Material properties

The chemical and physical properties of limestone widely depend on the way it was formed.

	Limestone	Quicklime
Molecular weight [kg/kmol]	100	56
Apparent density [kg/m^3]	2.7	1.5
Thermal conductivity [W/mK]	2.2	0.6
Melting point [°C]	-	2850

Table 3-3: Material properties of limestone and quicklime [9]

The real values of the specific heat capacity of lime and limestone, given by Barin et al. [39], are shown in Figure 3-17. The temperature dependence of the specific heat capacity of air and lime are similar. The specific heat capacity of lime can be approximated with the similar equation as for the gases in the temperature range 100 °C – 1300 °C:

$$c_{pCaO} = 0.84 \cdot \left(\frac{T}{T_0}\right)^{0.13} \tag{3-63}$$

$$c_{pCaCO_3} = 0.97 \cdot \left(\frac{T}{T_0}\right)^{0.25} \tag{3-64}$$

The temperature T has to be taken in K, $T_0 = 373$ K.

The mean value of specific heat capacity can be calculated using the following formula:

$$\bar{c}_p = \frac{1}{T - T_0} \cdot \int_{T_0}^{T} c_p(T) \cdot dT = \frac{c_p(T_0)}{n+1} \cdot \frac{(T/T_0)^{n+1} - 1}{T/T_0 - 1}. \tag{3-65}$$

The mean values of the specific heat capacity of lime, limestone and air are also presented in Figure 3-17.
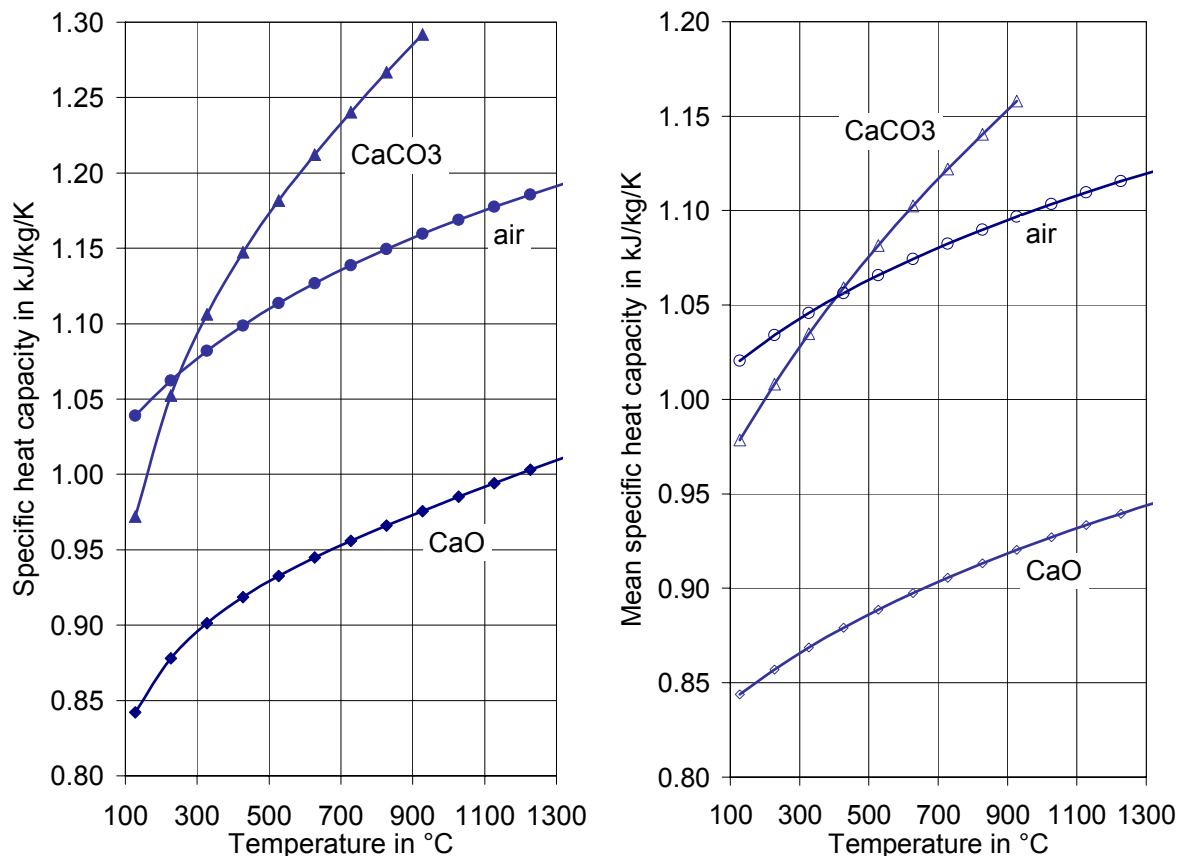
Figure 3-17: Specific heat capacity of air, lime and limestone as a function of temperature.

The decomposition enthalpy was taken 167000 kJ/kmol (relative to 900°C). The carbon dioxide equilibrium partial pressure was calculated with the equation [14]:

$$p_{eq} = 4 \cdot 10^7 \exp\left(-\frac{167}{R \cdot T}\frac{kJ}{mol}\right) bar \qquad (3\text{-}66)$$

Figure 3-18 shows the measured values of equilibrium partial pressure as well as the theoretical values given by Barin et al. [39].
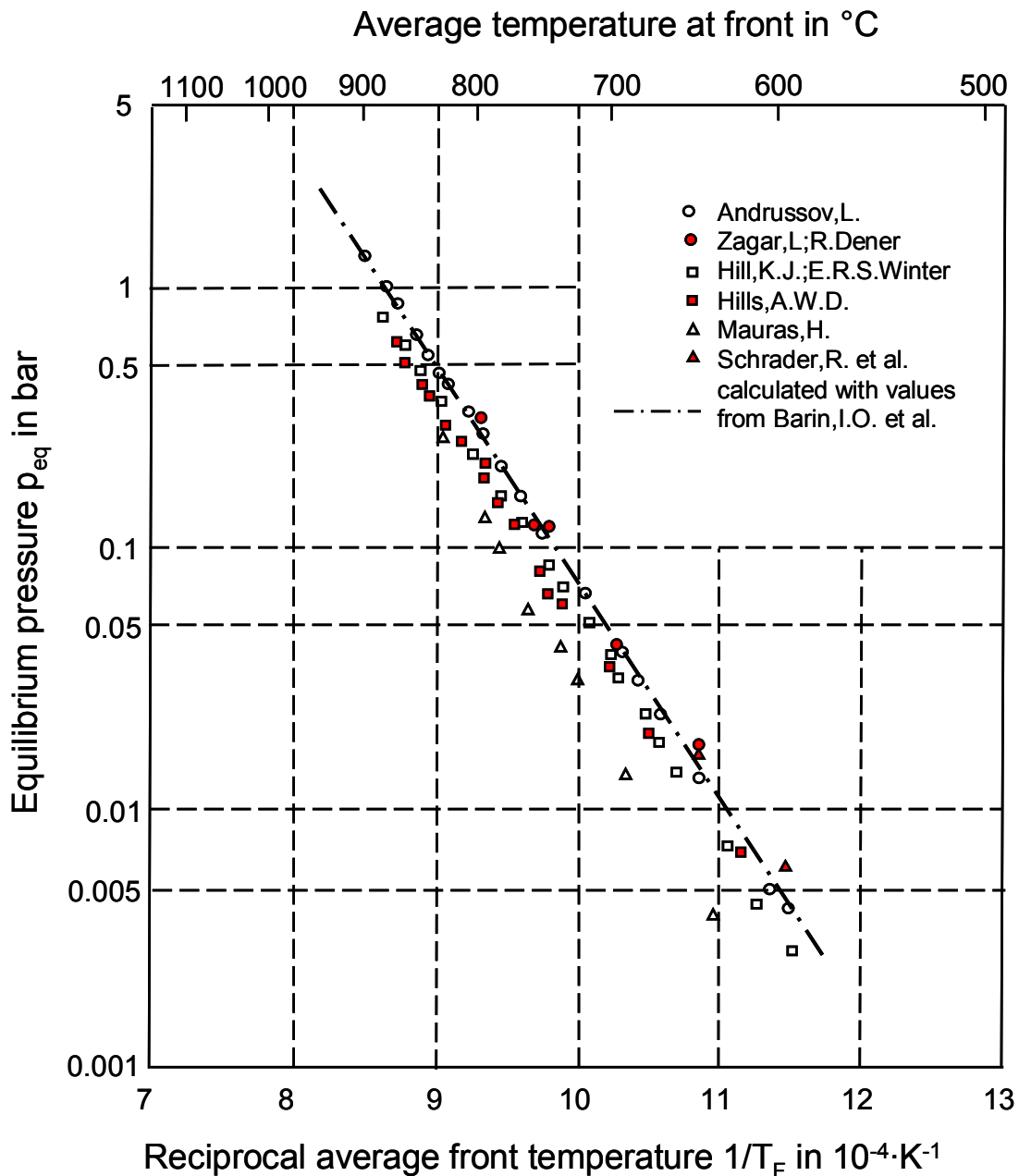
Figure 3-18: Equilibrium partial pressure of limestone decomposition [14].

Reaction coefficients for limestones of various origins are shown in Figure 3-19. For the calculations given in chapter 5 the mean value of 0.007 m/s was taken.

Figure 3-20 shows the values of calcium oxide thermal conductivity as a function of temperature. The calculations were carried out with the mean value of 0.6 W/mK.
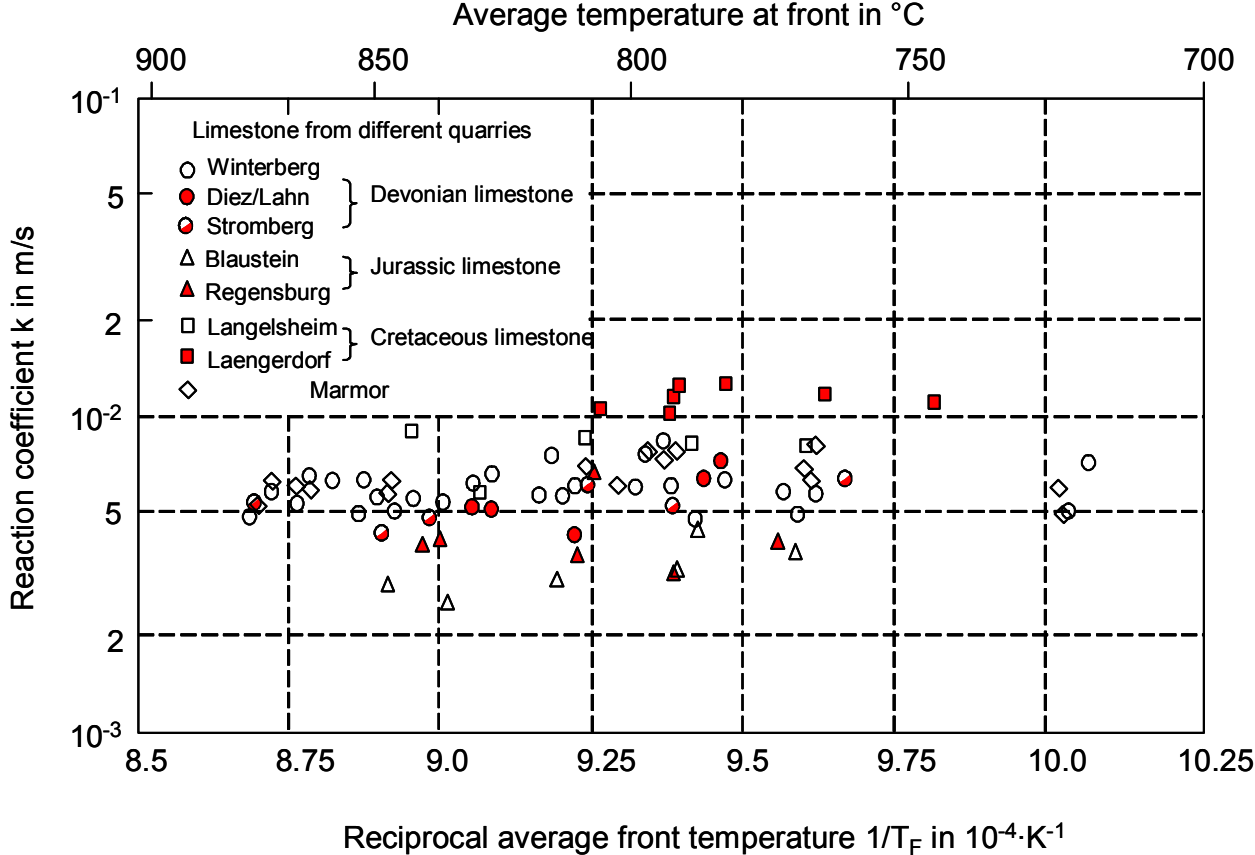
Figure 3-19: Reaction coefficient for different limestones [14].
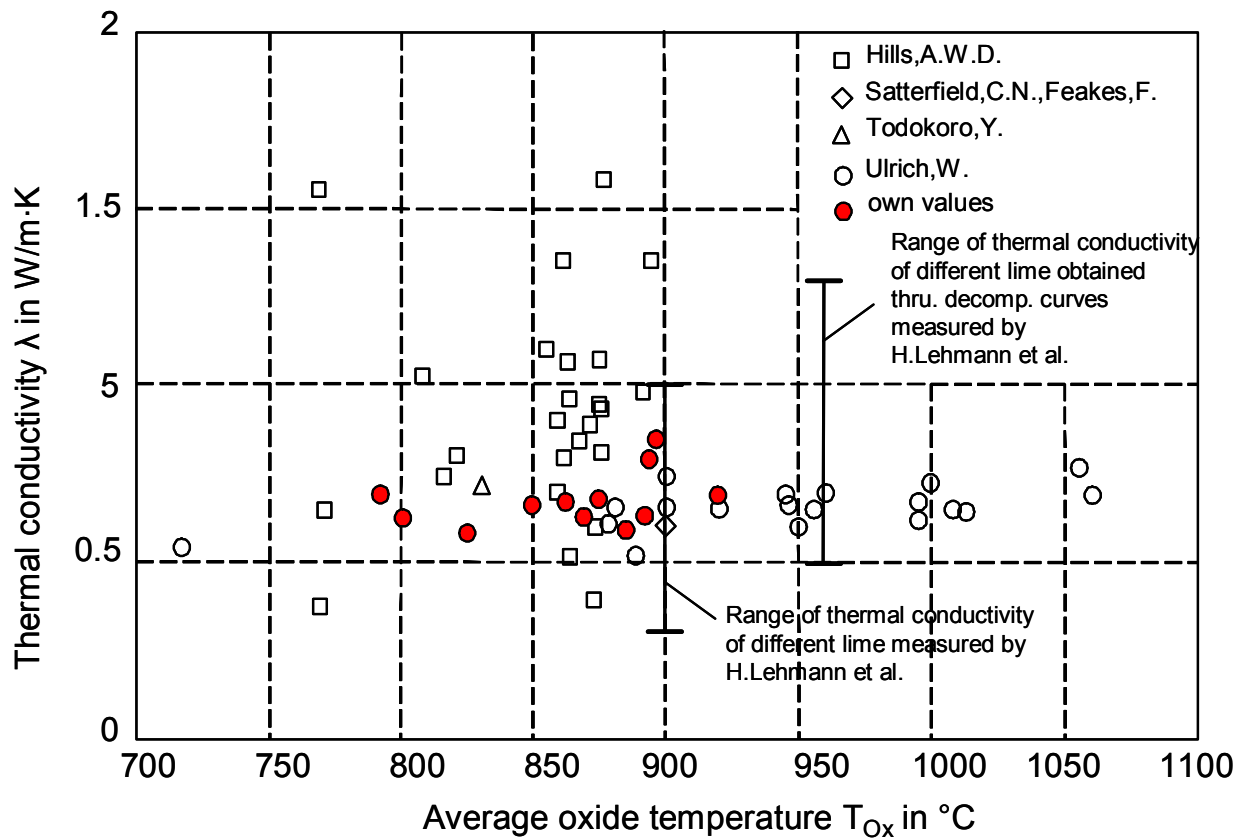
Figure 3-20: Thermal conductivity of calcium oxide [14].

The values of an effective pore diffusion coefficient as a function of temperature are shown in Figure 3-21. The values from different sources are scattered but show the same temperature dependence.

This dependence is described by the equation [14]:

$$D^P = 630 \cdot \exp\left(-\frac{160}{RT}\frac{kJ}{mol}\right)\frac{m^2}{s} \qquad (3\text{-}67)$$
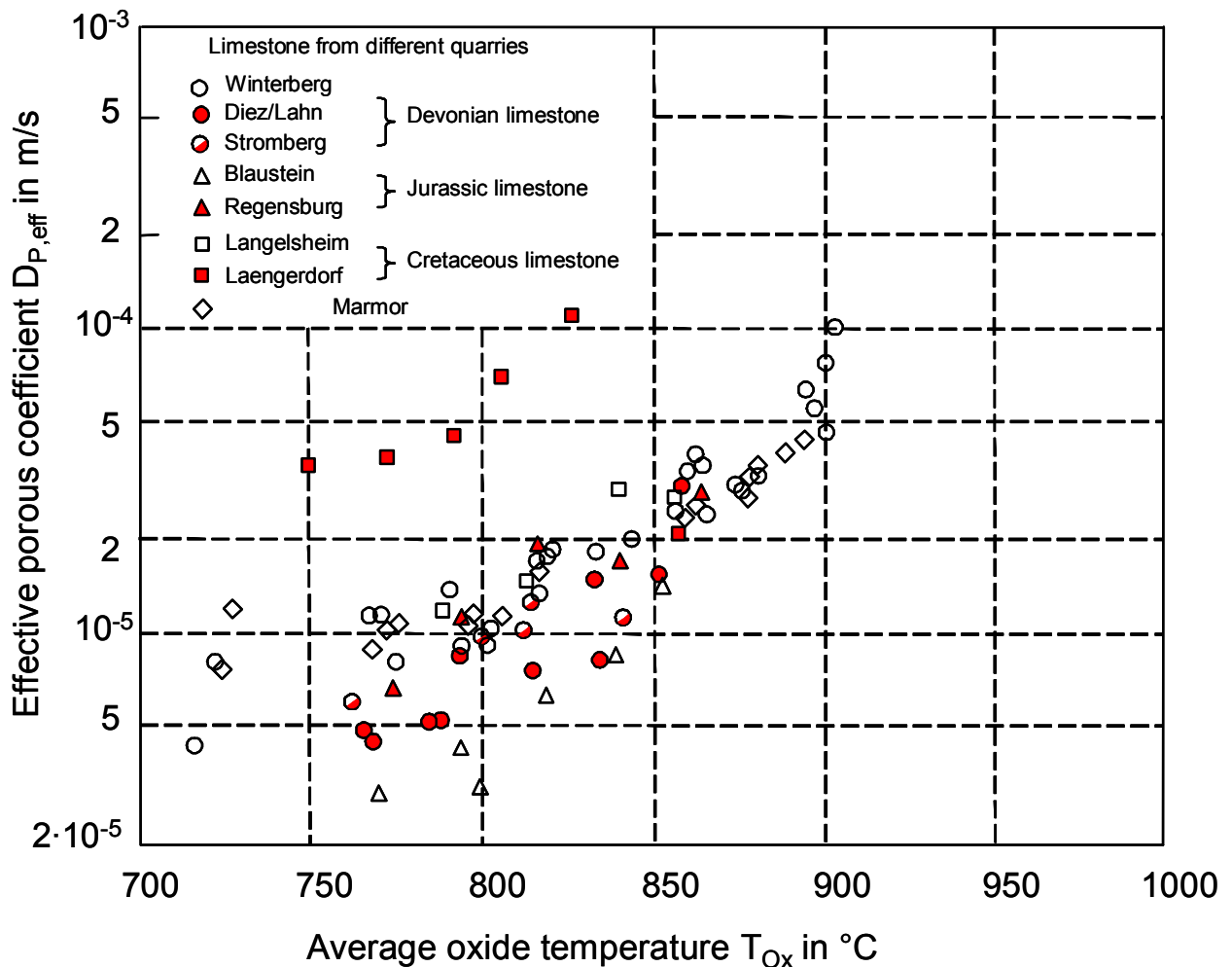
Figure 3-21: Effective pore diffusion coefficient as a function of temperature [14].

3.8 Quality of the quicklime

Production of the required quality of quicklime requires the selection of an appropriate limestone particle size, kiln design and fuel. It's possible to produce soft-, medium- and hard-burned lime. Soft-burned quicklime is lightly sintered and has a high reactivity to water. Hard-burned quicklime has been sintered as a result of over-burning at high temperatures. The quality is influenced by the particle's time-temperature history. Quicklime is often classified by its reactivity to water. It is measured by the rate of release of the heat of hydratation. The degree of burning may be taken as corresponding to the following approximate ranges (EN 459-2):

Soft $\qquad$ t_{60} < 3 min

Medium $\qquad$ t_{60} = 3 - 9 min

Hard $\qquad$ t_{60} > 9 min

where t_{60} is the time after which the solution reaches 60°C.

4. Mathematical model

4.1 Cooling zone

In the cooling zone the lime particles have to be cooled down from the burning temperature to the lowest temperature possible. The temperatures of 70°C to 80°C are considered as sufficiently low. Such temperatures are necessary so as not to thermally overload the following apparatus as well as the conveyor belt and to recover heat from the lime. Depending on the type of a kiln the preheated air emerging from the cooling zone is used in many different ways. It can completely flow into the reaction zone as one part of the total combustion air (e.g. normal shaft kiln), a part of the cooling air can be sucked off and then injected into the reaction zone or cooling air can be used as recirculation gas (e.g. annular shaft kilns).

The cooling down to the low temperatures is always possible, when the cooling air flow is appropriately increased. However, this flow should be as small as possible for optimization of the calcination process in the kiln. The less the cooling air is the larger can be the amount of the ambient air blown into the kiln with the fuel. This has two important advantages. If this air is preheated by the flue gas the energy consumption can be remarkably reduced. The air injected with the fuel can be used to improve the mixing in the cross-section and to equalize the temperature distribution. These effects will be considered in following articles.

In this chapter the influence of the amount of air, the particle size, and the bed length on the lime cooling will be considered comprehensively. The calculation had to be made numerically due to a high temperature variation and with it a high gas velocity and material values variations. Though, in practice it is easier to employ the analytical solution based on the heat exchanger theory. Therefore, it will be shown, by means of which mean values formation, these equations represent the satisfactory approximation.

The influence of the specific form of the lime particles and the size distribution is not describable. This is the highest uncertainty of all the calculations. Lime particles are simply characterized by the range of the width of the sieve mesh. Therefore, the particles have to be considered as spheres. As the particle size the mean value of sieve meshes should be taken into account.

The cooling zone is that part of a kiln in which the quicklime emerging from the burning zone is cooled before discharge. This zone begins where the burning zone ends (Figure 2-2). The solid mass at the end of the burning zone consists of quicklime particles with or without limestone cores. In this zone the down-flowing solid particles exchange heat with the up-flowing air. Air is introduced at the bottom of the kiln to supply enough oxygen for combustion of the fuel. In the cooling zone the calcination of any unreacted limestone remaining at the end of the burning zone, is considered insignificant in view of the extremely rapid drop of the gas temperature below the solid temperature.

The profiles of the mean solid and gas temperature are obtained from the energy balance, that the change of the enthalpy flow is equal to the transferred heat flow:

- gas

$$\frac{dT_{gas}}{dz} \cdot \dot{M}_{air} \cdot c_{pair} = \alpha(z) \cdot A \cdot (T_{solid} - T_{air}) \qquad (4-1)$$

- solid

$$\frac{dT_{solid}}{dz} \cdot \dot{M}_{solid} \cdot c_{psolid} = \alpha(z) \cdot A \cdot (T_{gas} - T_{solid}) \qquad (4-2)$$

where $\dot{M}$ is the mass flow, c_p is the specific heat capacity, and u is the overall heat transfer coefficient, which includes convective heat transfer from the gas phase to the particle surface and heat conduction within the particle. The lime surface per unit of length, in a section of length dz, can be calculated with the following equations:

$$A = A_{furnace} \cdot O_L \cdot (1 - \Psi) \qquad (4-3)$$

in which $A_{furnace}$ is the kiln cross-section area, Ψ is the void fraction, and O_L is the lime specific surface area. This specific surface area in m^2 per volume m^3 of the particle depends on the shape and on the size of the particle. The value of the surface area is unknown because of the irregular shape of the individual particles. Moreover, this area depends on the particle size, which value is distributed between the upper and lower mesh size. Therefore, the surface area is a parameter with a probability function, which is unknown. Only for the particles with defined shape the surface area can be calculated. For spheres as specific surface area is obtained:

$$O_L = \frac{6}{d_L} \qquad\qquad (4\text{-}4)$$

where d_L is the particle diameter.

Initial conditions are as follows:

$$T_{solid}(z=L) = 50°C$$
$$T_{gas}(z=L) = 20°C$$

The temperature profiles in the cooling zone can be calculated with an analytical solution for a counter-current heat exchanger if the heat transfer coefficient is constant. In the case of lime shaft kiln this coefficient changes with the length of the kiln. For the calculation of the length of the cooling zone, its mean value was taken. Equations for the calculation of the normalised temperature variation ε_i:

$$\varepsilon_i = \frac{1 - \exp[(C_i - 1)N_i]}{1 - C_i \exp[(C_i - 1)N_i]} \qquad\qquad (4\text{-}5)$$

the dimensionless transfer capability N_i:

$$N_i = \frac{1}{1 - C_i} \ln \frac{1 - C_i\,\varepsilon_i}{1 - \varepsilon_i} \qquad\qquad (4\text{-}6)$$

and the mean temperature difference Θ in counter heat exchanger [18]:

$$\Theta = \frac{\varepsilon_1 - \varepsilon_2}{\ln\dfrac{1 - \varepsilon_2}{1 - \varepsilon_1}} \qquad\qquad (4\text{-}7)$$

Meaning of the characteristic numbers:

$$\varepsilon_1 = \frac{\vartheta_1' - \vartheta_1''}{\vartheta_1' - \vartheta_2'} \qquad\qquad (4\text{-}8)$$

$$\varepsilon_2 = \frac{\vartheta_2'' - \vartheta_2'}{\vartheta_1' - \vartheta_2'} \qquad\qquad (4\text{-}9)$$

$$N_i = kA\big/\dot{W}_i \qquad\qquad (4\text{-}10)$$

$$\Theta = \frac{\Delta\vartheta_m}{\vartheta_1' - \vartheta_2'} = \frac{\varepsilon_i}{N_i} \qquad\qquad (4\text{-}11)$$

$$C_1 = \frac{\dot{W}_1}{\dot{W}_2} = \frac{\varepsilon_2}{\varepsilon_1} = \frac{N_2}{N_1} \qquad (4\text{-}12)$$

$$C_2 = \frac{1}{C_1} \qquad (4\text{-}13)$$
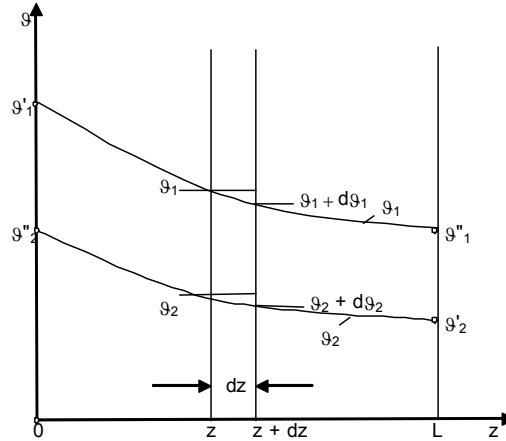
Figure 4-1: Temperature pattern in a counter-current heat exchanger [18]

$$A = A_{furnace} \cdot O \cdot (1 - \Psi) \cdot L \qquad (4\text{-}14)$$

Here $A_{furnace}$ is the kiln cross-section area, L is the cooling zone length, Ψ is the void fraction, and O is the lime specific surface area.

$$O = \frac{6}{d} \qquad (4\text{-}4)$$

The differential equations previously given are valid only for the mean temperature of the particle T_s. The heat transfer between the gas and the mean solid temperature is described as follows:

$$\dot{q} = k \cdot (T_s - T_g) \qquad (4\text{-}15)$$

where k is the overall heat transfer coefficient, which includes heat conduction from particle's core to its surface and convective heat transfer from particle's surface to the gas phase. This overall heat transfer coefficient can be described with the formula below:

$$k = \alpha_k = \frac{1}{\dfrac{1}{\alpha} + \dfrac{s/2}{\kappa \cdot \lambda}} \qquad (4\text{-}16)$$

in which κ is the transient factor, s/2 is the characteristic length and λ is the solid conductivity. For a counter current flow with a capacity flow ratio of 1, the transient factor κ equals:

$$\kappa = \begin{cases} 3 \text{ for plate} \\ 4 \text{ for cylinder} \\ 5 \text{ for sphere} \end{cases}.$$

These values can be taken with a sufficient accuracy for a capacity flow ratio up to 1.5.

Figure 4-2 shows the ratios of the cooling zone length calculated with the analytical solution to the length calculated using a numerical method. The maximum deviation between the analytical and numerical solution resulted for capacity flow ratio $\Omega = 1.4$. It can be seen that the deviations are in the range +2.5 % to -7.5 %. The values of T_{sL} and T_{s0}, given as an example in Figure 4-2, correspond to the highest solid temperature change during the cooling process. Other values result in lower solid temperature change and the analytical solution gives lower deviations from the numerical one. Therefore, the analytical solution on basis of the mean heat transfer coefficient can be used as a good approximation for describing the real process. Analytical calculations using a heat transfer coefficient for the mean gas temperature gave much higher deviations.
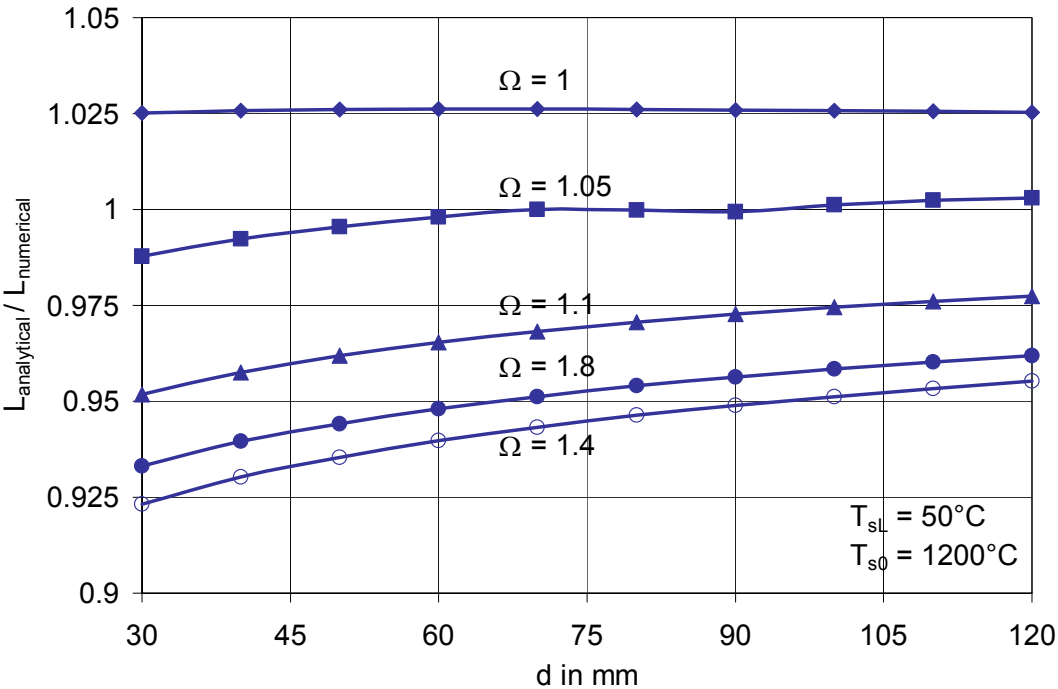
Figure 4-2: Deviations between the cooling zone length calculated with numerical method and the length calculated using the analytical solution.

At first the influence of the length of the cooling zone will be considered. The length is given or fixed by the geometrical design of the kiln. Only for coke fired normal shaft kiln the length is influenced by the process conditions. An input solid temperature T_{s0} of 1200 °C and air input temperature T_{gL} of 20 °C were chosen as an example. All results are obtained from numerical calculations. Figure 4-3 shows how the cooling zone length increases with the increasing particle diameter and decreasing Ω.

The lime outlet temperature T_{sL} is assumed to be 50 °C. For a cooling zone length of 6m and particle diameters > 100mm, Ω has to be higher than 1.1 in order to cool particles down to 50°C. If Ω < 1.1 it is not possible to cool such particles down to 50°C.
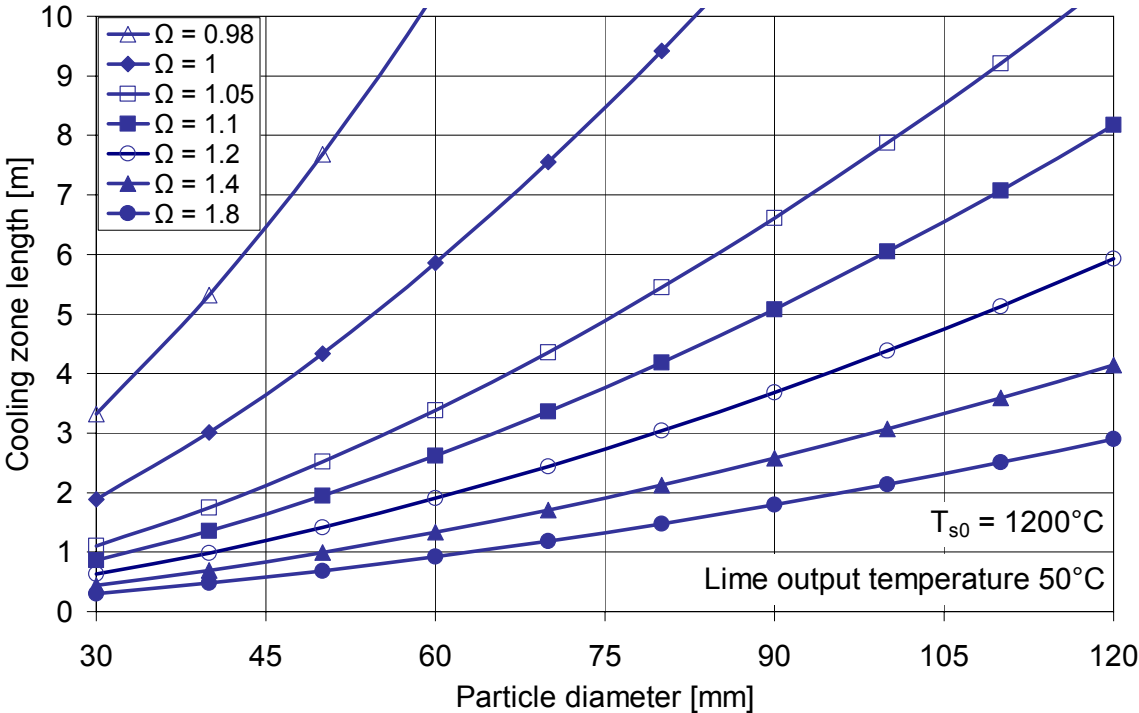
Figure 4-3: Cooling zone length as a function of particle diameter for different air flows.

Figure 4-4 shows the cooling zone length as a function of the lime output temperature for different capacity flow ratios and particle diameters. It can be seen how the cooling zone length increases with a decreasing lime outlet temperature. Considering large particles of 120 mm diameter, Ω = 1 and a cooling zone length of 6 m, it would not be possible to cool down such particles below 110°C. For these particles and cooling zone length Ω should to be increased to 1.1 in order to cool

particles down to 70°C. For the smallest particles of 30 mm diameter a length of 2 m is enough to get the lime outlet temperature as low as 50°C.

It should be mentioned that the lime outlet temperature is the temperature of the particles emerging from the shaft. On the way to a discharge there is further cooling of particles by radiation and conduction. The discharge temperature, which is usually measured, is lower than the outlet temperature. This difference can be 50-100 K.
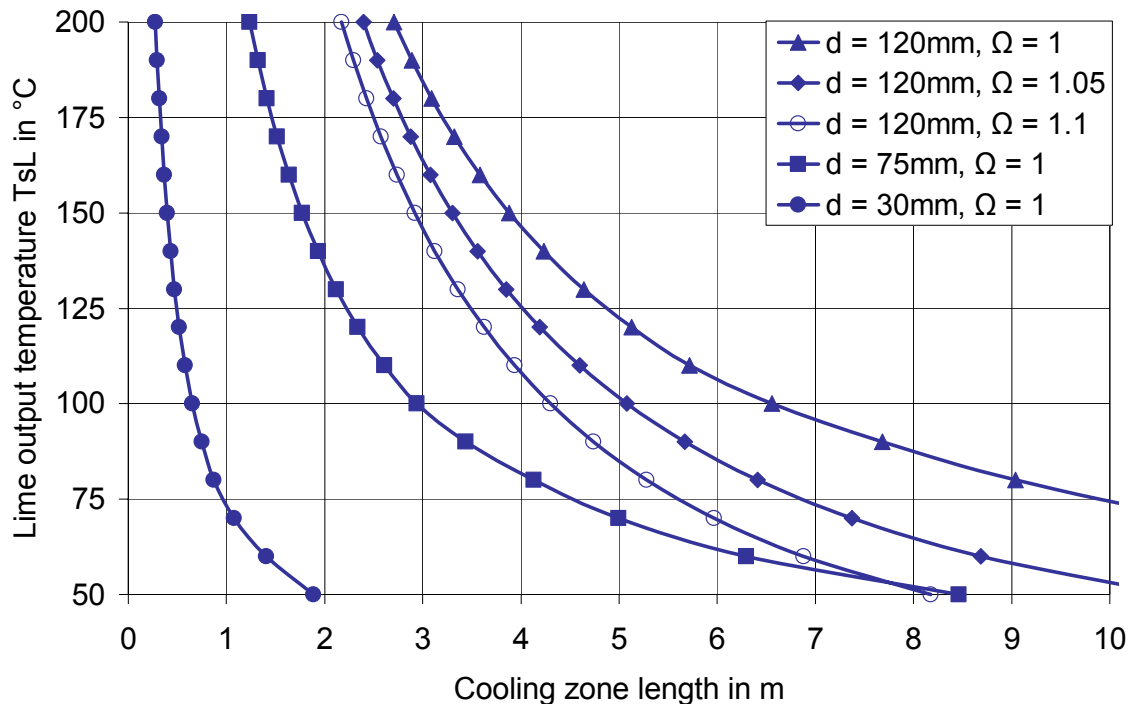
Figure 4-4: Cooling zone length as a function of lime output temperature for different particle diameters and air flows.

Figure 4-5 shows the cooling zone length's dependence on the capacity flow ratio Ω for particles of 80 mm diameter and the lime outlet temperature as a parameter. On a top scale the amount of air is expressed in m^3_{STP} air per kg lime. As can be seen, the cooling zone length changes slightly with Ω in a range of 1.1 - 1.3. For lower values the length rises sharply to reach a limiting value of Ω. Below this value it is not possible to reach the desired outlet temperature T_{sL}. E.g. for lime outlet temperature of 200°C the limiting value is $\Omega = 0.84$. For a given length of 6m Ω has to be increased from 0.84 to 1.03 to reduce the lime output temperature from 200°C to 50°C. The lower limit of the air flow is given by the energy balance. For a very long cooling zone the heat transfer area becomes so large that the temperature of the preheated air matches the lime temperature ($T_{g0} = T_{s0}$). This results for the specific air flow in:

$$\frac{\dot{V}_{STP}}{\dot{M}_s} = \frac{c_s}{c_g} \cdot \frac{1}{\rho_{gSTP}} \cdot \frac{T_{s0} - T_{sL}}{T_{s0} - T_{gL}} \cdot \tag{4-17}$$

From this equation can be seen that the higher the lime temperature T_{sL} is the lower is the specific air flow. It should be pointed out that the calculated air flow through the cooling zone consists of the air from a blower and of the false air. The false air make up to 30% of the total air flow.
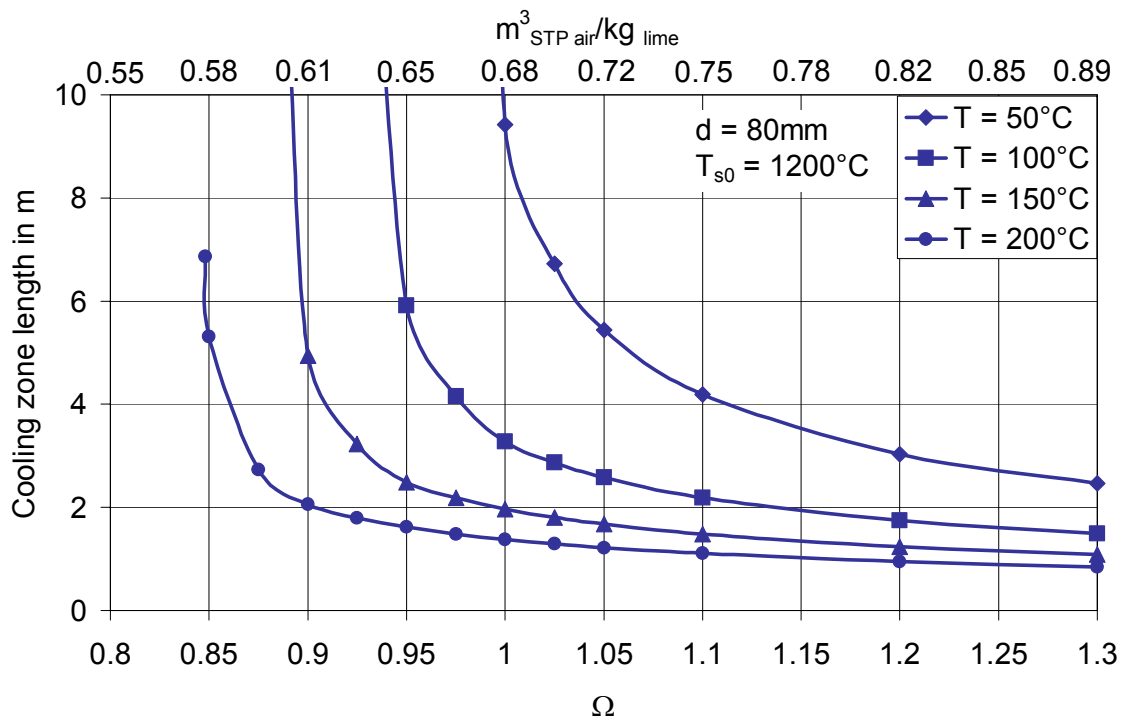
Figure 4-5: Cooling zone length as a function air flow for different lime output temperatures.

Figure 4-6 shows the lime output temperature as a function of the air mass flow for different particle diameters and a given cooling zone length of 4 m and 6 m. The smallest particles of 30 mm diameter can be cooled down to the air input temperature if Ω > 1.05. For Ω < 1 the lime outlet temperature T_{sL} significantly increases with decreasing Ω. For bigger particles this increase starts at higher Ω and is not that strong. If T_{sL} of 100°C is required, the air volumetric flow has to be 0.63 m^3_{STP}/kg$_{lime}$ for small particles and 0.69 m^3_{STP}/kg$_{lime}$ for particles of 120 mm diameter.

In a real process there is a particle size distribution. For the cooling zone length of 6 m and Ω =1, the particles of 30mm diameter would be cooled down to 50°C, while particles of 120mm diameter would leave furnace with the temperature of 110°C.
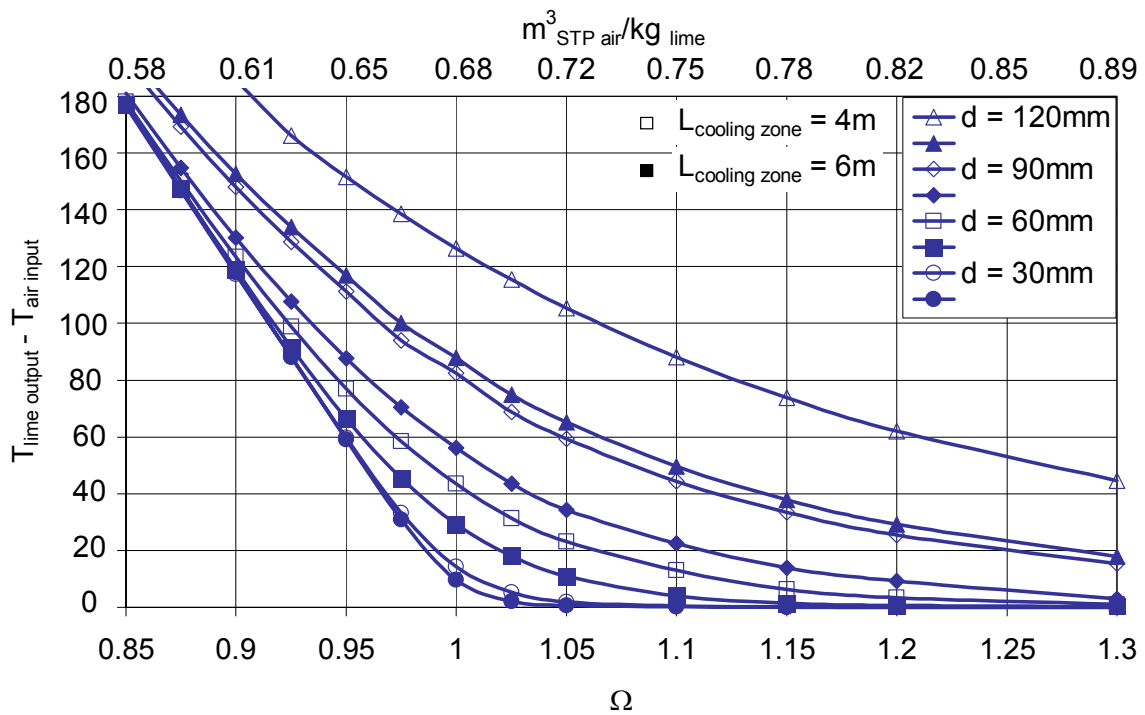
Figure 4-6: Lime output temperature as a function of the air flow for different particle diameters.

The lime discharge temperature strongly depends on the heat capacity ratio air/solid. The flow of the solid is here designated as the flow of lime. However, the flow of lime differs from the flow of the solid if residual CO_2 exists in the lime. In this case the capacity flow of the solid is larger that of the lime. If x_{CO2L} is the fraction of the CO_2 in lime the relationship is obtained to be:

$$c_{ps} = c_{pL} \cdot (1 + 0.9 \cdot x_{CO_2L})$$

(4-18)

4.2 Preheating zone

This zone is that part of a kiln where the limestone is heated by the exhaust gases to just below its dissociation temperature. The solid mass consists of limestone particles. In this zone the down-flowing solid particles exchange heat with the up-flowing flue gas.

The energy balances for solid and gas phase in this zone can be obtained:

- gas

$$\frac{dT_{gas}}{dz} \cdot \dot{M}_{gas} \cdot c_{pgas} = \alpha(z) \cdot A \cdot \left(T_{solid} - T_{gas}\right)$$

(4-19)

- solid

$$\frac{dT_{solid}}{dz} \cdot \dot{M}_{solid} \cdot c_{p\,solid} = \alpha(z) \cdot A \cdot \left(T_{gas} - T_{solid}\right) \qquad (4\text{-}20)$$

where A stands for limestone surface in a section of length dz.

The limestone surface per unit of length, in a section of length dz, can be calculated with the following equations:

$$A = A_{furnace} \cdot O_L \cdot \left(1 - \Psi\right) \qquad (4\text{-}3)$$

Boundary conditions are as follows:

$$T_{gas}\left(z = 0\right) = T_{fg}$$
$$T_{solid}\left(z = 0\right) = 20°C$$
$$T_{solid}\left(z = z_p\right) = 810 - 820°C$$

The limestone specific surface area:

$$O_L = \frac{6}{d_L} \qquad (4\text{-}4)$$

If the mean heat transfer coefficient is taken, the temperature profiles can be calculated with the equations valid for the counter-current heat exchanger. In the preheating zone the mass flow of gas is much higher than the mass flow of solid. This ratio depends and the kind of fuel and the air excess number. The temperature of the solid entering the furnace is ~20°C. Solid particles are preheated to the temperature of 810 – 820°C. This is a temperature of the beginning of the limestone decomposition and it depends on the carbon dioxide partial pressure in the preheating zone, which is dependent on the kind of fuel.

Figure 4-7 and Figure 4-8 show the preheating zone length as a function of quicklime output and particle diameter. Calculations were done for weak gas as a fuel, air excess number 1.1 and quicklime output temperature 50°C. In the first plot there is a preheating zone length calculated for the case if the flue gas temperature was 375°C. The second plot shows the preheating zone length calculated as if the flue gas temperature was 425°C, which means higher energy usage and bigger amount of gas in the preheating zone. The calculated length with the bigger gas to solid mass flow ratio is, unlike the cooling zone length, significantly shorter (almost by 50% for the biggest particles) than the length calculated in the first case.
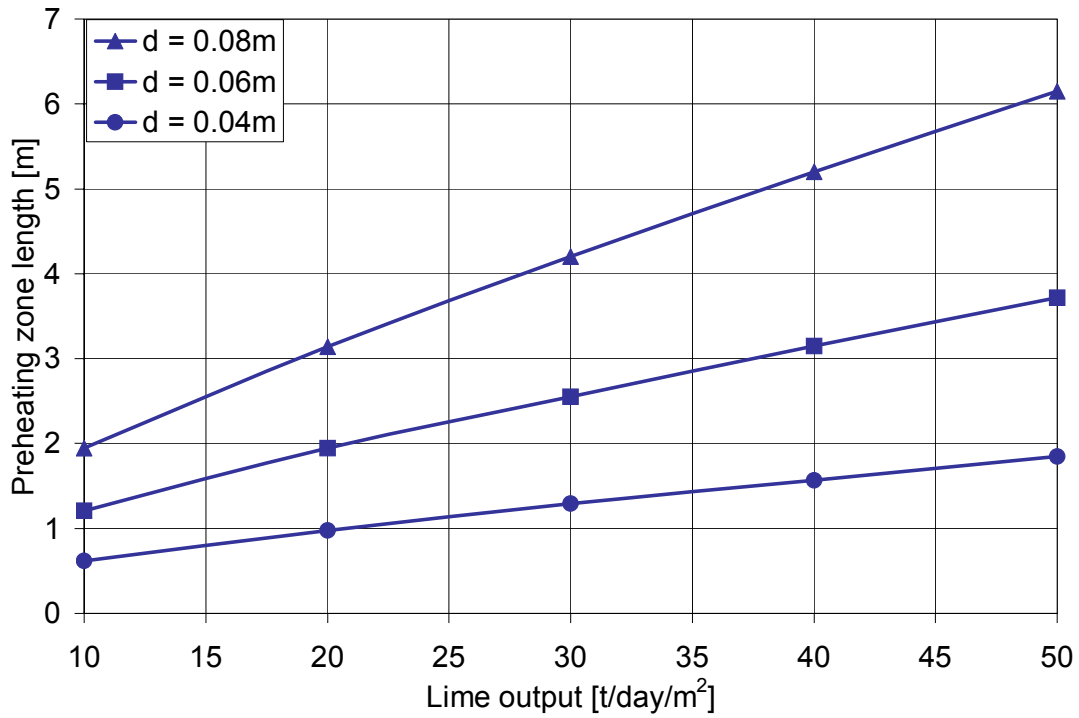
Figure 4-7 Preheating zone length as a function of particle diameter and lime output (T$_{output\ lime}$ = 50°C, T$_{flue\ gas}$ = 375°C).
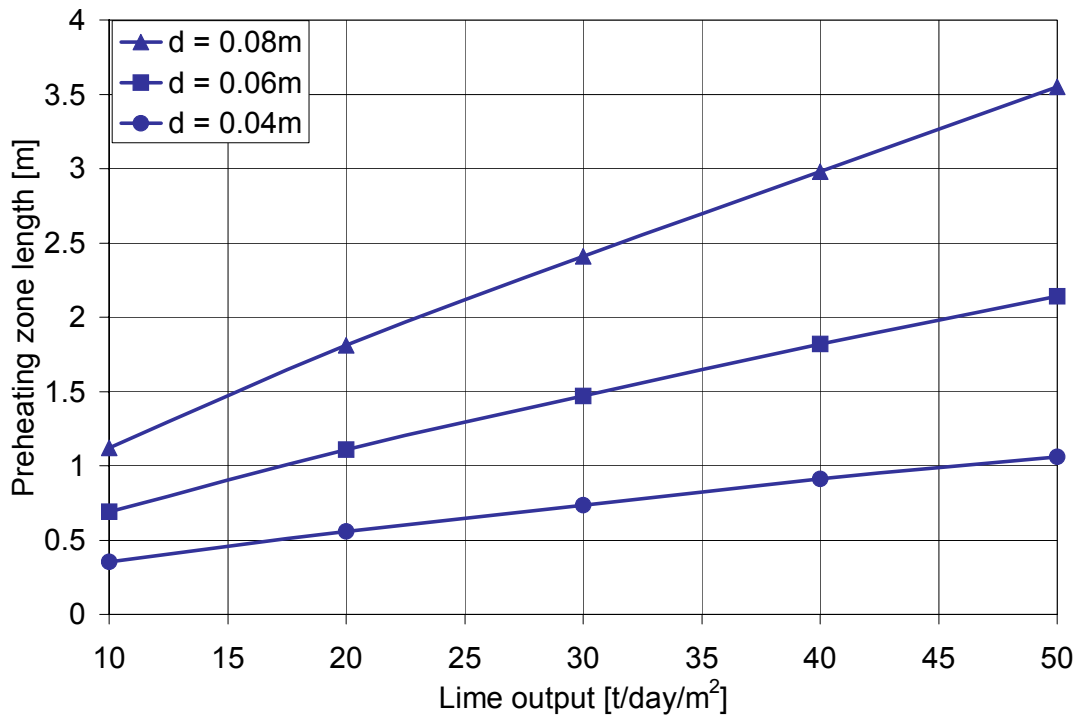
Figure 4-8 Preheating zone length as a function of particle diameter and lime mass flow (T$_{output\ lime}$ = 50°C, T$_{flue\ gas}$ = 425°C).

4.3 Burning zone

This zone is that part of a kiln in which reaction of the burden occurs. Fuel is burnt in preheated air. This produces energy at above 900°C and causes dissociation of the limestone into quicklime and carbon dioxide.

Figure 4-9 is a scheme for a lime shaft kiln section of length dz. The limestone and gas temperatures are denoted by T_{LS} and T_g respectively. The above mentioned temperatures depend on the z co-ordinate in the direction of flow of the solid.

$$\dot{M}_{LS} \cdot c_{LS} \cdot (T_{LS0} - T_{ref}) \qquad \left(\dot{M}_g + \frac{d\dot{M}_g}{dz} \cdot dz\right) \cdot c_g \cdot (T_{g1} - T_{ref})$$

$$\left(\dot{M}_{LS} + \frac{d\dot{M}_{LS}}{dz} \cdot dz\right) \cdot c_{LS} \cdot (T_{LS1} - T_{ref}) \qquad \dot{M}_g \cdot c_g \cdot (T_{g0} - T_{ref})$$
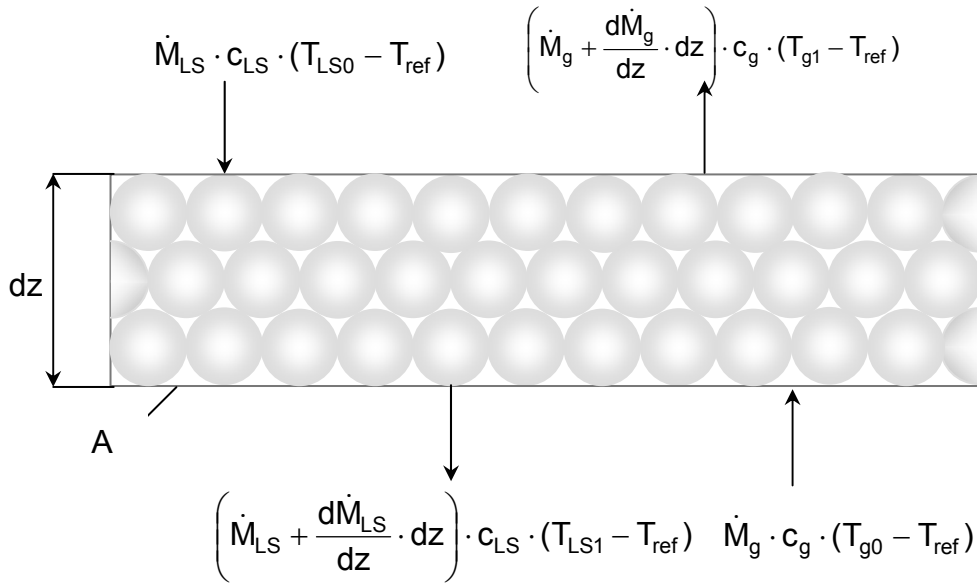
Figure 4-9: Scheme of a lime shaft kiln section of length dz.

By applying the first law of thermodynamics to a section of length dz the rate of heat transfer, $d\dot{Q}$, between fluid and solid through the surface element dA is found to be

$$d\dot{Q} = \dot{M} \cdot c \cdot dT \qquad (4\text{-}21)$$

Using the equation for the heat of reaction

$$d\dot{Q} = \dot{M} \cdot dU \cdot \Delta h \qquad (4\text{-}22)$$

where dU is the conversion degree, Δh is the reaction enthalpy

The energy balances for solid and gas phase are:

- gas

$$\frac{dT_{gas}}{dz} \cdot \dot{M}_{gas}(z) \cdot c_{p\,gas} = \frac{dU_{fuel}}{dz} \cdot h_u \cdot \dot{M}_{gas}(z) - \alpha(z) \cdot A \cdot (T_{gas} - T_{solid}) \qquad (4\text{-}23)$$

- solid

$$\frac{dT_{solid}}{dz} \cdot \dot{M}_{solid}(z) \cdot c_{p\,solid} = \alpha(z) \cdot A \cdot \left(T_{gas} - T_{solid}\right) - \frac{dU_{lime}}{dz} \cdot \frac{\Delta\tilde{h}}{\tilde{M}} \cdot \dot{M}_{solid}(z) \quad (4\text{-}24)$$

where A stands for limestone surface in a section of length dz.

The limestone surface per unit of length, in a section of length dz, can be calculated with the following equations:

$$A = A_{furnace} \cdot O_L \cdot \left(1 - \Psi\right) \tag{4-3}$$

The limestone specific surface area:

$$O_L = \frac{6}{d_L} \tag{4-4}$$

Initial conditions are as follows:

$$T_{solid}\left(z = z_p\right) = 810 - 820°C$$
$$T_{gas}\left(z = z_p\right) = T_{gas\,p}$$

The stone velocity is:

$$\frac{dz}{dt} = w \tag{4-25}$$

The temperature at which the decomposition begins depends on the kind of fuel, while the gas temperature in the beginning of this zone is obtained from the calculation of the preheating zone.

The conversion degree of fuel (U_{fuel}) is a function of the gas temperature, oxygen and carbon dioxide concentration. Both reactions: fuel combustion and limestone decomposition are coupled along this zone.

Heat is mainly transported by convection. The heat transfer coefficient in this part of the furnace varies with the length of the zone. It is a function of the particle diameter, void fraction and gas temperature.

4.4 Air preheating zone

It is that part of the furnace in which the air is preheated to the temperature higher than the solid temperature. This zone begins when the temperature of solid and gas are equal and ends at the point where fuel is introduced into the furnace. There is only one chemical reaction that takes place - fuel combustion. Any further decomposition of limestone is not possible as the solid is cooled down by the gas.

4.5 Influencing parameters
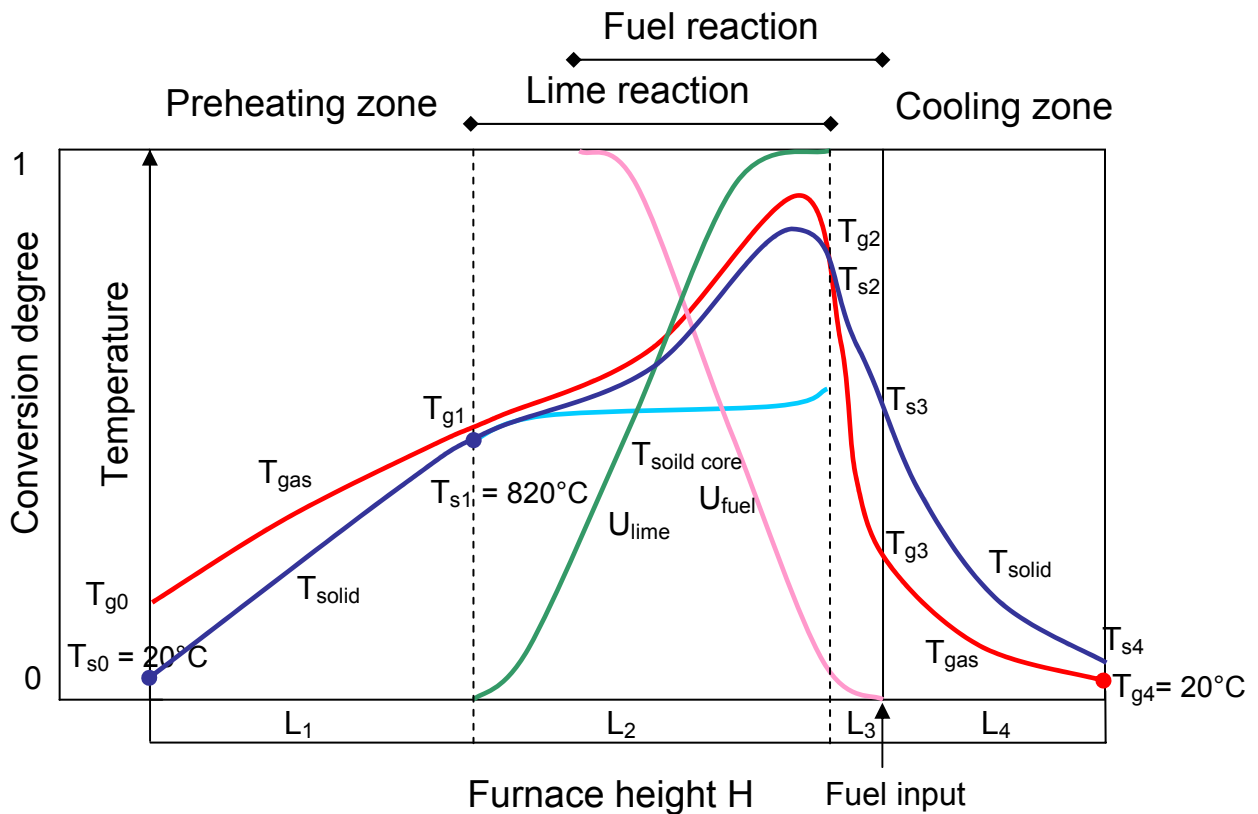
Figure 4-10: Temperature and conversion profiles in normal shaft kilns.

The normal shaft kiln, described in this work, is a vertical counter-current moving bed reactor with the upward flow of hot kiln gases passing counter-current to the downward flow of solid particles. The fuel is injected directly to the burning zone. Figure 4-10 shows the principal temperature and conversion degree profiles in a normal shaft kiln. The solid input temperature T_{s0} and the air input temperature T_{g4} are the only temperatures that are known.

The parameters, which are searched for, are:

- the height of the kiln H, which influences the investment cost
- the energy usage E, which influences the operating cost

Both parameters depend on each other.

The variables, which can be adjusted, are:

- the size of the limestone particles d
- kind of fuel, the reaction of fuel
- the cooling zone length L_4
- the output of lime

82

4.6 Solution

4.6.1 Problem description

The principal temperature and conversion degree profiles in a normal shaft kiln are shown in Figure 4-10. The known parameters: the solid input temperature T_{s0} and the air input temperature T_{g4} are on the opposite sides of the kiln. It makes the mathematical description of the furnace a boundary-value problem, and not the initial-value problem, which would be easier to solve.

The calculations should be started on both sides of the range (at the top and at the bottom of the kiln). In the beginning there are two zones without reaction: one at the top of the furnace – the preheating zone, another at the bottom of the furnace – the cooling zone. Between the preheating and the cooling zone is the reaction zone with limestone calcination and fuel combustion taking place. In this part of the furnace equations describing the temperature changes are coupled with the equations describing chemical reactions. Only the total length of all zones is known but not the length of each of them. If the calculations were started at the bottom of the furnace, it wouldn't be known at which point the limestone calcination ends. Neither would be known if the calcination was complete.

Within the reaction zone there is a range with a very strong temperature change and a range with a very small temperature change with a little difference between gas and solid temperature (transition to the preheating zone). Such problem is called stiff and requires special methods for efficient numerical solution.

The main difficulty in solving the set of the equations describing a normal shaft kiln is that it is a stiff, boundary-value problem with coupled reactions. Additionally the zones length and the limestone conversion degree depend on the solution.

None of the commercial solutions available in the programming library gave any solution to this problem.

4.6.2 Method of solution

In order to get the most effective mathematical description, the furnace was divided into 4 zones (Figure 4-10):

1. the preheating zone, where the stones are preheated to the decomposition temperature

2. the burning zone, where the limestone calcinations and fuel combustion take place

3. the air preheating zone, where the air emerging form the cooling zone is preheated to the temperature higher than the solid temperature

4. the cooling zone, where the lime particles are cooled down before discharge

The energy and mass balances were done separately for each of the four zones but all zones are coupled unlike the models described in literature [19], [20]. The energy and mass balance for each zone required the assumption of the energy usage E, which was corrected iteratively latter on. From the energy balance the flue gas temperature T_{g0} was obtained, which transforms the boundary- value problem into the initial-value problem. The flue gas temperature T_{g0} depends not only on the energy usage but also on the lime output temperature T_{s4}, which is a function of T_{s3}, which depends on the solution. The analysis of the energy balance showed that the limestone calcination accounts for ~75% of the energy usage, the heat loss as the flue gas enthalpy makes up to ~24% of the energy usage, while the heat loss as the lime enthalpy is only ~1% of the energy usage. Therefore the fluctuations of the lime output temperature don't have such strong influence on the energy usage as the variations of the flue gas temperature. This was the reason of transforming the boundary-value problem in initial-value problem with the initial conditions (the flue gas temperature T_{g0} and the limestone input temperature T_{s0}) placed at the top of the furnace and not at the bottom of the furnace.

This problem requires the iterative determination of the zone length, except from the cooling zone length, which is known. Instead of that the solid temperature between zone 3 and 4 T_{s3} has to be determined.

Figure 4-11 shows the way the solution was obtained. The length of the cooling zone is given by the position of the fuel injection jets. The temperature of the air leaving the cooling zone depends on the amount of air introduced to this zone. The maximum amount of air in the cooling zone depends on the energy usage. The minimum amount of air in the cooling zones is the one required to cool down the solid particles to a required temperature (usually ~80°C). Depending on the amount of air in the cooling zone, the temperature of the air that leaves this zone varies.

The total length of three other zones is known but not the length of each of them. The flue gas temperature depends on the fuel usage and the temperature of the air emerging from the cooling zone. The preheating zone length depends on the flue gas temperature and the amount of gas in this zone, which is given by the fuel usage. For the assumed flue gas temperature and the fuel usage the length of the preheating zone is calculated. The burning zone begins where the solid reaches

the decomposition temperature. The gas and solid temperatures in the beginning of this zone are obtained from the calculation of the preheating zone. The burning zone is this part of the furnace, where the limestone calcination takes place. The end of this zone is indicated by the end of the calcination. If the reaction is not complete the burning zone ends where the gas temperature is lower than the solid temperature. If the calcination is not complete the fuel usage has to be adjusted and the zones have to be modelled with an adjusted fuel usage. It has to be repeated as long as the assumed conversion degree and the calculated one are the same. The solid and gas temperature at the end of this zone as well as the solid and gas temperatures at the end of the cooling zone are the boundary conditions for the calculation of the air preheating zone (zone 3), which length comes out by subtraction of the preheating and burning zones length from the total length of these three zones. If the convergence in this zone is not achieved, the fuel usage has to be changed and all the zones have to be modelled again. This iteration process is repeated as long as the convergence is achieved.
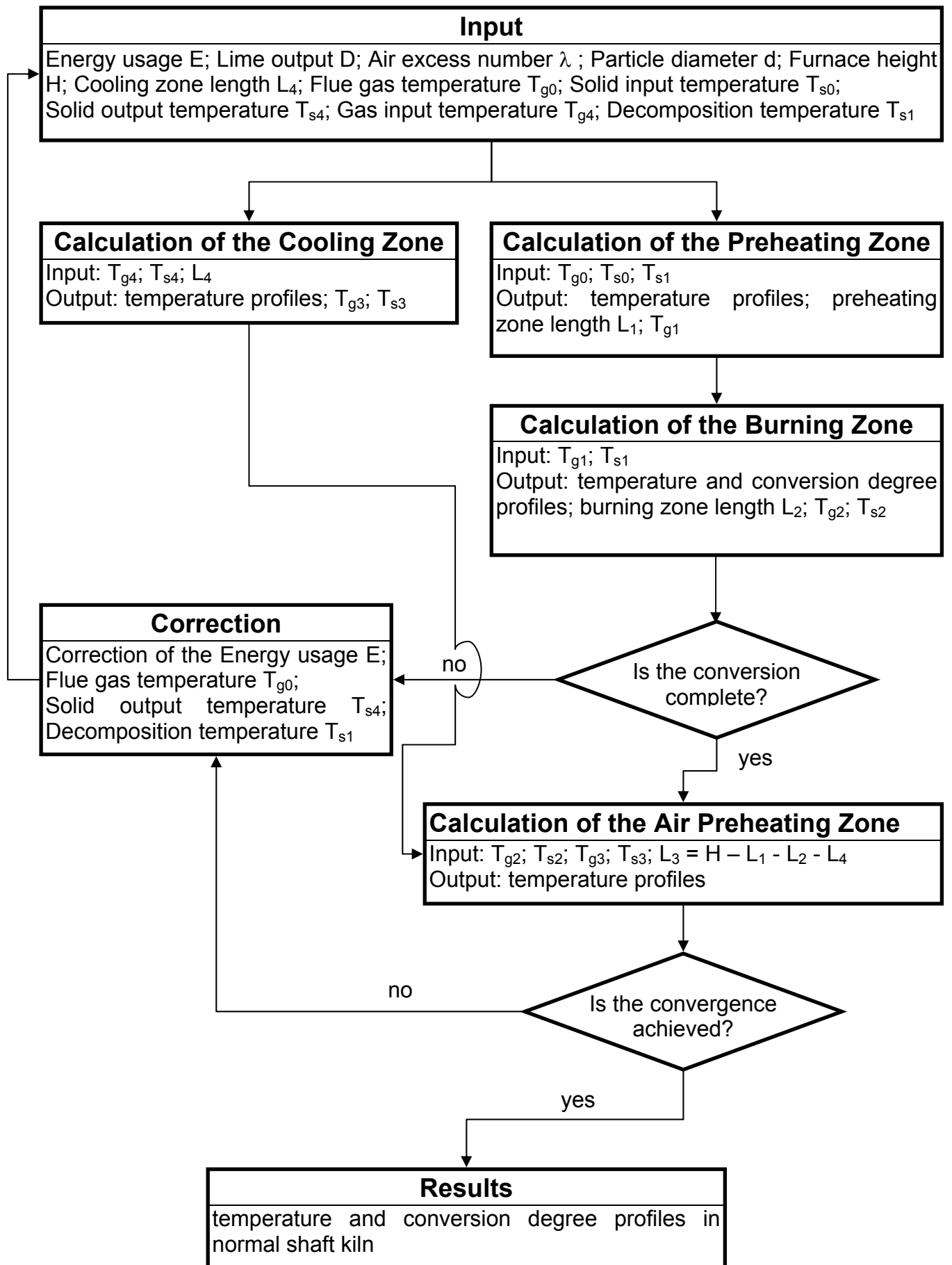
Figure 4-11: Algorithm of the calculation of the zone length, the temperature and the conversion degree profiles in normal shaft kiln.

4.6.3 Numerical solution

The numerical model described in this work includes gas and solid phase heat conduction and radiation, gas diffusion, and heat and mass transfer between the gas and particle surface. Chemical reactions include fuel combustion in the gas phase and limestone thermal decomposition, both reactions are coupled. Limestone decomposition is modelled with finite rate kinetics.

The model contains a system of ordinary differential equations. It is a boundary-value problem where the boundary conditions are distributed between two points. The solution of such a problem has to be determined iteratively. The functions for this type of problem use finite difference methods. Finite difference equations are set up on a mesh of points and estimated values for the solution on the grid points are chosen. These estimates are used as starting values for Newton iteration to solve the finite difference equations. The method is unlikely to be successful when the solution varies rapidly over short ranges. This is the case, when the limestone calcination takes place – in the beginning the gas temperature changes slightly while at the end of the reaction there are very strong gas temperature changes. As it was not possible to achieve convergence with the finite difference method this part of the furnace had to be treated as an initial-value problem and solved with another method.

The problem that appeared in this case was that the solution contains rapidly decaying transient term. The analysis of the functions showed that there are two such terms in equations: one is the term describing the limestone conversion degree decays rapidly when the reaction is about to be complete, another is the gas temperature in the transition range from the reaction zone to the preheating zone. Such problems are called stiff and require special methods for efficient numerical solution. Therefore the Runge-Kutta method of 4th order was applied. Unfortunately the Runge-Kutta method didn't give any solution when one of the terms is equal 0. Therefore the combination of both methods (Runge-Kutta and finite difference) was necessary. The equations describing the preheating and the burning zone are solved with Runge–Kutta method, while the air preheating zone is modelled with finite difference method.

For the given energy usage the length of the preheating zone and the gas temperature between the preheating and the burning zone are calculated. The function used, computes an approximate solution at a sequence of points. The critical task in this case is a correct choice of the step size. Obtained values are the input values for the calculation of the burning zone.

The air preheating zone mathematically represents the two-point boundary-value problem with assigned boundary values for a system of ordinary differential equations. The solution method uses deferred correction technique and Newton iteration. Initially the boundary values of the variables must be specified, some in the beginning, some at the end of the range. Also the estimates of the remaining boundary values have to be supplied. These and all boundary values are used in constructing an initial approximation to the solution. The approximated solution is corrected by a finite-difference technique with deferred correction allied with Newton iteration.

The error tolerance was taken 1.0e-4. The step size was 0.02m.

5. Results

The total length of the preheating, burning and air preheating zone is 9.5m. For the calculations it was assumed that all particles are spheres of the 0.08m diameter, solid input temperature is 20°C, and there is no carbon monoxide in the flue gas. The stones were preheated to 820°C. As the energy demand depends strongly on the flue gas temperature, this temperature was taken as a parameter. Calculations were done for the quicklime output 26.3 t/day/m^2.

Figure 5-1 show the calculated temperature and conversion degree profiles in a shaft kiln for weak gas as a fuel, with the function $U_{fuel} = \exp(-0.2z^2)$ describing the fuel conversion degree. Initially the solid temperature rise is sharp and it becomes slighter with the decreasing temperature difference between gas and solid. When the solid temperature reaches 820°C (after ~3.5m) the limestone decomposition begins. It indicates the beginning of the burning zone. In this zone initially the rise of solid surface and core temperature is very slight. In this section both reactions, limestone decomposition and fuel combustion, are quite slow. As the fuel combustion reaction rate increases, the gas and solid surface temperatures rise gets sharper and reach a maximum at the end of the zone. During the decomposition process the core temperature increase is slight, getting sharper at the end of the reaction. When the limestone decomposition is complete it reaches the value of ~1100°C. When the solid and gas temperatures are the same no further decomposition is possible (after ~7.5m). This point indicates the beginning of the air preheating zone. In this zone there is only one chemical reaction – fuel combustion. On the length of 9.5m air emerging form the cooling zone is mixed with cold fuel and the gas phase has at this point the mean temperature of ~400°C. In its up-ward flow along the furnace gas enthalpy increases due to heat generated by the combustion and heat transferred from the solid particles.
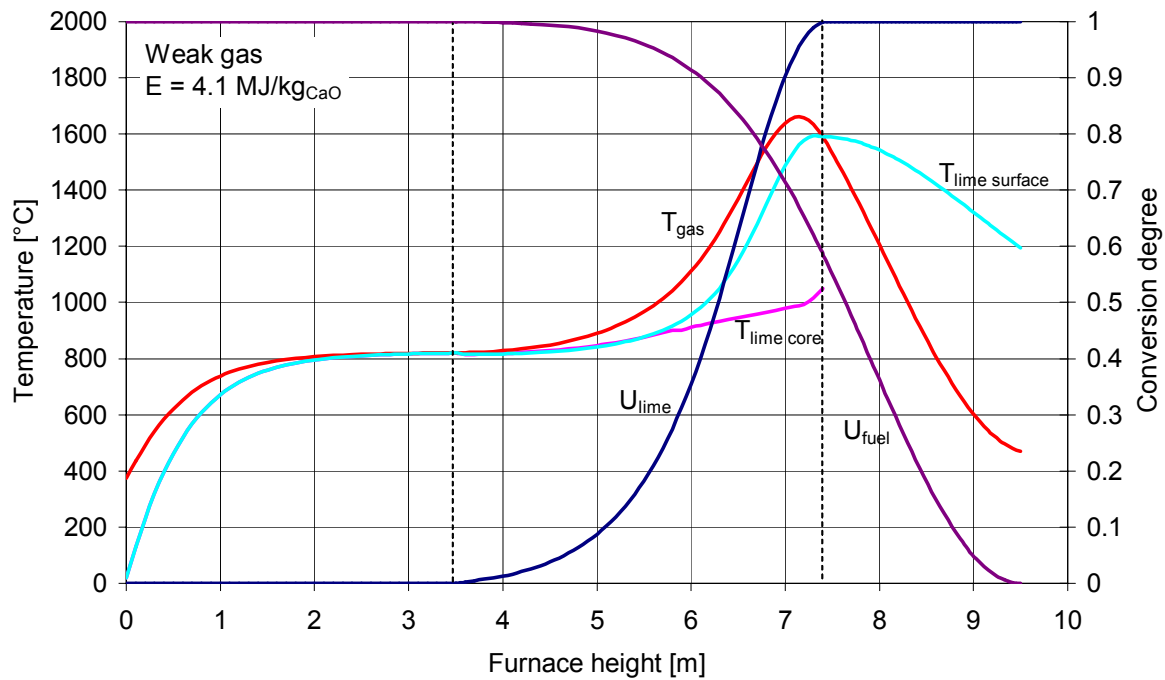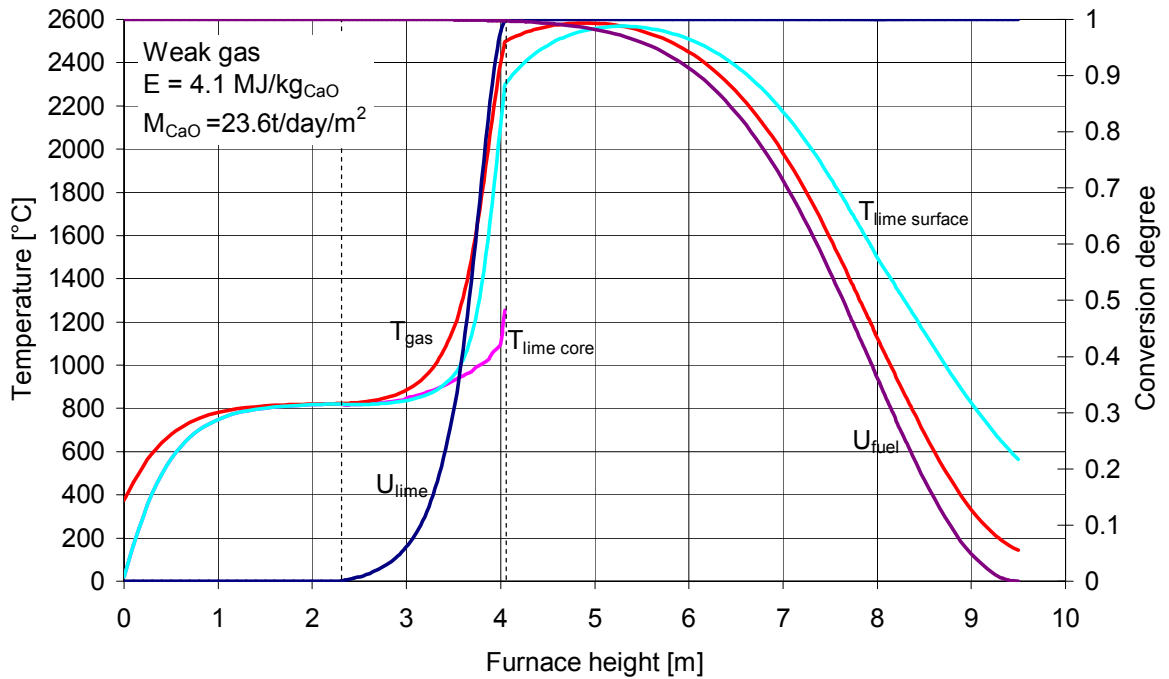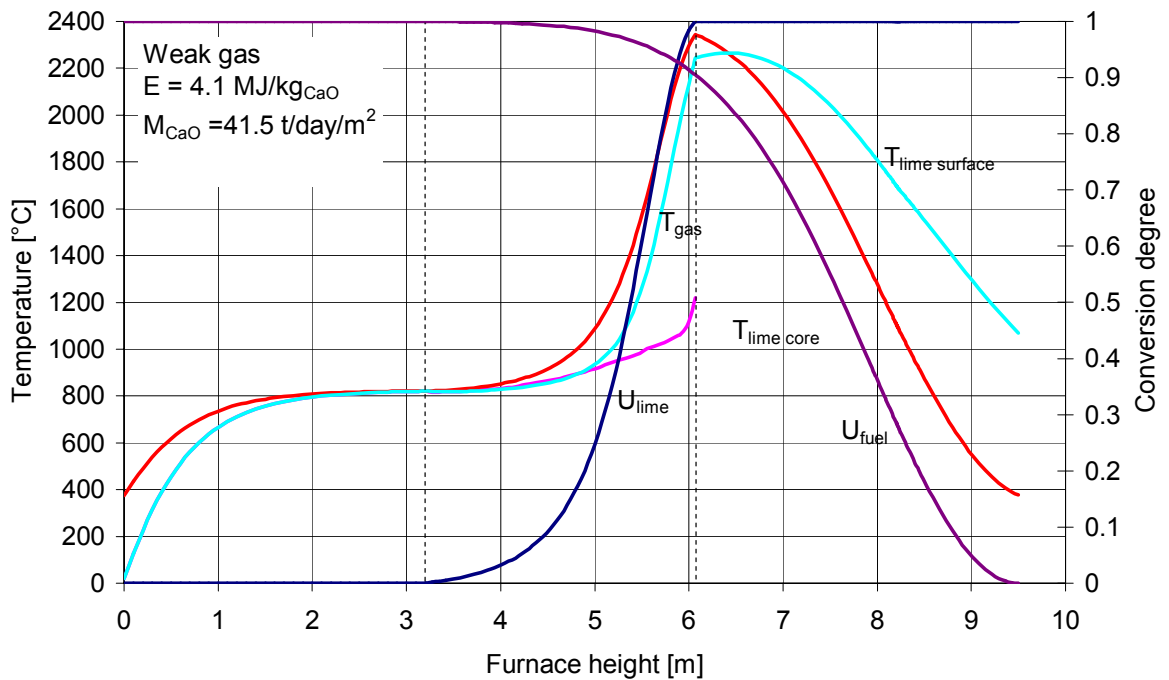
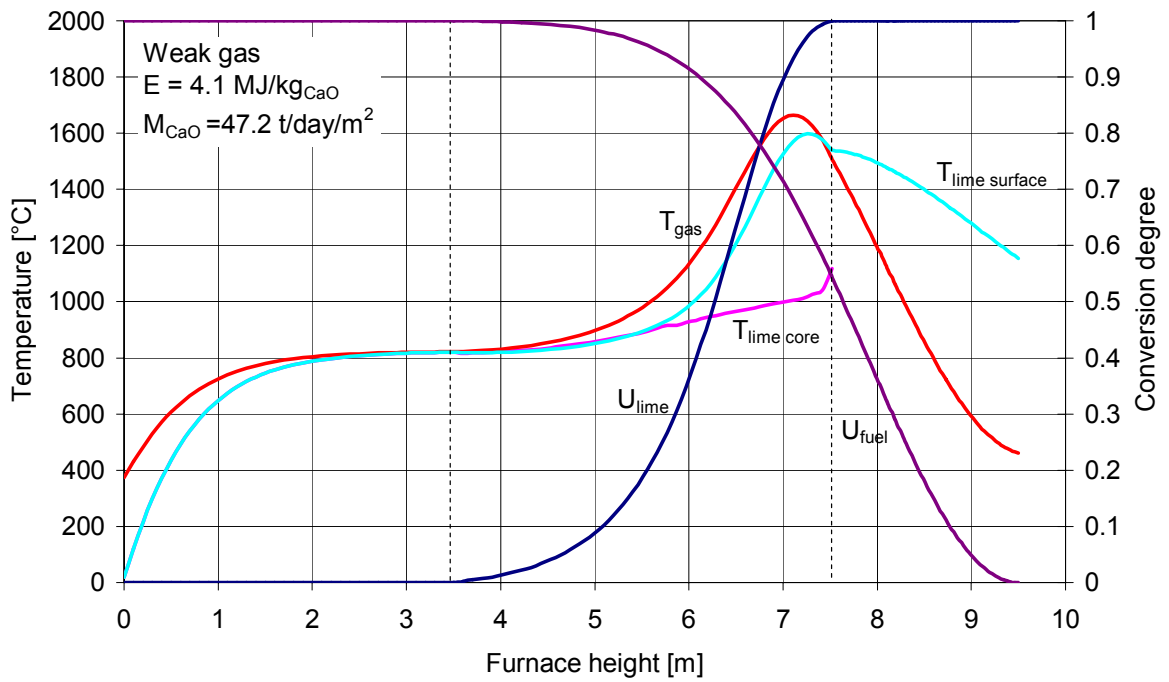**Figure 5-1: The temperature and conversion degree profiles in the preheating and the burning zones. Plots involve weak gas as a fuel, lime output 26.3t/day/m², particle diameter 0.08m, air excess number 1.1; flue gas temperature 375°C, energy usage 4.1 MJ/kg$_{CaO}$**

Figure 5-2 shows the temperature and conversion degree profiles for different flue gas temperatures and thus energy consumptions. Accordingly to the increase of the flue gas temperature raises the intensity of limestone decomposition that ends in shorter distance from the process beginning. With the higher energy usage the maximum gas temperature and the flue gas temperature are higher, while the lime temperature entering the cooling zone does not vary significantly from the value of 1200°C for all three cases.

(a)
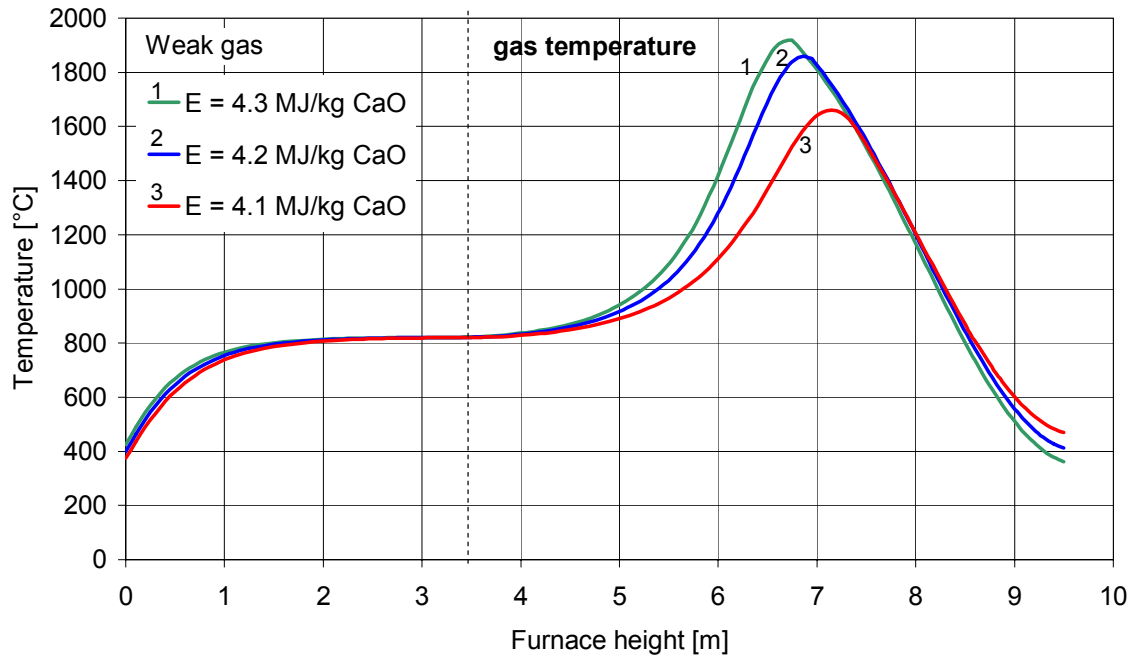
(b)
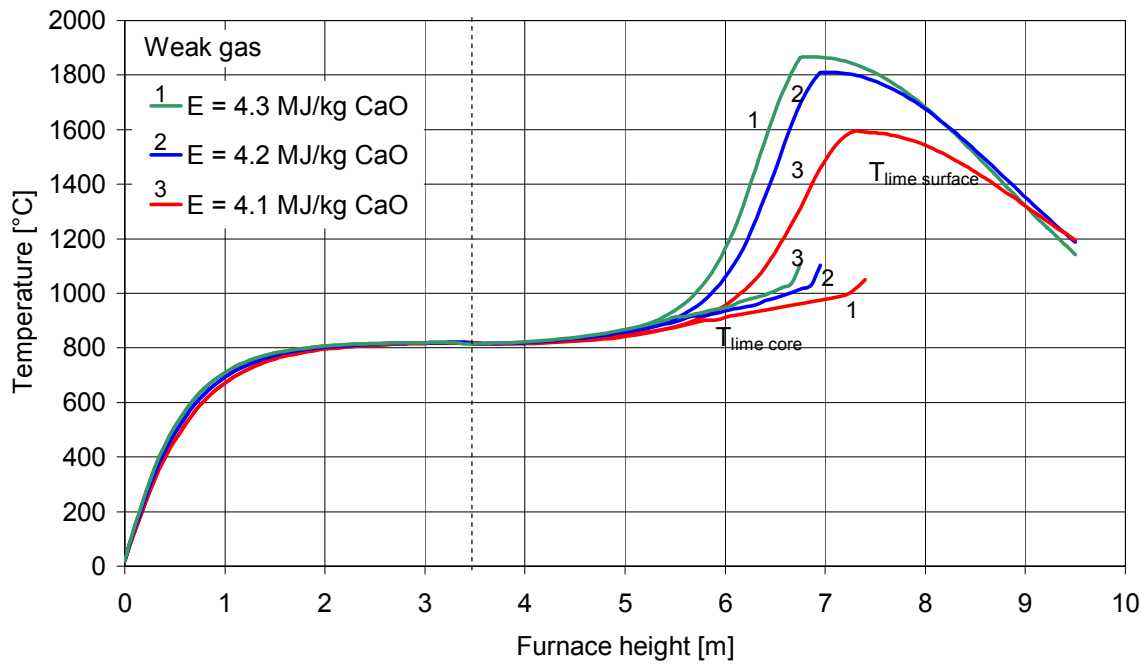
(c)
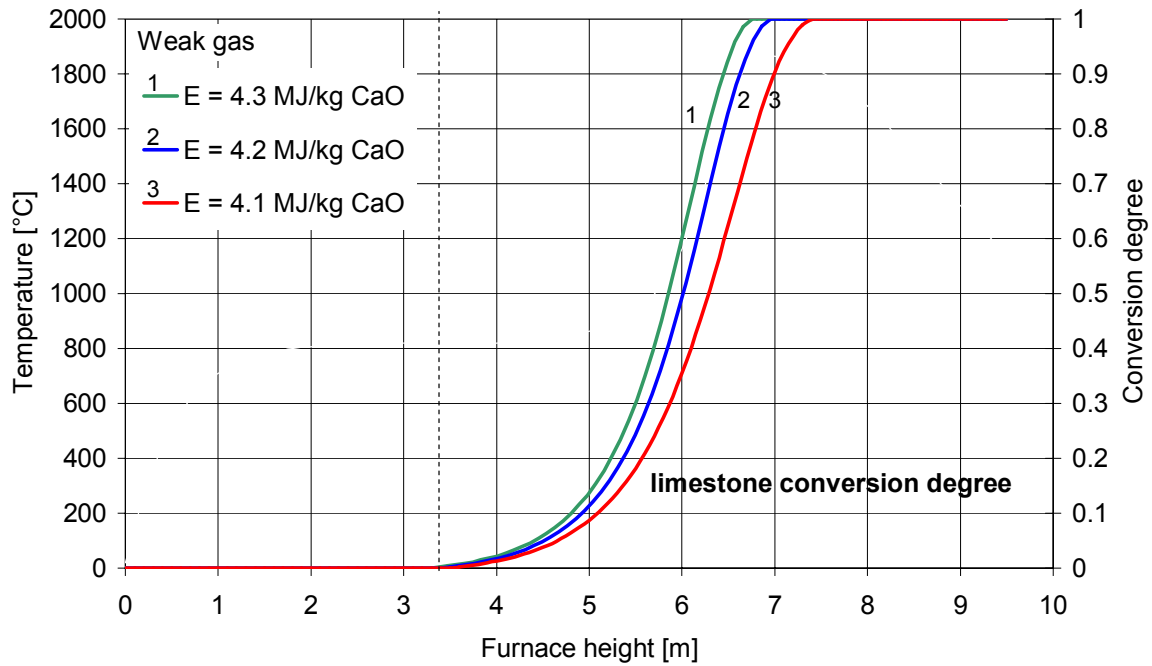
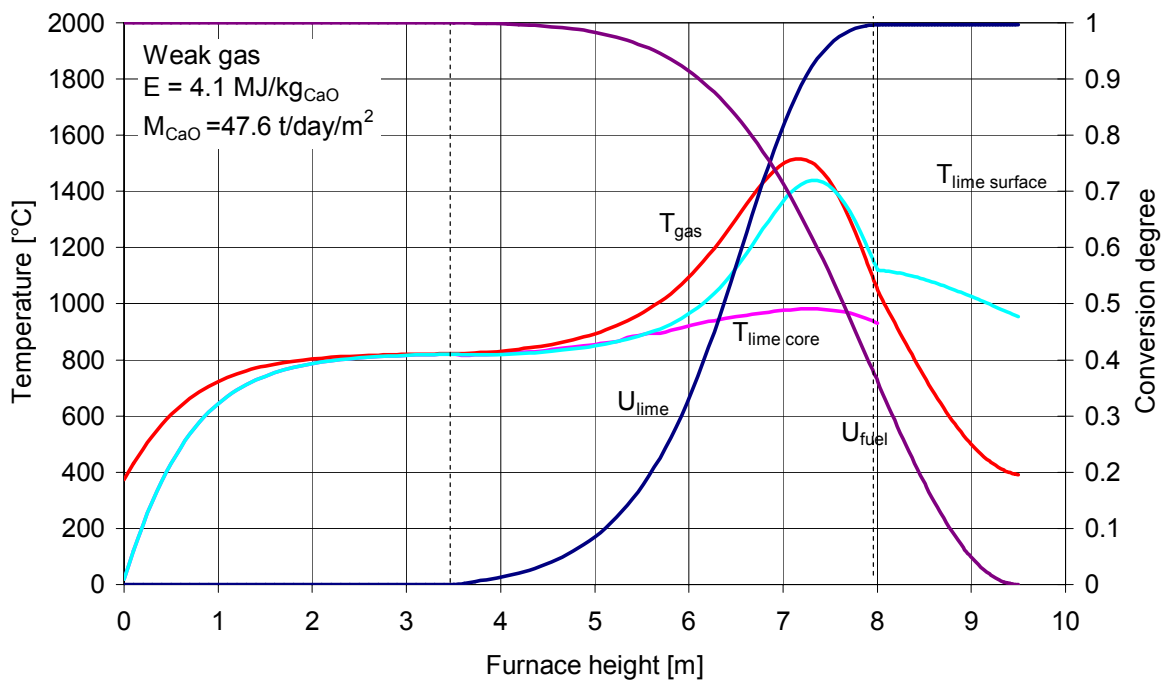**Figure 5-2: The temperature and conversion degree profiles in the preheating and the burning zones. Plots involve weak gas as a fuel, lime output 26.3t/day/m², particle diameter 0.08m, air excess number 1.1;**

Figure 5-3 shows the temperature and conversion degree profiles for different fuel conversion degree profiles. If the fuel burns slowly the maximum gas temperature is lower then for the faster combustion. The decomposition time is longer but the process begins earlier (after ~2.5m) than in the previously described cases. If the fuel reacts on the length of 2.5m, the gas temperature is almost equal to the adiabatic combustion temperature. The reactions of limestone decomposition and fuel combustion do not overlap in this case. The solid temperature entering the cooling zone varies significantly for both cases.

(a)

(b)

93
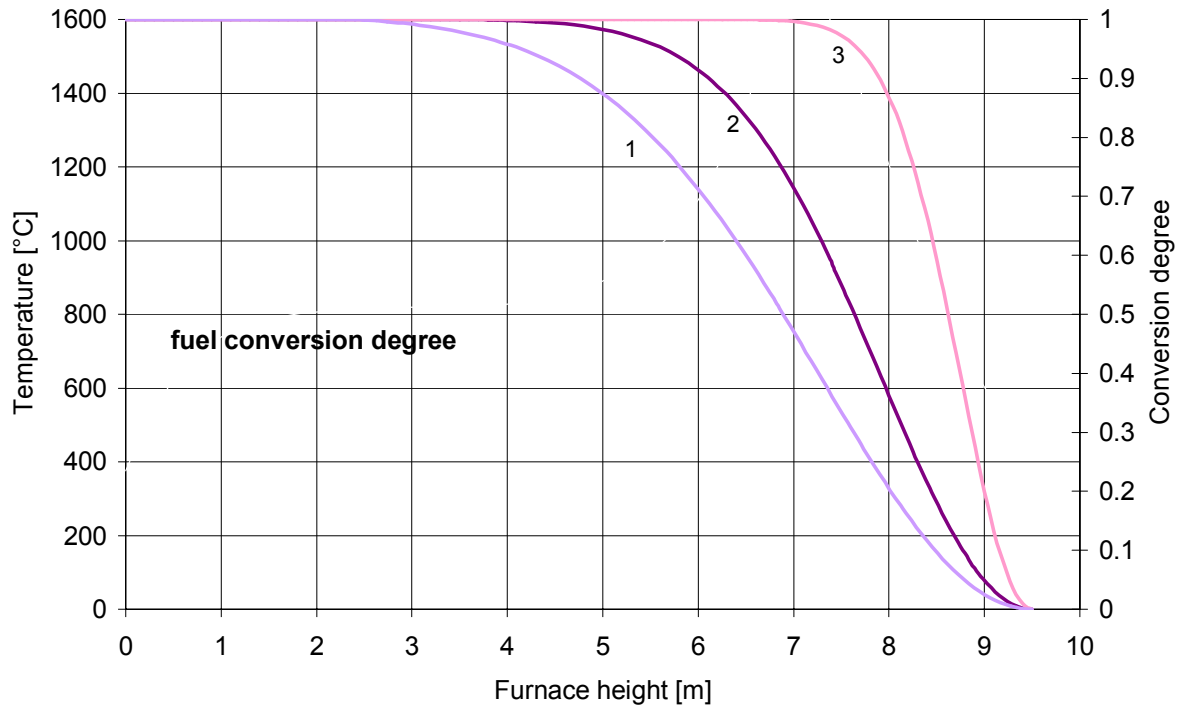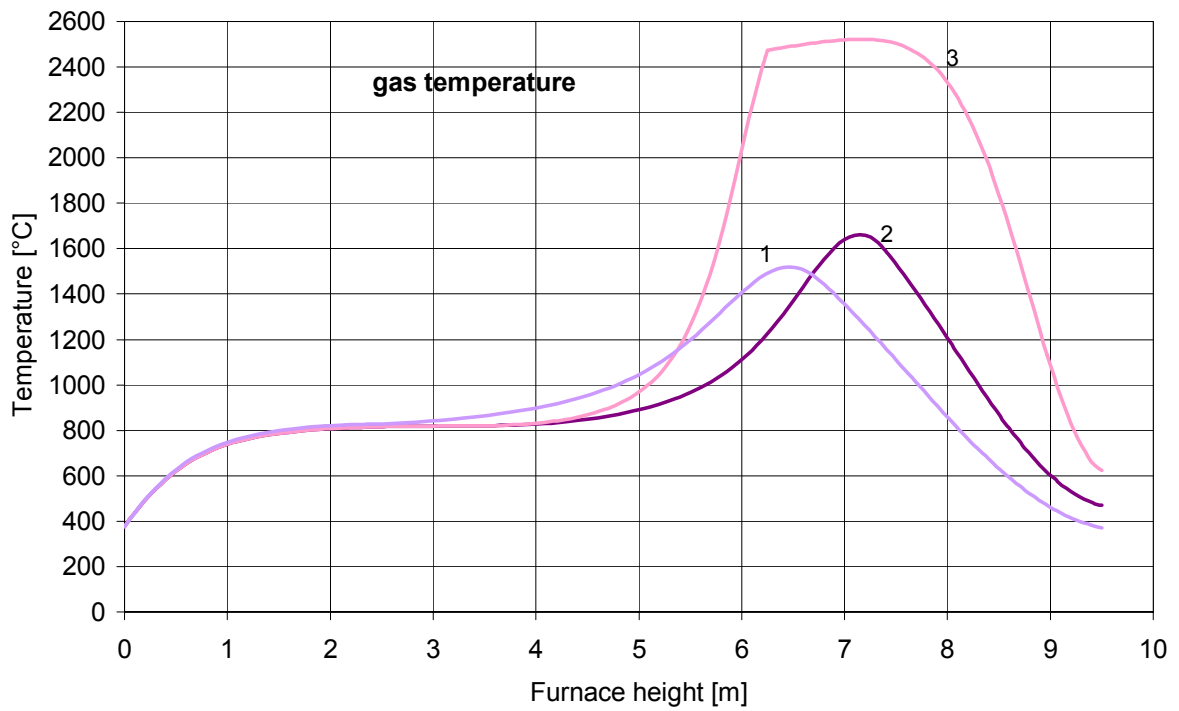
(c)
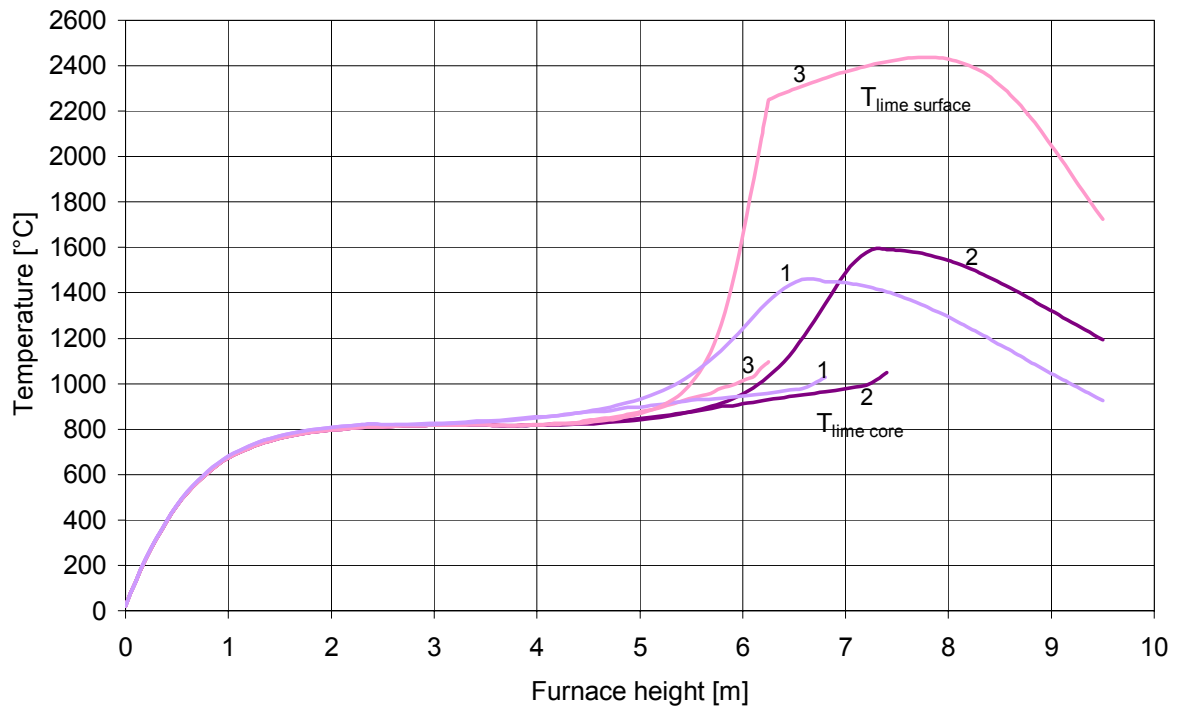
(d)
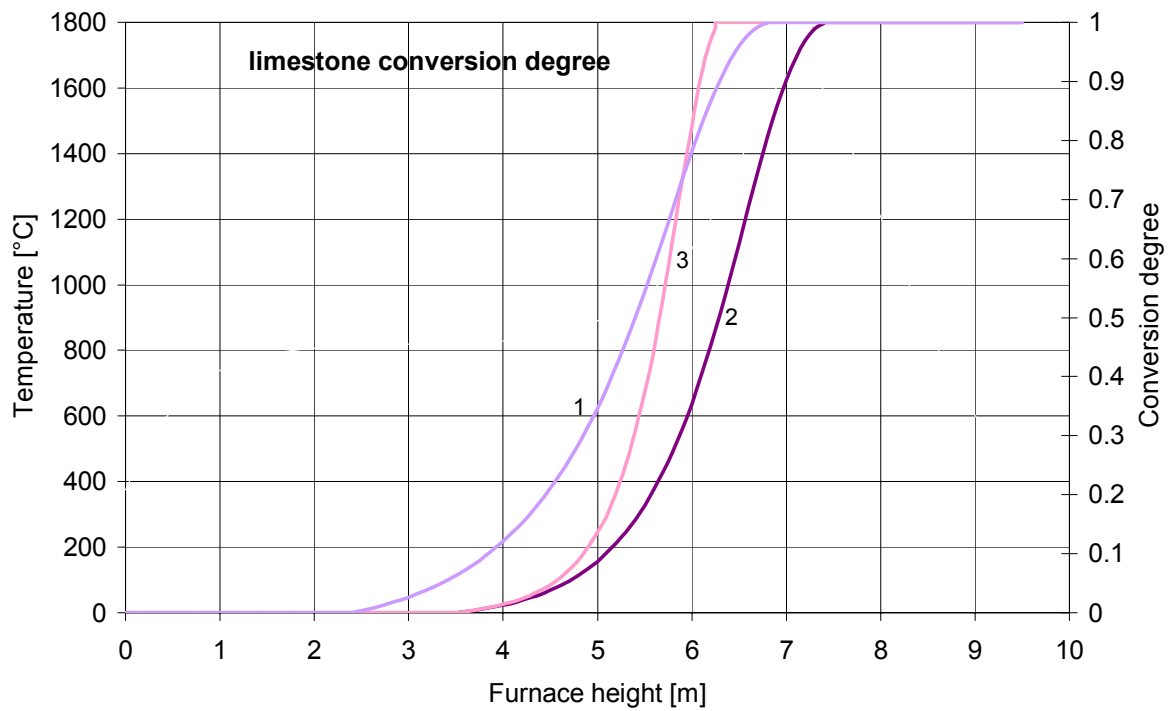
Figure 5-3: The temperature and conversion degree profiles in the preheating and the burning zones. Plots involve the flue gas temperature 375°C, weak gas as a fuel, lime output 26.3t/day/m^2, air excess number 1.1, energy usage 4.1 MJ/kg$_{CaO}$ and particle diameter 0.08m; (1) U$_{fuel}$ = exp(-0.1z^2); (2) U$_{fuel}$ = exp(-0.2z^2); (3) U$_{fuel}$ = exp(-0.95z^2);

Figure 5-4 and Figure 5-5 show the calculated temperature and conversion degree profiles in a shaft kiln for natural gas as a fuel. Figure 5-4 shows the profiles for different flue gas temperatures and thus energy consumptions. The tendencies observed are the same as in the case of the weak gas. The maximum gas temperature is higher than the one calculated for the weak gas.

(a)
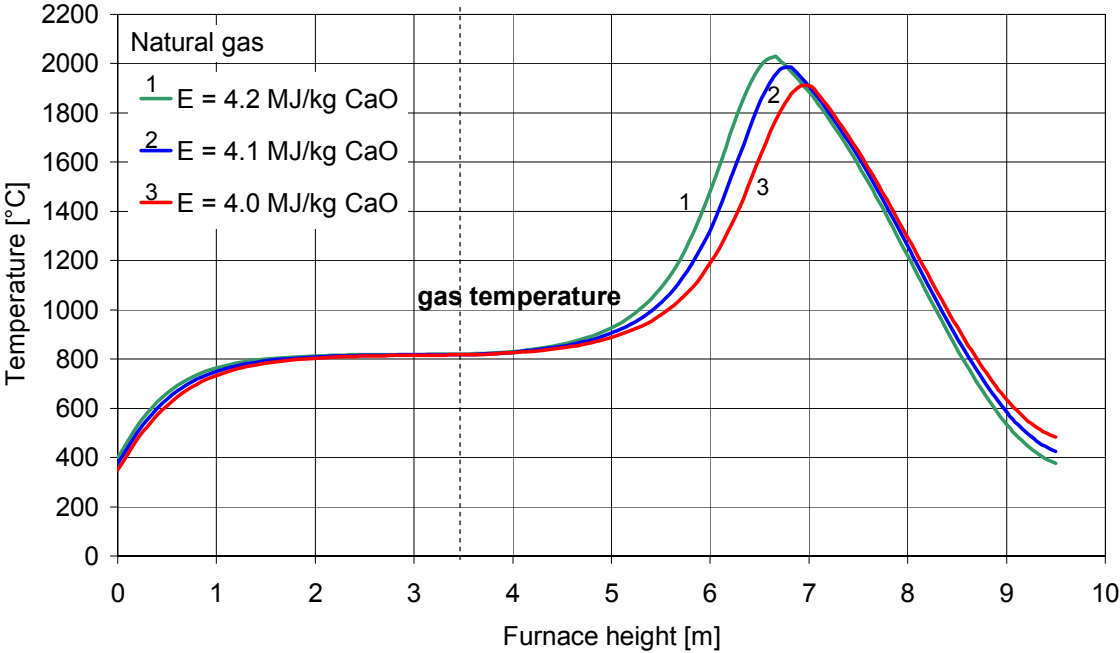
(b)
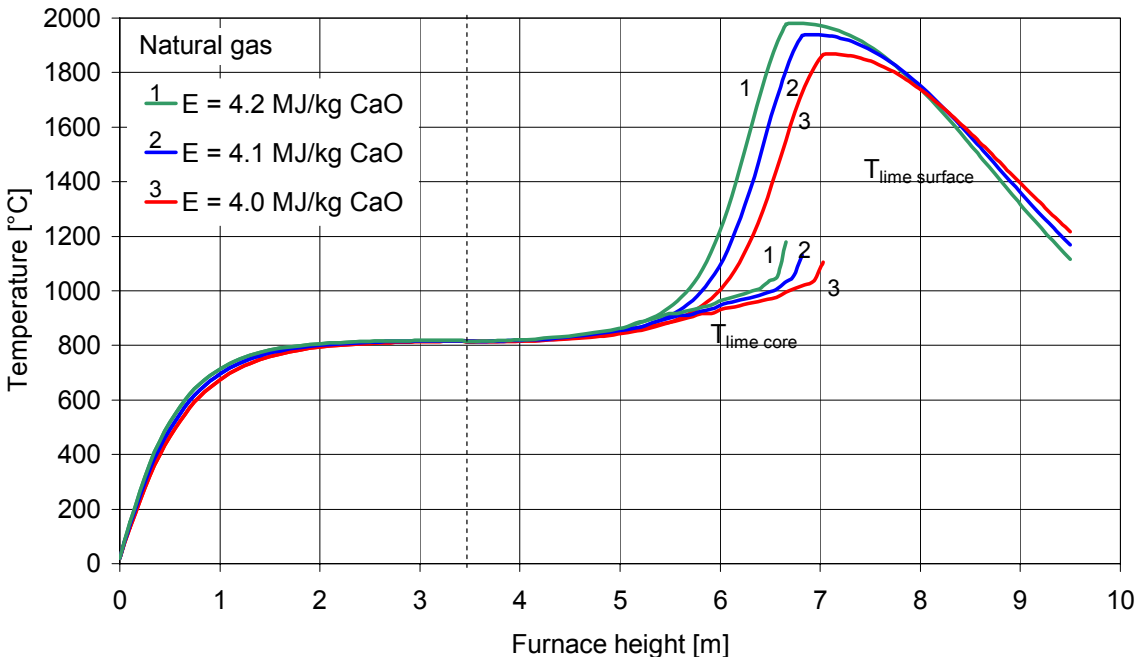
(c)
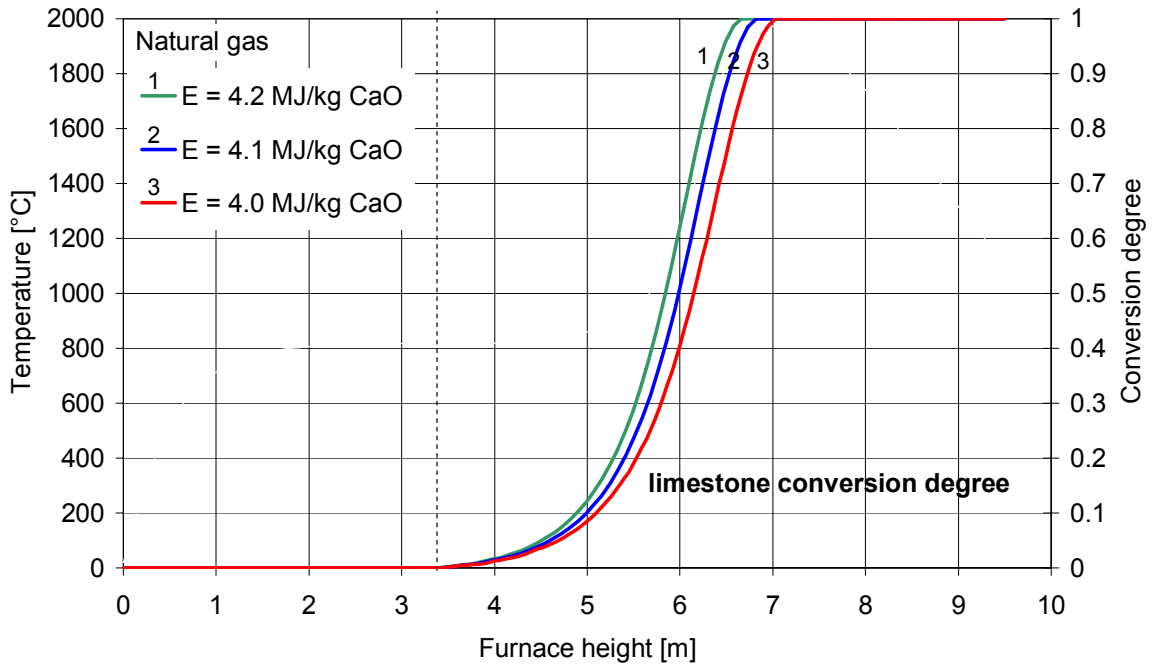
Figure 5-4: The temperature and conversion degree profiles in the preheating and the burning zones. Plots involve natural gas as a fuel, lime output 26.3t/day/m^2, air excess number 1.35, and particle diameter 0.08m.

Figure 5-5 shows the temperature and conversion degree profiles for different fuel conversion degree profiles. Also in this case the same tendencies are observed as in the case of the weak gas.

(a)
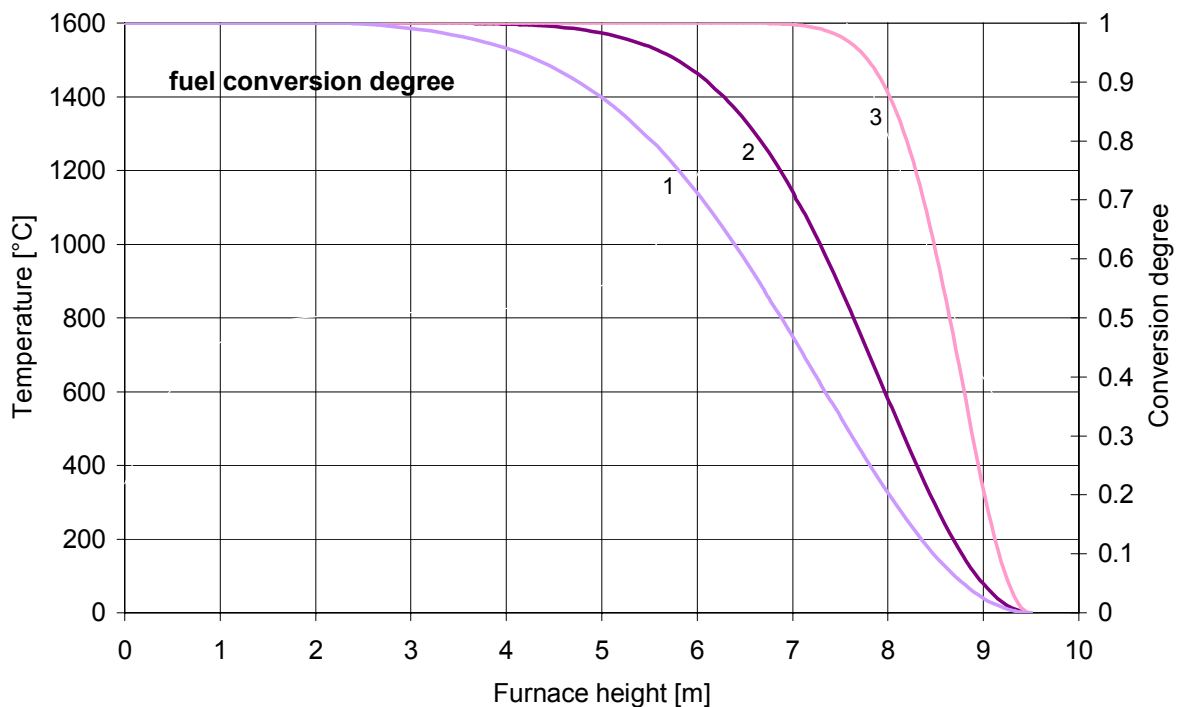
(b)
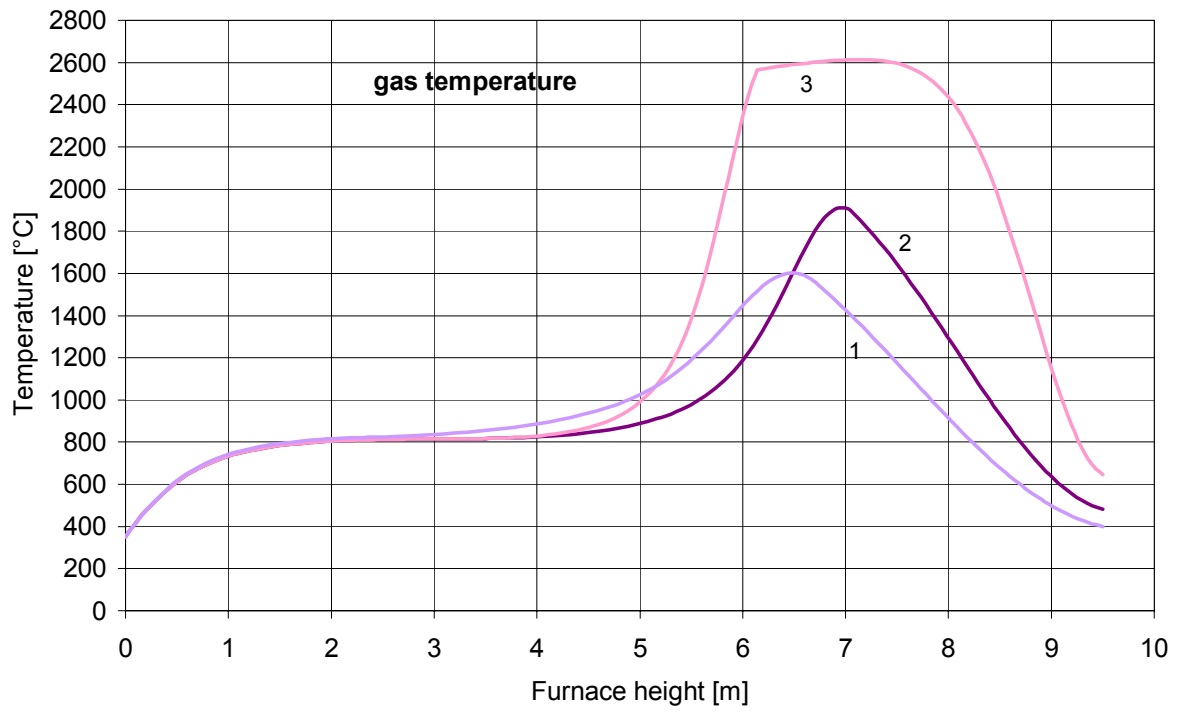
(c)
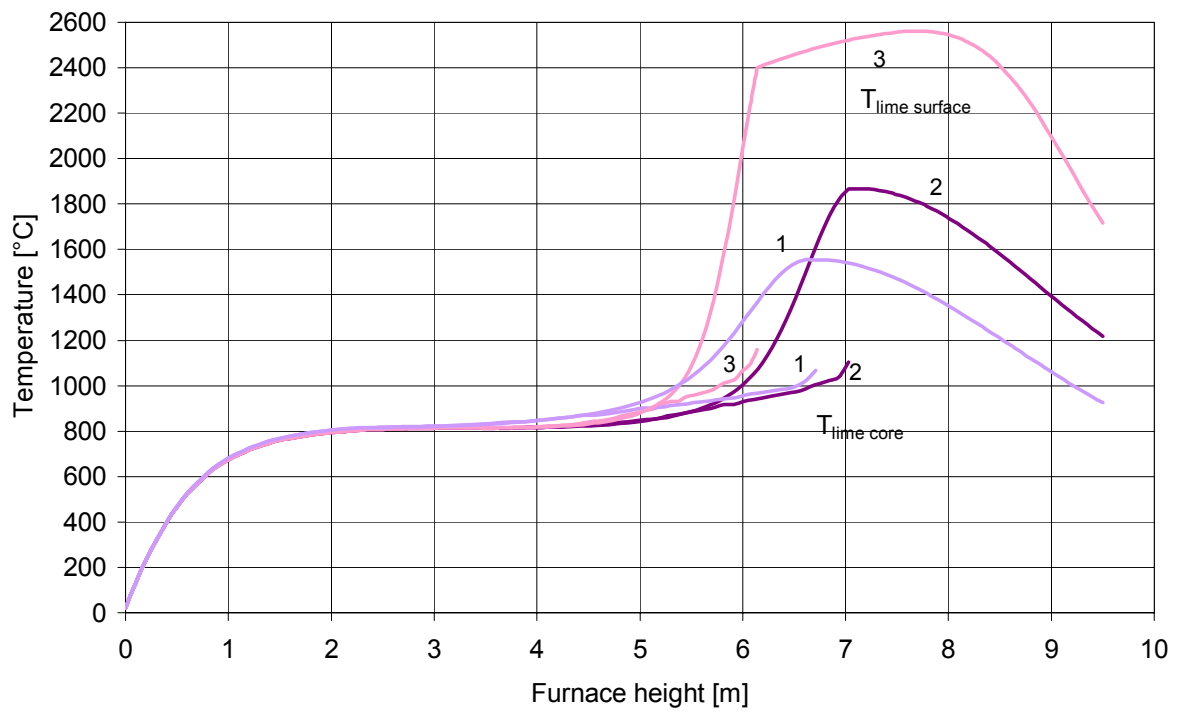
(d)
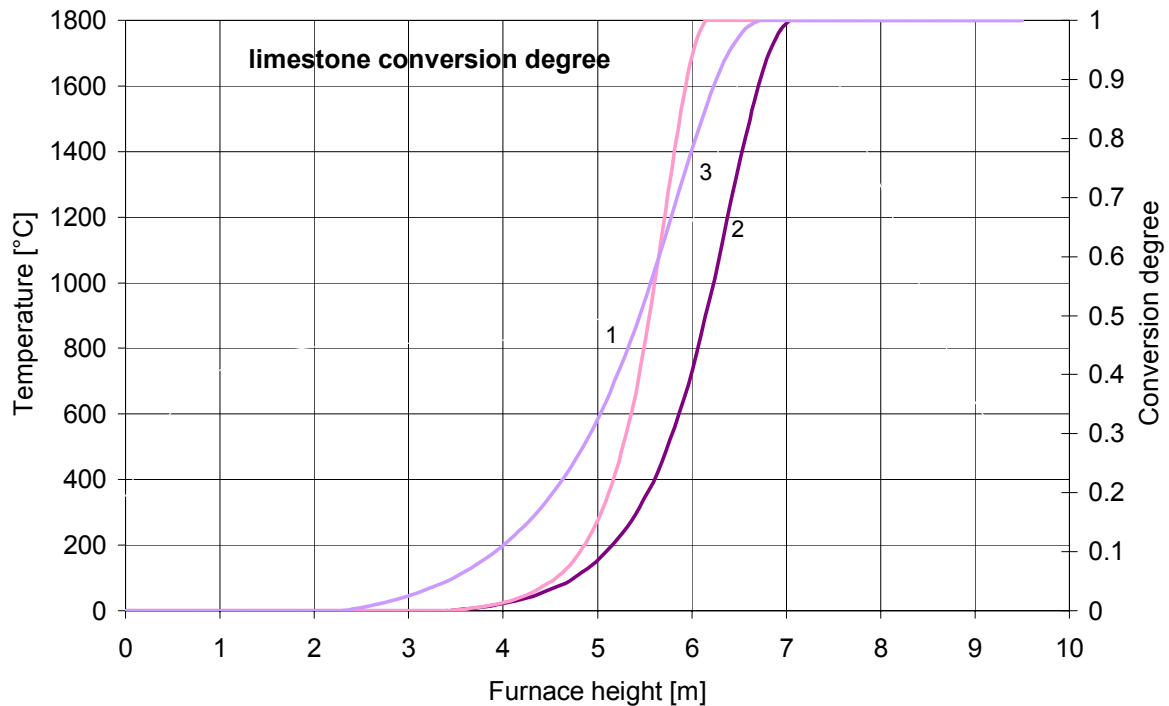
Figure 5-5: The temperature and conversion degree profiles in the preheating and the burning zones. Plots involve the flue gas temperature 350°C, natural gas as a fuel, lime output 26.3t/day/m², air excess number 1.35, energy usage 4.0 MJ/kg$_{CaO}$ and particle diameter 0.08m. ; U$_{fuel}$ = exp(-0.1z²); U$_{fuel}$ = exp(-0.2z²); U$_{fuel}$ = exp(-0.95z²);

Figure 5-6 and Figure 5-7 show the calculated temperature and conversion degree profiles in a shaft kiln for lignite as a fuel. Figure 5-6 shows the profiles for different flue gas temperatures and thus energy consumptions. The tendencies observed are the same as in the case of both before regarded fuels. The maximum gas temperature is higher than the one calculated for the weak gas but lower than the one calculated for the natural gas.

(a)
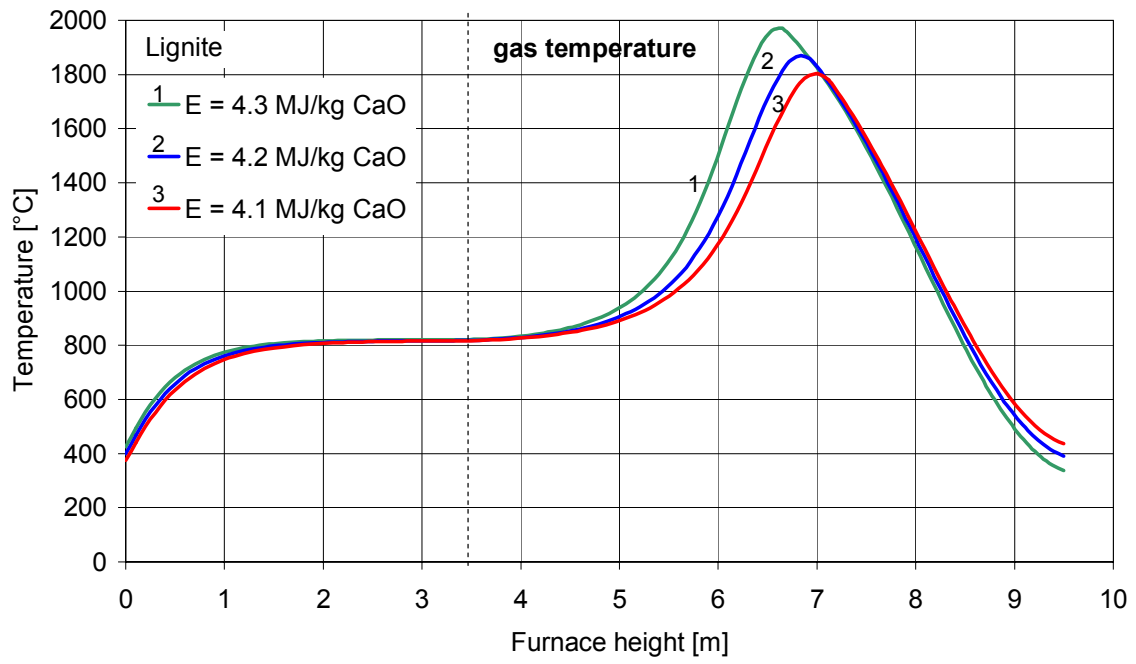
(b)
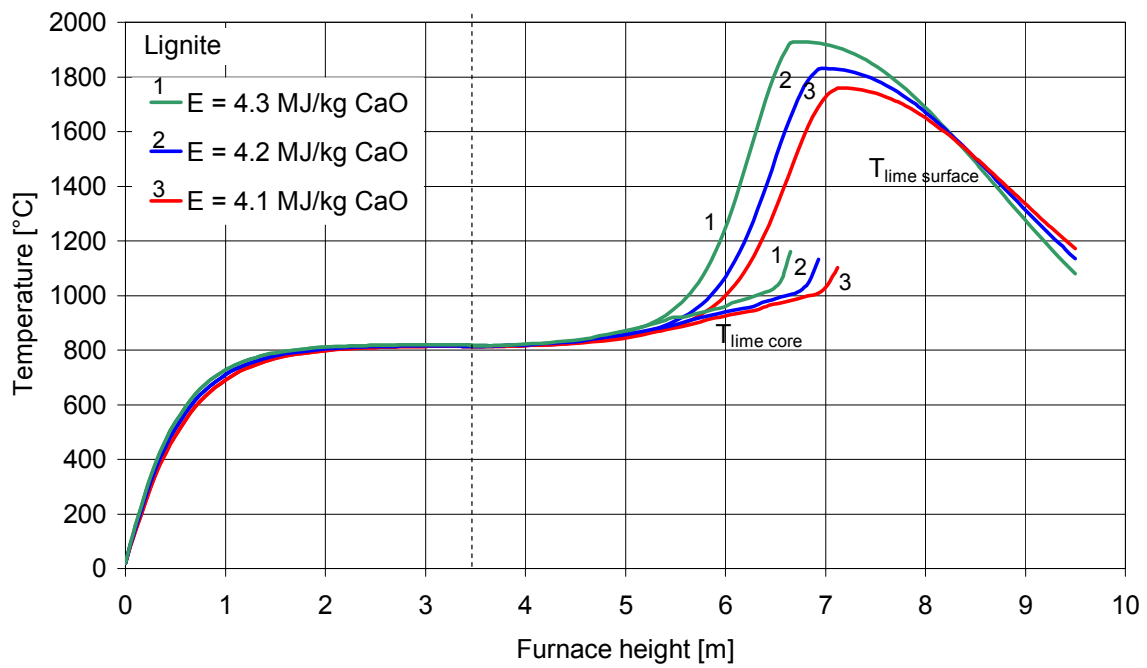
(c)
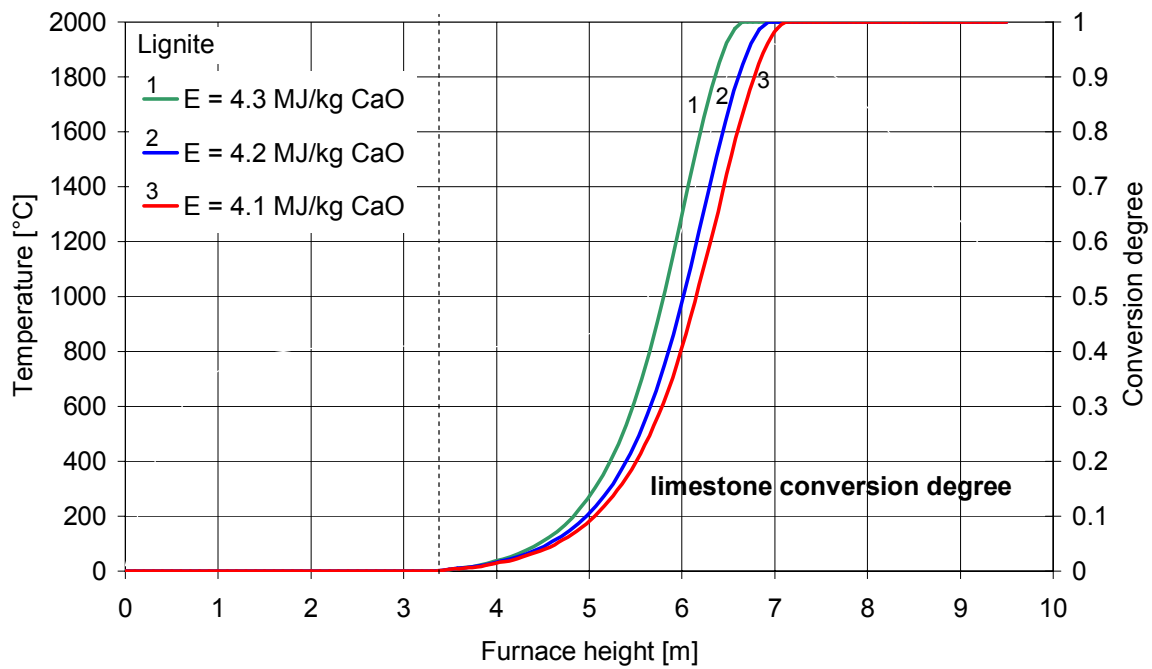
Figure 5-6: The temperature and conversion degree profiles in the preheating and the burning zones. Plots involve the flue gas temperature 375°C, lignite as a fuel, lime output 26.3t/day/m^2 , air excess number 1.4, energy usage 4.1 MJ/kg$_{CaO}$ and particle diameter 0.08m.

Figure 5-7 shows the temperature and conversion degree profiles for different fuel conversion degree profiles. Also in this case the same tendencies are observed as in the case of the both before regarded fuels.

(a) fuel conversion degree
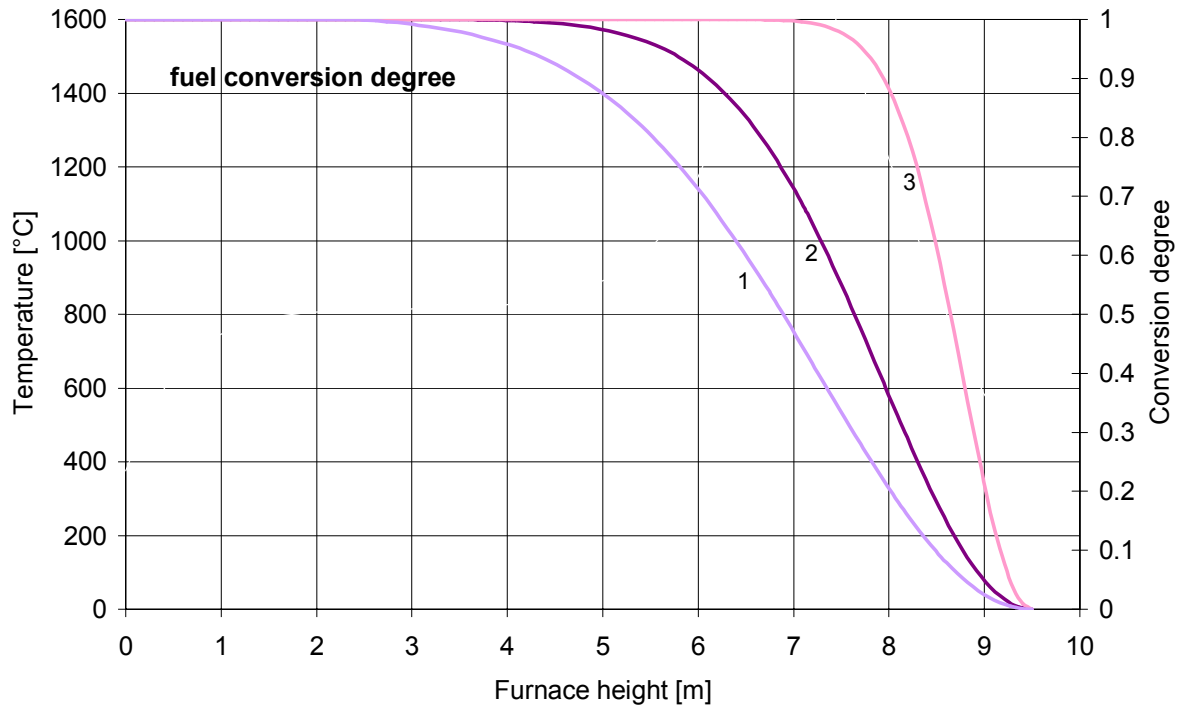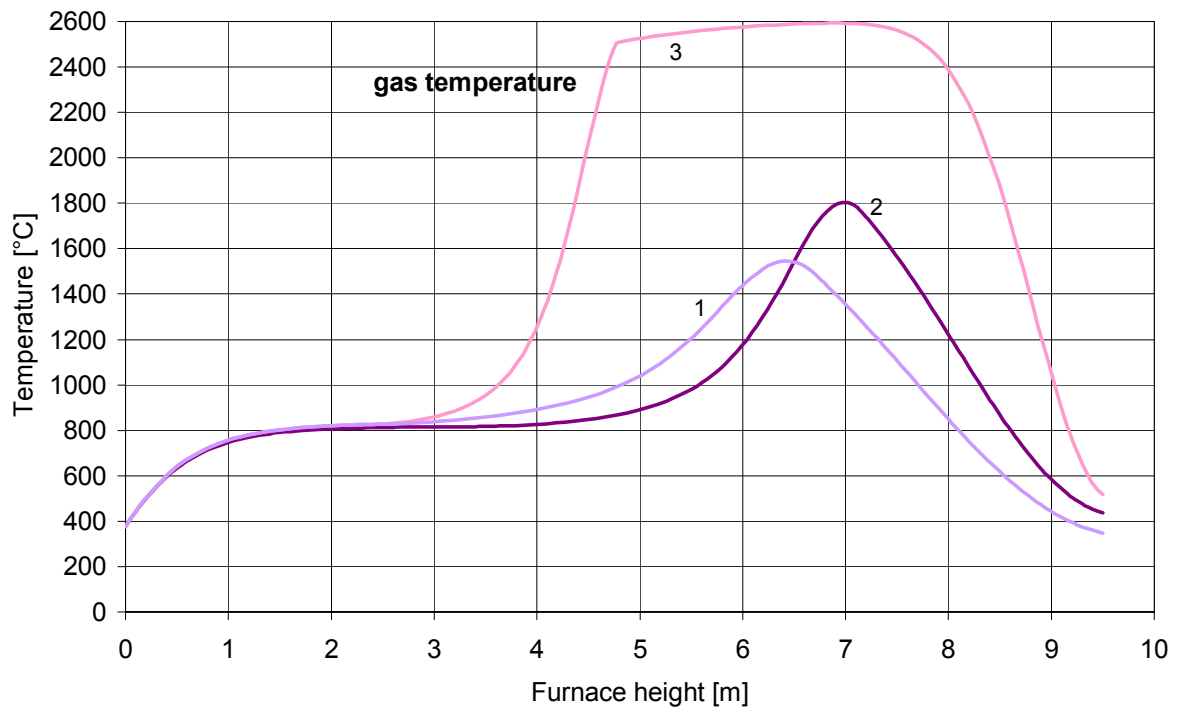
(b) gas temperature

(c)
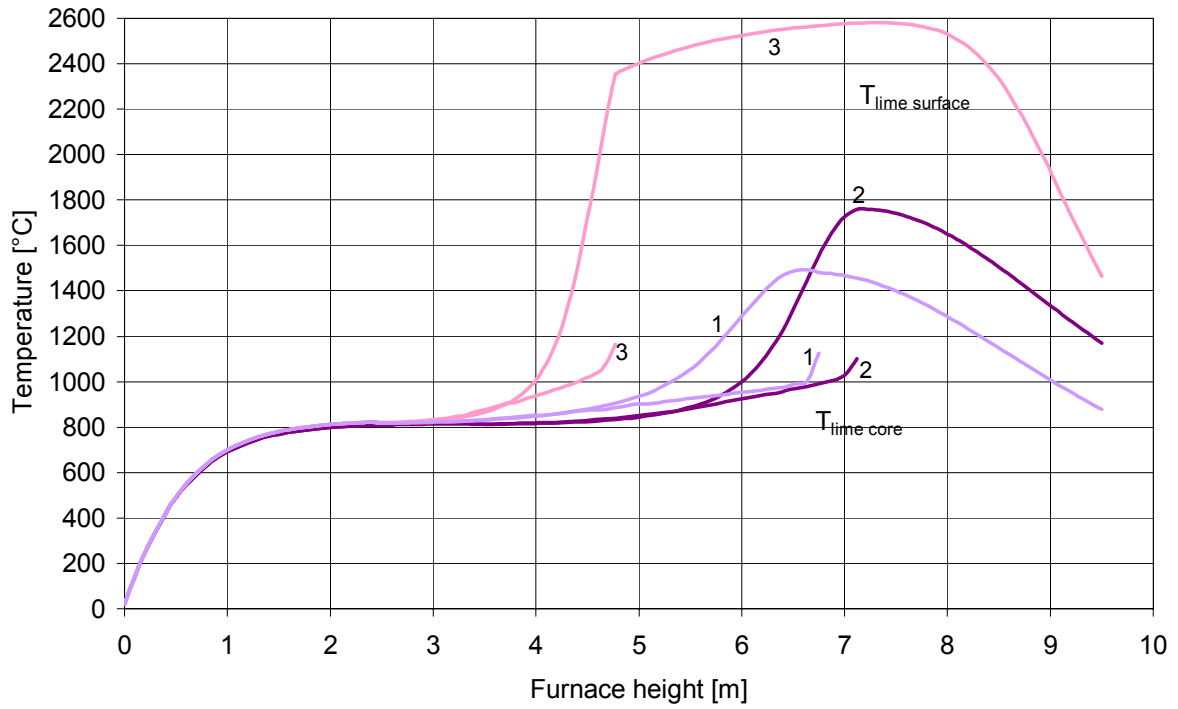
(d)
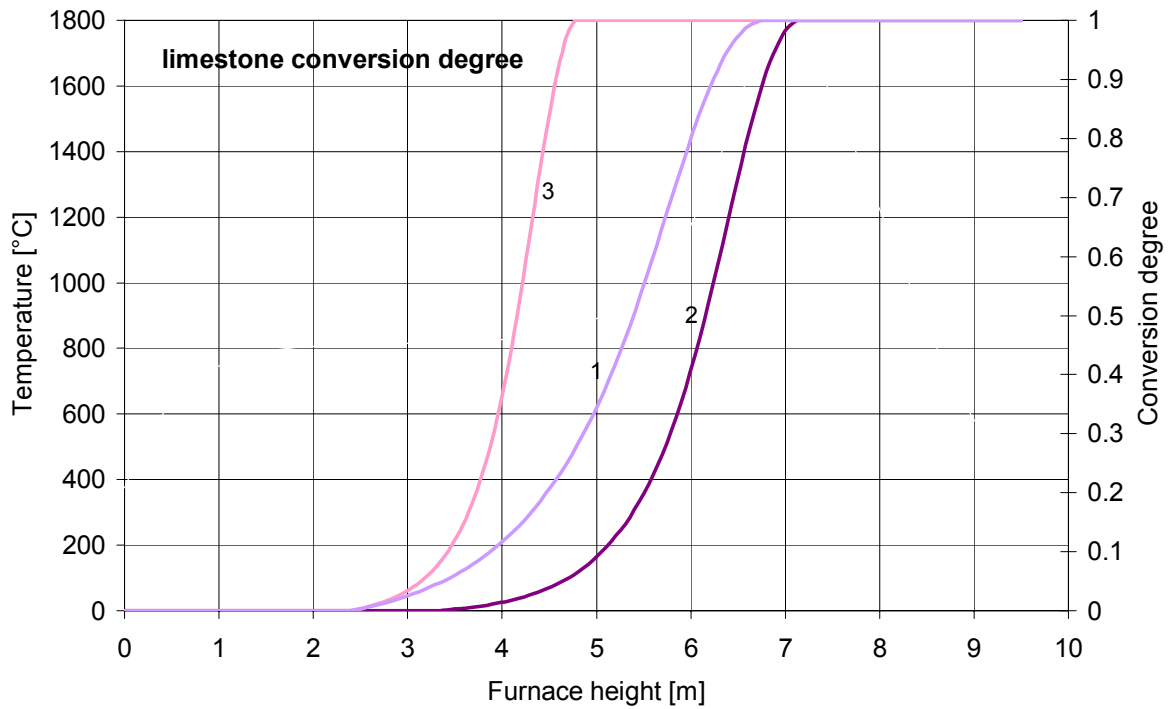
Figure 5-7: The temperature and conversion degree profiles in the preheating and the burning zones. Plots involve the flue gas temperature 375°C, lignite as a fuel, lime output 26.3t/day/m^2 , air excess number 1.4, energy usage 4.1 MJ/kg$_{CaO}$ and particle diameter 0.08m. ; U$_{fuel}$ = exp(-0.1z^2); U$_{fuel}$ = exp(-0.2z^2); U$_{fuel}$ = exp(-0.95z^2);

Figure 5-8 shows the calculated temperature and conversion degree profiles in a shaft kiln for weak gas as a fuel. The lime output was assumed 10% higher than the one taken for the calculations shown in Figure 5-1 (a). Increase of the mass flow of solid results in lower maximum gas temperature and incomplete limestone decomposition.
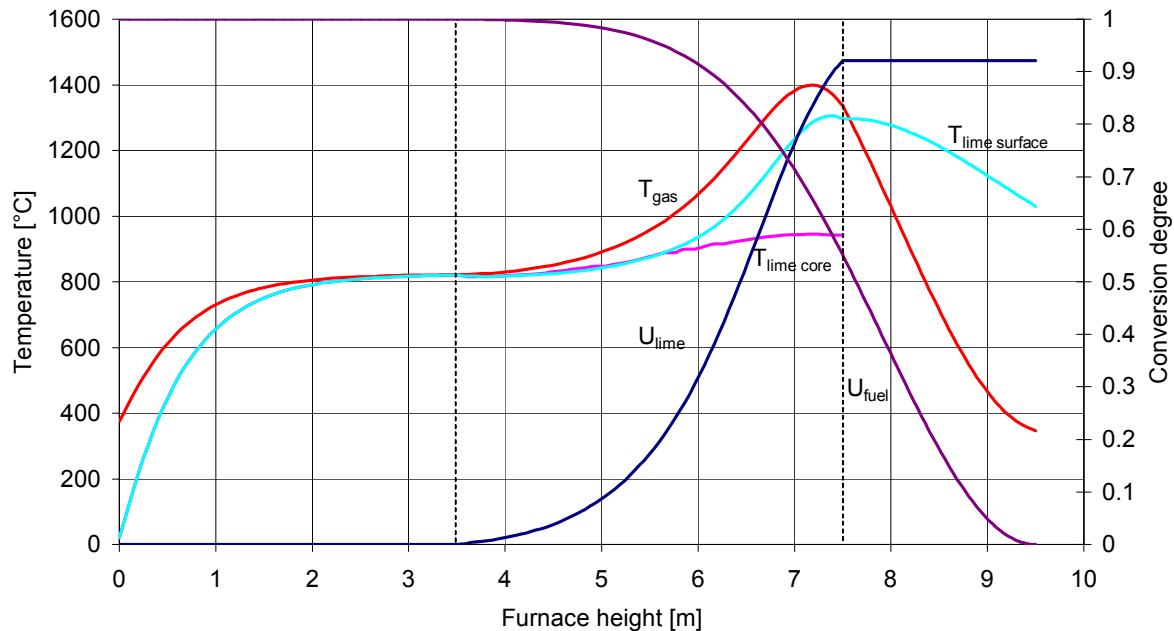
Figure 5-8: The temperature and conversion degree profiles in the preheating and the burning zones. Plots involve the flue gas temperature 375°C, weak gas as a fuel, lime output 29.0t/day/m², air excess number 1.1, energy usage 4.1 MJ/kg$_{CaO}$ and particle diameter 0.08m.

Independently on the kind of fuel the maximum gas temperature is proportional to the energy usage, while the gas and solid temperatures at the end of the air preheating zone seem not to be that strongly influenced by the energy usage.

Figure 5-9 shows the calculated temperature and conversion degree profiles in a shaft kiln for weak gas as a fuel for the particles of 0.06m diameter. The lime output in Figure 5-9 (a) was the same as the one taken for the calculations shown in Figure 5-1 (a). The preheating zone is much shorter as in the case of particles of 0.08m diameter. The reaction is much faster complete. The whole energy produced by fuel combustion is used to preheat the gas, which results in its very high temperature. Figure 5-9 (b), (c), and (d) show the calculated temperature and conversion degree profiles for the increasing lime output. The preheating zone gets longer with increasing lime output and maximum gas temperature gets smaller as part of the produced energy is at the same time used for the calcination. Figure 5-9

103

(c) shows the temperature and conversion degree profiles for the maximum lime output with complete calcination. Figure 5-9 (d) shows the temperature and conversion degree profiles for incomplete calcination.

(a)

(b)

Figure 5-9: The temperature and conversion degree profiles in the preheating and the burning zones. Plots involve the flue gas temperature 375°C, weak gas as a fuel, air excess number 1.1, energy usage 4.1 MJ/kg$_{CaO}$ and particle diameter 0.06m. (a) lime output 23.6 t/day/m^2, (b) lime output 41.5 t/day/m^2, (c) lime output 47.2 t/day/m^2, (d) lime output 47.6 t/day/m^2,

6. Conclusions

Conclusion considering the numerical solution:

- In order to get the most efficient mathematical description of the furnace, it had to be divided into 4 zones:

  1. the preheating zone, where the stones are preheated to the decomposition temperature

  2. the burning zone, where the limestone calcinations and fuel combustion take place

  3. the air preheating zone, where the air emerging form the cooling zone is preheated to the temperature higher than the solid temperature

  4. the cooling zone, where the lime particles are cooled down before discharge

- Neither finite difference method nor Runge – Kutta method were successful with the solution of the equations describing the temperature and conversion degree profiles in the whole furnace. The combination of both methods (Runge – Kutta for calculation of the preheating, the burning and the cooling zone; finite difference method - for the air preheating zone) was necessary to give a satisfactory result.

- The energy usage and thus the flue gas temperature, lime output temperature, and the preheating, the burning and the air preheating zone length had to be determined iteratively

Conclusion considering the furnace performance:

- With the help of the model the energy usage and the quality of lime can be predicted.

- The energy usage depends on the kind of fuel and the gas and solid temperature difference between the preheating and the burning zone.

- The smallest energy usage is obtained for the natural gas and the highest - for the weak gas.

- For a given fuel the energy usage can be lowered by lowering the air excess number.

- The quality of lime depends on the lime temperature.

- The maximum lime temperature depends on the energy usage. The higher the energy usage, the higher the maximum lime temperature.

- The maximum lime temperature depends also on a fuel conversion. For the slow fuel combustion the maximum lime temperature was lower than the one obtained for the faster fuel combustion.
- The kind of fuel has an influence on the maximum lime temperature. The highest temperatures were obtained for the natural gas. T They were lower for the lignite and the lowest for the weak gas.
- The maximum lime temperature dependence on the lime output was determined. The increase of the lime output results in decrease of the maximum lime temperature. If the lime output is too big the complete conversion is not possible
- The maximum lime output depends on the particle size.

Outlook:
- In its present state the mathematical model deals only with spheres of the same size. In the future the model should be extended to different particle size and shape.
- The conversion degree of fuel (in present state of model approximated by a function $U_f = \exp(-az^2)$) should be described as a function of oxygen concentration, air excess number and kind of fuel.
- It would be advisable extend the model to another type of furnace e.g. with multi-level fuel injection system.

7. Nomenclature

A	area	[m^2]
a	thermal diffusivity	[m^2/s]
b	shape factor	-
c	specific heat capacity	[J/kgK]
d	particle diameter	[m]
D^P	pore diffusion coefficient	[m^2/s]
f$_a$	form factor	-
h	calorific value	[J/kg]
H	height of the furnace	[m]
Δh	reaction enthalpy	[J/mol]
k	reaction coefficient	[m/s]
L	zone length	[m]
L$_0$	characteristic length	[m]
$\dot{M}$	mass flow rate	[kg/s]
$\tilde{M}$	molar mass	[kg/kmol]
O	specific surface area	[m^2/m^3]
p	pressure, partial pressure	[Pa]
R	molar (universal) gas constant	[J/molK]
R$_i$	resistance of sub-process I	[K/W]
s	mean beam length	[m]
s/2	characteristic length	[m]
T	temperature	[K]
t	time	[s]
U	conversion degree	-
w	superficial velocity	[m/s]
x	mass fraction	-
z	co-ordinate	[m]

Greek letters

α	heat transfer coefficient	[W/m^{2}K]
β	mass transfer coefficient	[m/s]
ε	emissivity	-
ϑ	temperature	[°C]
λ	heat conduction coefficient	[W/mK]
ν	kinematic viscosity	[m^2/s]
η	dynamic viscosity	[kg/m/s]
ρ	density	[kg/m^3]
ρ_{1S}	volume concentration of CO_2	[kg/m^3]
ρ_{0S}	coke initial density	[kg/m^3]
σ	Stefan-Boltzmann constant	[W/m^{2}K^4]
φ	view factor	-
Ψ	void fraction	-

Subscripts

a	air
eq	equilibrium
f	fuel
g	gas
k	chemical reaction

LS   limestone
LB   quicklime
lam   laminar
m   average
rad   radiation
s   surface, solid
turb   turbulent
u   ambient
α heat transfer
β mass transfer
λ heat conduction
δ reaction front

8. References

[1] Canadian Minerals Yearbook for Lime, 1998.

[2] U.S. Geological Survey, Minerals Yearbook, 1999.

[3] U.S. Geological Survey, Mineral Commodity Summaries, February 2000.
   http://minerals.usgs.gov/minerals/pubs/commodity/lime/

[4] U.S. Geological Survey, Mineral Commodity Summaries, January 2001.
   http://minerals.usgs.gov/minerals/pubs/commodity/lime/

[5] U.S. Geological Survey, Mineral Commodity Summaries, January 2002.
   http://minerals.usgs.gov/minerals/pubs/commodity/lime/

[6] European Commission D6 III: European Minerals Yearbook. Second edition 1996-7. Luxembourg 1998

[7] European Commission: Reference Document on Best Available Techniques in the Cement and Lime Manufacturing Industries, March 2000.

[8] Kehse, G., de Meester, E., Wermbter, H., Zelkowski, J.: Untersuchungen zur Entwicklung einer praxisorientierten Methodik und Apparatur zur Kontrolle der Brenneigenschaften grobkörniger Brennstoffe. 3. European Lime Conference, European Lime Association, Munich 2000.

[9] Oates, J.A.H.: *Lime and Limestone: Chemistry and Technology, Production and Uses*. Wiley-VCH, 1998.

[10] Höltje, W.: *Alternatives to coke as fuel for conventional shaft kilns*. Zement-Kalk-Gips 1 (1989), pp. 21-26

[11] Specht, E.: *Combustion Technology* – handout for Master of Quality, Safety & Environment Program, Otto-von-Guericke-University Magdeburg

[12] Tsotsas, E.: *Product quality in process and chemical engineering* – handout for Master of Quality, Safety & Environment Program, Otto-von-Guericke-University Magdeburg

[13] VDI Wärmeatlas . 8th Edition. Springer Verlag Berlin Heidelberg, 1997.

[14] Specht, E.: *Kinetik der Abbaureaktionen*. Cuvillier Verlag, Göttingen, 1993.

[15] Jeschar, R.: *Heat transfer in pelletizing with mixed feed*. Archiv für das Eisenhüttenwesen 35 (1964), H.6

[16] Jeschar, R., Specht, E., Alt, R.: *Grundlagen der Wärmeübertragung*. Viola-Jeschar-Verlag, Goslar,1990.

[17] Kainer, H., Specht, E., Jeschar, R.: *Pore diffusion, reaction and thermal conduction coefficient of various limestones and their influence on decomposition time.* Zement-Kalk-Gips 7 (1986), pp. 214-219.

[18] Baehr, H.D., Stephan, K.: *Heat and mass transfer.* Springer, 1998.

[19] Verma, C.L.: *Simulation of lime shaft kilns using mathematical modelling.* Zement-Kalk-Gips 12 (1990), pp. 576-582.

[20] Verma, C.L., Dave, N.G., Saraf, S.K.: *Performance estimation vis-à-vis design of mixed-feed lime shaft kiln.* Zement-Kalk-Gips 9 (1988), pp. 471-477

[21] Gordon, Y.M., Blank, M.E., Madison, V.V., Abovian, P.R.: *New Technology and Shaft Furnace for High Quality Metallurgical Lime Production.* Proceedings of Asia Steel International Conference – 2003, Jamshedpur, India, April9-12, 2003, Volume-1, p.p. 1.b.1.1-1.b.1.6

[22] Günther, R,: *Verbrennung und Feuerungen.* Springer-Verlag Berlin Heidelberg New York, 1974, p. 163.

[23] Ergun, S.: *Fluid flow through packed columns.* Chem. Engng. Prog. 48 (1952) 2, p.p. 89/94.

[24] Brauer, M.: *Grundlagen der Einphasen- und Mehrphasenströmungen.* Sauerländer Verlag, Aarau u. Frankfurt 1971.

[25] Molerus, O.: *Fluid-Feststoff-Strömungen. Strömungsverhalten feststoffbeladener Fluide und kohäsiver Schüttgüter.* Springer-Verlag, Berlin, 1982.

[26] Molerus, O.: *Principles of Flow in Disperse Systems.* Chapman & Hall, London 1993.

[27] Schweinzer, J.: *Druckverlust in und gaskonvektiver Wärmeübergang an Festbetten und Wirbelschichten.* Dissertation, University Erlangen-Nürnberg 1987.

[28] Gnielinski, V.: vt „verfahrenstechnik" 12 (1978), Nr. 6, p.p. 363/66.

[29] Gnielinski, V.: vt „verfahrenstechnik" 16 (1982), Nr. 1, p.p. 36/39.

[31] Hottel, H. C., u. A. F. Sarofim: *Radiative Transfer.* New York: McGraw-Hill 1967.

[32] Nußelt, W.: *Der Wärmeübergang in der Verbrennungskraftmaschine.* VDI-Forsch.-Heft Nr. 264. (1923) Düsseldorf: VDI-Verlag.

[33] Schack, A.: Z. Techn. Phys. 15 (1924) p. 267.

[34] Hottel, H. C.: Trans. amer. Inst. Chem. Engs. 19 (1927) p. 173.

[35] Elsasser: Harvard Meteorological Series No. 6, Harvard University Cambridge, Mass. 1942.

[36] Mayer, H.: *Method of Opacity calculations LA-647.* Los Alamos, October. 1947.

[37] Goody, R. M.: Quart. J. Roy. Meteorol. Soc. 78 (1952) p. 165.

[38] Plass, G. N.: J. Opt. Soc. Am. 48 (1958) p.p. 690/703.

[39] Barin, I., Knacke O.: *Thermochemical properties of inorganic substances.*
Springer-Verlag, Berlin, 1973.

9. Table Index

10. Figure Index

116

117

Lebenslauf

Persönliche Daten

Name: Agnieszka Maria Bes
Geburtsdatum: 15.11.1974
Geburtsort: Zabrze – Polen
Staatsangehörigkeit: Polnisch
Familienstand: Ledig

Schulausbildung & Studium

1996 – 1998   **Pädagogisches Studium** im Zentrum für Forschung und didaktische Fortbildung an der Schlesischen Technischen Universität – Gliwice, Polen.

1993 – 1998   **Dipl.-Ing. Chemie**
Spezialfach: Polymer und Kunststofftechnologie
Studium an der Schlesischen Technischen Universität – Gliwice, Polen.

1989 – 1993   **Abitur**
Liceum Ogolnoksztalcace Nr. 1– Gliwice, Polen.

Berufliche Erfahrung

- **ab März 2002**
  Wissenschaftliche Mitarbeiterin, an der Otto-von-Guericke Universität – Magdeburg.

- **September 1998 – Juni 1999**
  Lehrerin für Chemie, Oberschlesisches Edukationszentrum – Gliwice, Polen.

- **Praktikum:**
  - Lehrerin für Chemie, Liceum Ogolnoksztalcace Nr. 5, Gliwice, Polen, März-April 1998.

  - Abteilung für Qualitätskontrolle, Polifarb Cieszyn-Wroclaw S.A., Cieszyn, Polen, Juli 1997.